A thesis submitted in partial fulfillment for the requirements of the

Degree of Doctor of Philosophy from Faculté des sciences, Université Mohammed V-Agdal

Option: Computer Engineering and Telecommunication

Submitted by
RACHID SAADANE

Indoor UWB Channel Characterization and Modeling based on an Information Theoretic approach and SAGE algorithm.

Defended in 10 July , 2007 before the jury including:

M. Chefchaouni INPT, Rabat Morocco	President
D. Aboutajdine, Fsr, Rabat, Morocco	Thesis supervisor
A. Menouni, EURECOM, Sophia Antipolis, France	Thesis supervisor
M. A. Lagunas CTTC Barcelona Espagne	Reader
M. Debbah Supelec Paris, France	Reader
R. Knopp EURECOM, Sophia Antipolis, France	Examiner
M. Hamri Fsr, Rabat Morocco	Examiner
N. Zahid Fsr, Rabat Morocco	Examiner
M. Wajih Maroc Telecom	Invited

rachid.saadane@gmail.com

Avant Propos

Les travaux présentés dans ce mémoire ont été effectués en collaboration entre : Laboratoire de Recherche en Informatique et Télécommunications à la Faculté des Sciences de Rabat sous la direction de Monsieur Driss Aboutajdine et l'institut Eurecom Sophia Antipolis sous la direction de Madame Aawatif Menouni Hayar.

En premier lieu, je tiens à remercier le **C**entre **N**ational de la **R**echerche **S**cientifique et **T**echnique pour l'octroi de la bourse d'excellence qui m'a permis de mener mes travaux de recherche de thèse dans de bonnes conditions.

Je tiens à remercier avec gratitude et délicatesse mes directeurs de thèse Mr. Driss Aboutajdine, Professeur d'enseignement Supérieur à la faculté des sciences de Rabat et Mme. Awatif Menouni Hayar, Maître de Conférences à l'Institut Eurecom pour leur encadrement et leur suivi rigoureux tout au long de la réalisation de ce travail. Mes remerciements s'adressent aussi à Mr. Raymond Knopp, Professeur à l'Institut Eurecom pour les aides qu'il m'a apportées surtout au début des mes travaux de recherche. Je saisie l'occasion pour remercie Dr. Helmut Hofstetter pour les fructueuses collaborations que nous avons eues.

Je tiens à remercier, aussi, Messieurs les membres du jury, Professeur Noureddine Zahid de la faculté des sciences de Rabat, Professeur Mohammed Hamri de la faculté des sciences de Rabat, Professeur M. Chefchaouni directeur de INPT Rabat, Professeur Miguel Angel Lagaunas du Centre Tecnològic de Telecomunicacions de Catalunya de l'université de Catalunya, Professeur Raymond Knopp de l'institut Eurecom, Professeur Mérouan Debbah de l'école supérieure de l'électricité de paris et Mr. Mohammed Wajih directeur à Maroc Telecom, pour leurs attentions et leurs commentaires constructifs sur mon travail.

Je saisie l'occasion aussi pour remercier Dr. Mohammed Derdar, Mr. A. Jilbab, Dr. Tayeb Sadiki pour les fructueuses discussions que nous avons eues et qui m'ont fortement aidées pour l'élaboration de ce document.

Je m'adresse, également, à mes amis d'Eurecom à qui je dois un grand merci, Tarik, Taoufik, Hicham, Issam et Younesse et Abdellah, je n'oublie pas les gestes fraternels et inoubliables qu'ils ont faits pour moi lors de mes séjours scientifiques en France.

Une pensée particulière aux chers collègues du Laboratoire de Recherche en Informatique et Télécommunications: ELhaj Saoud, Youssef, Brahim, Benayad, My Ahmed, Hicham, Jamal, Ouadoudi, Mohammed, Mohamed, Amine, Adil, Hamadi, Najlae, Samira, Manal, Hassan, Sanaa, Hicham, Tarik, Brahim, Aziz, Sanaa, Siham, Fadoua, Fedwa, Leila, Aouatif, Zhour, Naoual, Khalid, Nabil, Reda, Ibrahim, Hinde, Fatim-ezzahra, Imane...

Un merci spécial à mes amis de la faculté, surtout Ismail, Abdelilah, Said, Lamouar, youssef, Mourad, Lhacene, Zouhair...
Enfin, je remercie tous ceux qui ont contribué de près ou de loin à la mise à terme de ce modeste travail.

Abstract

Models of radio channel propagation are indispensable in the analysis and design of wireless communication systems. They are used to predict power and interference levels and analyze other properties of the radio link. The main goal of this dissertation is to provide a set of tools that allow the researchers in the field of Ultra Wide Bandwidth (UWB) communication systems to investigate the performances of those proposed algorithms and communication system schemes.

Based on a set of UWB channel (from 3 to 9 GHz) measurements under both Line of Sight (LOS) and Non Line of Sight (NLOS) conducted recently at Eurecom Institute. A Vector Network Analyzer is used to measure the frequency channel response of the frequency bandwidth of interest. An Omnidirectional antennas are used for both the transmitter (Tx) and receiver (Rx) antennas. Probability and cumulative density of received signal, power variation and pathloss fluctuations are evaluated. An estimation of m-parameter for each delay and its probability density function are given away (for NLOS). We have find that the Weibull power density function (pdf) fits the experimental measurements. Besides, an investigation of pathloss shows no dependency between frequency and the pathloss, but the pathloss and central frequency present a correlation. We have also found that most measurements characterized by a shadowing fading fit a lognormal distribution and the small fading distribution seemed to have a value of $\tilde{m} = 1$, which corresponds to a Rayleigh distribution.

In the second part of this thesis we use a new approach for characterizing the second-order statistics of indoor UWB channels using channel sounding techniques. These are based on an eigendecomposition of the channel auto-covariance matrix, which allows for the analysis of the growth in the number of significant Degrees of Freedom (DoF) of the channel process as a function of the signaling bandwidth as well as the statistical correlation between different propagation paths. We show empirical eigenvalue distributions as a function of the signal bandwidth for both LOS and NLOS situations. Moreover, we give examples where paths from different propagation clusters show strong statistical dependence. And to confirm the saturation of DoF with channel bandwidth increasing, the theoretic information is used. Firstly we evaluate the number of DoF using AIC and MDL, and secondly we investigate the channel entropy.

In the UWB propagation context, a physical phenomenon must be taken in consideration. Analyzing these phenomena the UWB radio channel is affected by various propagation mechanisms, particularly reflection, transmission, scattering and diffraction. We have analyzed by multiplicity of simulations of the diffractions and reflections as function of channel bandwidth, the materiel properties and the displacements types. After that, we have proposed a new UWB channel model. The presented model is, in fact, based on physical propagation effects and UWB channel measurements conducted at Eurecom. In order to do this, a Space Alternating Generalized Expectation Maximization (SAGE) algorithm is used to estimate the model parameters. The Simulations show that the proposed model presents a good fit to measurement data and is easy to implement.

Résumé

L'objectif principal de ce travail de thèse est d'offrir un ensemble d'outils permettant aux chercheurs et aux industriels dans le domaine des communications Ultra Large Bande (ULB) d'examiner et évaluer les performances des transmissions mobiles en se basant sur le modèle proposé.

La caractérisation et la modèlisation des canaux de propagation sont indispensables pour la conception et l'implémentation des systèmes de communications. Cette caractérisation donne naissance à des modèles qui seraient utilisés pour la prédiction et l'évaluation de niveaux de puissance et les interférences, ainsi que pour analyser d'autres propriétés des liaisons radio.

Dans les systèmes de communications mobiles, notamment la technologie ULB, les canaux ne sont pas caractérisés par un modèle universel unique. Ce travail donc a pour objectif de mettre en place une évaluation de tous les paramètres éventuellement pris en compte lors de modélisation du canal.

Le travail est subdivisé en deux parties majeures, la première a été consacrée au le volet expérimental de l'étude, l'ensemble des mesures que nous avons a faites se sont basées sur deux modes de topologies: Avec visibilité directe (ou Line Of Sight) et Sans visibilité directe (Non Line Of Sight) entre l'émetteur et le récepteur. Pour faire le sondage, nous nous sommes servis d'un analyseur vectoriel des réseaux et des antennes omnidirectionnelles.

A la fin de la récolte des mesures expérimentales, la fonction densité de probabilité (PDF) et la fonction de distribution cumulative (CDF) du signal reçu sont évaluées. Une évaluation de la variation de la puissance en est déduite . Une étude des effets à grandes et à petites échelles montrent bien qu'il n'y a pas de dépendance entre la fréquence et la perte par propagation (ou Path Loss), par contre, la corrélation entre elle n'est pas négligeable. L'étude a montré, que les effets à petites échelles peuvent être représentés par une distribution de Rayleigh tandis que Les effets d'évanouissement sur la majorité des mesures suivent une distribution Lognormal.

La seconde partie porte sur l'évaluation et la présentation d'une nouvelle approche qui consiste en une caractérisation des statistiques d'ordre deux d'un canal ULB en utilisant les technique de sondage canal. Cette approche est basée sur une décomposition en sous espaces propres de la matrice d'auto covariance du canal afin d'évaluer l'évolution des degrés de liberté (DDL) en fonction de la bande du signal, et aussi, pour analyser la corrélation entre les multi trajets de propagation. Nous déduisons une distribution empirique des valeurs propres du canal en fonction la largeur de la bande pour les deux cas de figures LOS et NLOS.

L'étude de l'évolution de nombre du DDL en fonction de la largeur de bande a montré une saturation à partir d'une certaine bande de fréquence. Pour confirmer ce résultat, nous avons fait appel aux fondements de la théorie d'information en se basant, d'une part, sur les deux critères Akaik Information Cretirion (AIC) et Maximum Description length (MDL) tout en examinant le comportement en fonction de la fréquence, puis, comparé ceci avec une autre approche basée sur l'étalement du retard (ou delay spread) et d'autre part, nous avons évalué la fonction d'entropie en fonction de la fréquence qui a montré aussi une saturation du nombre de degrés de liberté.

Ainsi, vu que les systèmes ULB sont très sensibles aux effets de transmissions de réflexions et de diffractions, il est très important de mettre en évidence l'influence de ces phénomènes dans le processus de propagation. Pour cela, nous avons analysé, par une série de simulations, les différents mécanismes cités ci-dessus en fonction de la largeur de la bande et la nature des obstacles qui les causent. Cette analyse, nous a permis, donc, de pouvoir proposer un nouveau model de canal moyennant l'algorithme de Space Alternating Generalized Expectation Maximization (SAGE). Les résultats obtenus ont été comparés et validés avec les mesures expérimentales.

Contents

List of Figures

List of Tables

ACRONYMS

Here are the main acronyms used in this document.

1G	First Generation
2G	Second Generation
⋮	⋮
4G	Fourth Generation
AIC	Akaike's Information Criterion
Atem	Atelier of transmission electromagnetic
AWGN	Additive White Gaussian Noise
BAN	Body Area Network
CDF	Cumulative Distribution Function
CIR	Complex Response Impulse
FCC	Federation Communication Commit
FFT	Fast Fourier Transform
HDR	High Data Rate
GOF	Goodness-Of-Fit
IFFT	Inverse Fast Fourier Transform
i.i.d.	independent and identically distributed
KL	Karhunen-Loeve
ISI	Inter-Symbol Interference
LAN	Local Area Network
LOS	Line-of-Sight
MDL	Maximum Description Length
MEM	Maximum Entropy Modeling
MMSE	Minimum Mean-Square Error
MIMO	Multiple-Input Multiple-Output
ML	Maximum Likelihood
NLOS	Non Line-of-Sight
MPC	Multi–Path Components
MRC	Maximum Ratio Combining
PAWN	Personal Area Wireless Network
PDP	Power Delay Profile
PDF	Probability Distribution Function
RF	Radio Frequency

RSIB	Remote
RT	Ray Theory
Rx	Receiver
SS	Spread Spectrum
SNR	Signal-to-Noise Ratio
S–V	Saleh-Valenzuela
SVD	Singular Value Decomposition
QoS	Quality of Service
TL	Threshold Level Tx
Transmitter	
US	Uncorrelated Scattering
UWB	Ultra-Wideband
UMTS	Universal Mobile Telecommunications Services
VAN	Vector Network Analyzer
WPAN	Wireless Personal Area Networks
WG	Working Group
ZF	Zero Forcing
WLAN	Wireless Local Area Network
w.r.t.	with respect to

INTRODUCTION AND THESIS OUTLINE

Due to recent developments in digital consumer electronics technology, Ultra Wideband (UWB) is becoming more attractive for low cost personal communication applications. UWB systems are now emerging across a variety of commercial and military applications, including communications, radar, geolocation, and medical. Third generation wireless and beyond (3 G mobile and 4 G mobile). First generation commercial wireless UWB products are anticipated to be widely deployed soon. This has been fueled by a demand for high frequency utilization and a large number of users requiring simultaneous multidimensional high data rate access for applications of wireless internet and e-commerce.

UWB systems are often defined as systems that have a relative bandwidth larger than 25 % and/or an absolute bandwidth of more than 500 MHz (FCC). The UWB systems using large absolute bandwidth, are robust to frequency-selective fading, which has significant implications on both design and implementation. Among its important characteristics, the UWB technology are low power devices, accurate localization, high multipath immunity, low complexity hardware structures and carrier-less architectures [Sch93, WS98]. Additionally, the spreading of the information over a very large frequency range decreases the spectral density and makes UWB technology deployment compatible with existing systems.

For designing and implementing any wireless communication system, channel sounding and modeling are a basic necessity. Several theoretical and practical studies, have shown an extreme difference with respect to narrowband channels [CWM02b, KP02, SHKD04]. In the area of UWB channel modeling, the researchers are interested to characterize the path loss law, shadowing, multipath delay spread, coherence bandwidth, average multipath intensity profile and received amplitude distribution of the multipath components...

In this thesis, based on UWB channel measurements conducted at Eurecom Institute we have used a new approach to analyze the UWB channel. It is based on the sub space eigen-analysis and the light of Information Theory tools. The analysis of UWB channel sub-space, has shown, for both LOS and NLOS settings, a saturation of the number of eigen–values equivalently the number of DoF versus the bandwidth. Other important results about UWB channel characterization are shown, for example the small and large scale fading are evaluated. In the last part of this thesis we have presented a simple realistic channel model based on the channel characterization and UWB channel propagation phenomena analysis.

In this thesis two hypotheses are also assumed. The first one is that the indoor channel is assumed to be time invariant because the transmitter and the receiver are static and no motions take place in the channel. The second one is that the signal excitation is assumed to be close to an ideal Dirac-Delta impulse which means that the received signal can be seen as a good approximation of the channel impulse response.

This thesis is comprised of two parts: Following a brief introduction to the issues of UWB tech-

nology, systems and channel models in Chapter 1 and 2. In the first part of this thesis, we will address UWB channel measurements like first step to UWB channel characterization and modeling and present experimental results of UWB channel propagation in Indoor environment. In Chapter 3 we will present different sounding techniques in time and frequency domains. Lastly, we will present UWB channel measurements campaign conducted at Eurecom Institute in Mobile Communication Laboratory. Chapter 4 reports on experimental and statistical results and analysis of UWB channel propagation in Indoor, Outdoor and Corridor environments. In this Chapter, we have characterized some channel parameters (Path loss, Power variation, time desperation parameters...). Most of them are compared to those reported on the previous UWB channel measurements companies [SHKA05a, SAH07].

In the second part of this thesis which includes Chapters 5 and 6 we use firstly a new approach to analyze an UWB indoor radio propagation channel by performing an eigen-decomposition and observing the scaling of the number of significant eigenvalues with channel bandwidth. And secondly, we develop a new UWB channel model based on UWB channel measurements conducted at Eurecom Institute and UWB propagation phenomena analysis. In Chapter 5 we investigate empirically the UWB channel energy behaviors and the scaling of the number of significant eigenvalues with channel bandwidth [SHKD04, HKS05]. In the second part of this Chapter we apply Akaike information criterion (AIC) and Minimum Description Length (MDL) to estimate the number of DoF of an Ultra WideBand channel in an in-door environment. We evaluate our solution under both scenarios, LOS and NLOS [SHKA05b, SAHK07].

In Chapter 6 we develop a new UWB channel model based on physical propagation effects and UWB channel measurements conducted at Eurecom Institute [SAH06, SH06, SHAH07b, SHAH07a].

CHAPTER

1

UWB TECHNOLOGY AND SYSTEMS

1.1 Introduction

In this chapter, we present a brief scope of UWB technology and we provide an overview of the existing communication systems in the literature. Our intent here is to provide sufficient description of UWB technology to allow interpretation of both the characterization and modeling results. Specifically, the overview is intended to allow the reader of this thesis to connect the UWB technology with their use. We do not include a comprehensive discussion in all areas, since that is already obtainable in several selected references, e.g., [Mol, Mol05]. We begin this chapter with a short scope of UWB technology. This includes an UWB definition, UWB characteristics, advantages, drawbacks and their applications with respect to UWB waveform properties. Next, a typical receiver adapted to UWB communication systems is described, and a brief description of UWB antennas is provided. In addition, we present a discussion on radio frequency propagation. Its objective is to present briefly the effects of the dominant propagation mechanisms like reflection, diffraction, transmission and scattering on UWB channel impulse response. To explain the relation between these mechanisms and channel propagation, a brief interpretation of effects caused by multipath propagation both in time and frequency domain is presented.

1.2 Brief Scope of UWB Technology

1.2.1 UWB Definition

When UWB technology was proposed for civilian applications, there were no definitions for the signal. The Defense Advanced Research Projects Agency (DARPA) provided the first definition for UWB signal based on its fractional bandwidth B_f of the signal. The first definition provided that a signal can be classified as an UWB one if B_f is greater than 25%. The fractional bandwidth is defined as follows [Tay95].

$$B_f = 2\frac{f_H - f_L}{f_H + f_L} \tag{1.1}$$

where f_L and f_H respectively are cut off frequencies, respectively. In February 2002, the FCC issued the FCC UWB rulings that provided the first radiation limitations for UWB, and also permitted the technology commercialization [FCC02]. The final report of the FCC First Report and Order [Com02] was publicly available during April 2002. The document introduced four different categories for allowed UWB applications (see 1.2.2), and set the radiation masks for them.

The prevailing definition has decreased the limit of B_f at the minimum of 0.25, defined using the equation above. Also, according to the FCC UWB rulings the signal is recognized as UWB if the signal bandwidth is 500 MHz or more. The radiation limits by FCC are presented in Table 1.1 for indoor and outdoor data communication applications, the figure 1.1 shows the FCC proposed mask for UWB signal Indoor.

In Europe, the regulation of UWB is still in progress. The process begun later than in the USA, and while the FCC regulation was published, European Conference of Postal and Telecommunications Administrations (CEPT) were finalizing a report on UWB spectrum sharing. Individual European regulators were supposed to base their regulations on the report. In October 2004, Electronic Communication Committee (ECC) published a draft of a new ECC Report 64 on the protection requirements of radio communication systems below 10.6 GHz from generic UWB applications.

Table 1.1: FCC radiation limits for indoor and outdoor communication applications

Frequency in GHz/environement	Indoor (EIRP in dBm)	Outdoor (EIRP in dBm)
$0.960 - 1.610$	-75.3	-75.3
$1.610 - 1.990$	-53.3	-63.3
$1.990 - 3.100$	-51.3	-61.3
$3.100 - 10.600$	-41.3	-41.3

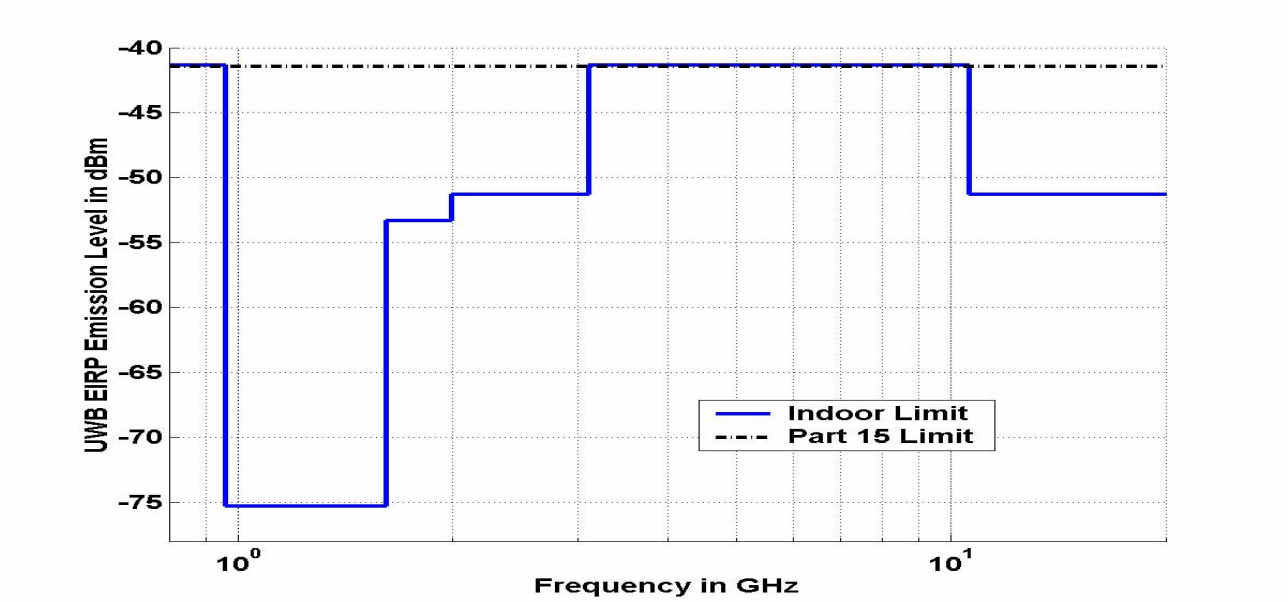

Figure 1.1: FCC UWB Emission Limit for Indoor Systems

1.2.2 UWB Technology Applications

Now, most computer and consumer electronic devices -everything from a digital camcorder and DVD player to a mobile PC and a high-definition TV (HDTV)- require wires to record, play or exchange

data. UWB will eliminate these wires, allowing people to “unwire” their lives in new and unexpected ways. Through UWB [Cor07]:

1. A digital camcorder could play a just-recorded video on a friend’s HDTV without anyone having to fiddle with wires.
2. A portable MP3 player could stream audio to high-quality surround-sound speakers anywhere in the room.
3. A mobile computer user could wirelessly connect to a digital projector in a conference room to deliver a presentation.
4. Digital pictures could be transferred to a photo print kiosk for instant printing without the need of a cable.
5. An office worker could put a mobile PC on a desk and instantly be connected to a printer, scanner and Voice over IP (VoIP) headset.

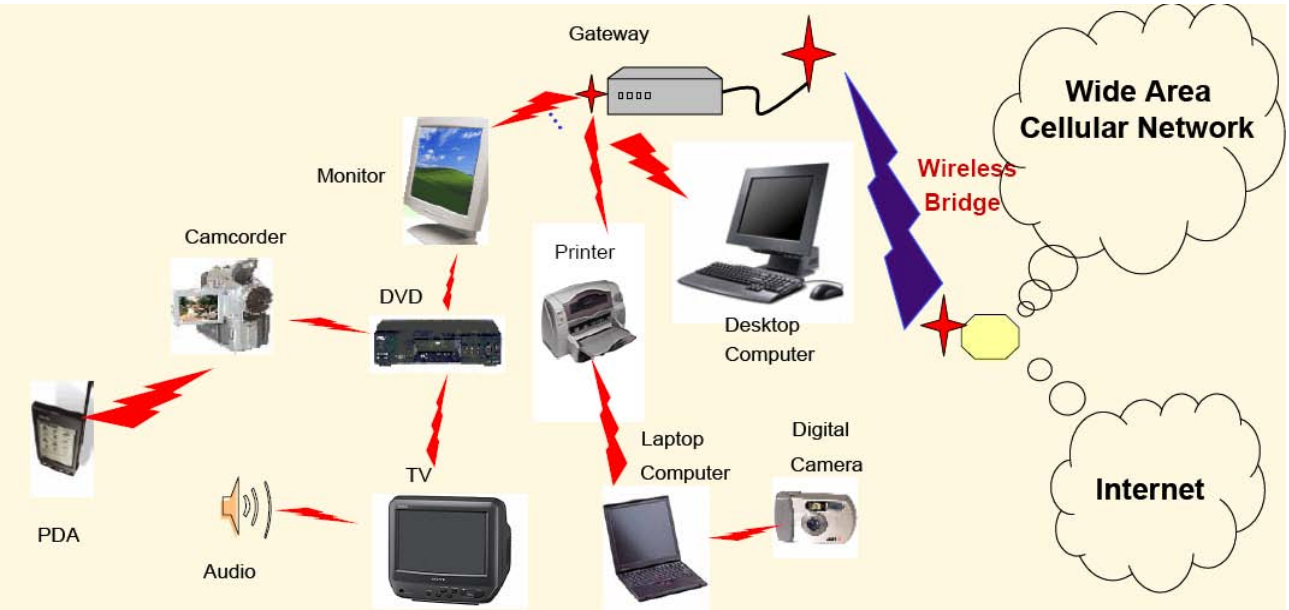

Figure 1.2: UWB devices in WPAN

The figure 1.2 shows the UWB devices will be the important components in Wireless Personal Area Network (WPAN).

1.3 UWB Signals

1.3.1 UWB and the Waveform Properties

UWB has a number of advantages and disadvantages that make it attractive for consumer communications applications. In particular, UWB systems have:

1. Very wide fractional and absolute radio frequency bandwidth.

Advantages	Disadvantages	Applications
-High rate communications. -Potential for processing gain. -Low frequencies penetrate walls, ground.	-Potential interference to existing systems. -Potential interference from existing systems.	-High-rate WPAN7. -Low-power, stealthy commis. -Indoor localization. -Multiple access.

2. Very short pulses

Advantages	Disadvantages	Applications
-Direct resolvability of discrete multipath components. -Diversity gain.	-Large number of multipaths. -Long synchronization.	-Low-power combined communications and localization.

3. Persistence of multipath reflections

Advantages	Disadvantages	Applications
- Low fade margins. -Low power.	-Scatter in angle of arrival.	-NLOS communications indoors and on ships.

4. Carrierless transmission

Advantages	Disadvantages	Applications
- Hardware simplicity. -Small hardware.	-Inapplicability of super-resolution beam-forming.	-Smart sensor networks.

1.3.2 UWB Signal Pulse Shape

UWB signals can be modeled by Gaussian monopulses. The use of monopulse with a very short pulse width in time domain produces a wide bandwidth signal in frequency domain. The center frequency and the bandwidth can be determined, based on the monopulse's width. The Gaussian waveform in time domain is given by equation 1.2.

$$w(t) = \frac{t}{\tau} e^{\frac{-t}{\tau}2}, \tag{1.2}$$

where τ is time decay constant that determines the monocycles duration and t is time. A typical received UWB pulse shape, sometimes known as a Gaussian doublet. There are several ways for generating an UWB signal as shown in the Figure 1.3: first sub-figure (top) shows an UWB signal (pulse) with length $T_p = 1e^{-8}$ seconds and composed by $N_c = 8$ cycles of a sinusoidal waveform (Central Frequency $= 0.8$ GHz, Bandwidth $= 0.2$ GHz and Fractional Bandwidth = 0.25). The second sub-figure (bottom) shows an UWB signal (pulse) with length $T_p = 1e^{-9}$ seconds and composed by $N_c = 8$ cycles of a sinusoidal waveform (Central Frequency $= 8$ GHz, Bandwidth $= 2$ GHz and Fractional Bandwidth = 0.25). Figure 1.4 shows, on the left, an UWB signal generated using a Gaussian pulse with length $T_p = 1e^{-10}$ seconds. On the right, it presents power spectral density of this Guassian pulse (Bandwidth $= 5$ GHz).

The most UWB systems use this Gaussian pulse or its derivative because its shape is easily generated.

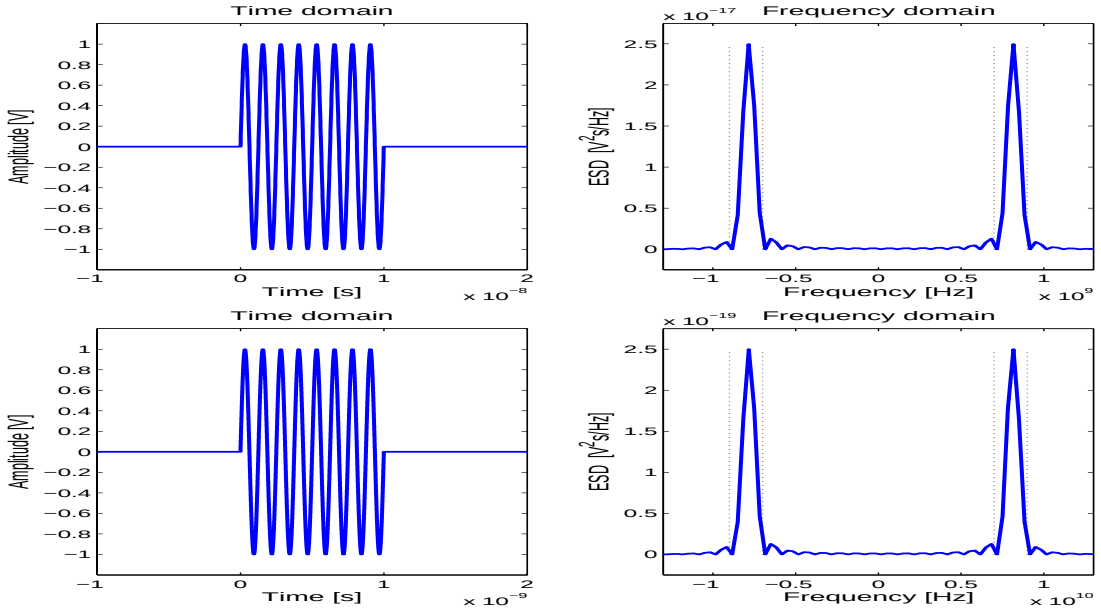

Figure 1.3: An example of an UWB signal generation, Signal bandwidth .2 GHz (top), Signal bandwidth 2 GHz (bottom)

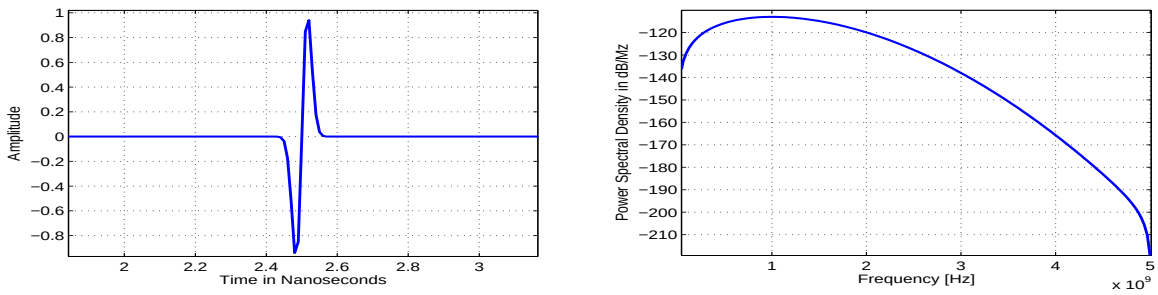

Figure 1.4: Gaussian pulse in time domain (left), Power Spectral Density of Gaussian pulse (right)

1.3.3 UWB signal Power Spectral Density

The power spectral density (PSD) is defined as:

$$PSD(P, \Delta f) = \frac{P}{\Delta f} \tag{1.3}$$

where P is the power transmitted in watts (W), Δf is the bandwidth of the signal in hertz (Hz), and the unit of PSD is (W/Hz). In the UWB systems the power spectral density is generally considered to be extremely low, especially for communication applications. As well known the signal frequency and signal time are inversely proportional. Narrow band signals or sinusoidal systems have narrow frequency occupation, Δf, and long time duration Δt. For an UWB system the pulses have a short t that corresponds a very wide bandwidth Δf. In Table 1.2, we present some typical values of PSDs for traditional wireless communication applications.

Table 1.2: Power spectral density of some wireless communication systems

System	Transmission power [W]	Bandwidth [Hz]	Power spectral density [W/MHz]
Radio	50 kW	75 kHz	$666,600$
Television	100 kW	6 MHz	$16,700$
2G Cellular	10 mW	8.33 kHz	1.2
802.11a	1 W	20 MHz	0.05
UWB	1 mW	7.5 GHz	0.013

1.4 Indoor Radio Frequency Propagation

1.4.1 Wireless channel

In a wireless channel shown in Figure 1.5, the transmitted wave interacts with the physical environment in complex ways, and arrives at the receiver along a number of paths, referred to as multi–paths. The ratio of transmitted and received field strengths, i.e. the propagation loss, is determined by the distance due to the square-law spreading and ground reflections, as well as absorption by materials and foliage in the propagation path.

1.4.2 Radio Propagation Mechanisms

In a typical indoor environment, due to reflection, refraction, Diffraction and scattering of radio waves by structures inside a building, the transmitted signal most often reaches the receiver by more than one path, resulting in a phenomenon known as multipath fading. In wide band (and UWB) pulse transmission, the effect is to produce a series of delayed and attenuated pulses (echoes) for each transmitted pulse. Figure 1.6 presents the dominant propagation mechanisms. These mechanisms are briefly described in the following.

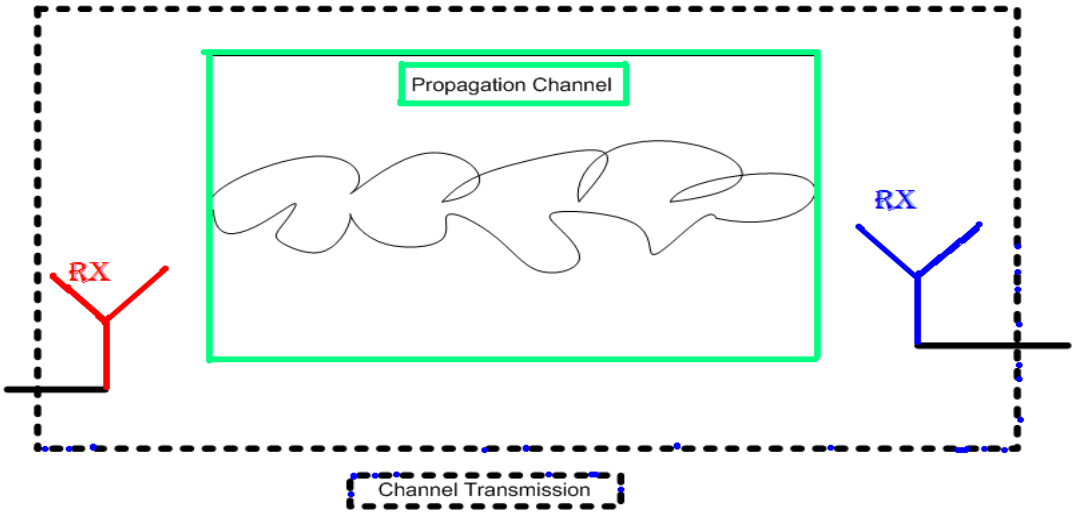

Figure 1.5: General illustration of the UWB channel (here antennas are a part of the channel)

1. Reflection: Reflection occurs when electromagnetic waves impinge upon an obstacle whose dimensions are considerably larger than the wavelength of the incident wave ($\lambda << D$). Multiple reflections can also occur. The obstacle occurs reflection can be the surface of the earth, buildings or walls. A reflected wave can either decreases or increases the signal level at the reception point. In cases where many reflected waves exist, the received signal tends to be very unstable. This phenomenon is commonly referred to as multipath fading and the signal is often Rayleigh distributed.

2. Diffraction: Diffraction occurs at obstacle edges or at corners and as a result, radio waves are bent and additionally attenuated ($\lambda >> D$). However, diffraction allows the reception of radio waves when NLOS is present especially in urban or rural environments. In indoor environments, diffraction can be generally ignored.

3. Scattering: Scattering occurs when the propagation path contains obstacles whose dimensions are comparable ($\lambda \approx D$) or smaller ($\lambda >> D$) than the wavelength and when the number of obstacles per unit volume is large. Rough surfaces small objects or other irregularities produce scattered waves. The nature of this phenomenon is similar to diffraction except that the waves are scattered in a greater number of directions. Scattering is the most difficult phenomenon to predict. A simple approach to account for surface roughness and calculate the reduction in the amplitude of the specular component is implemented by multiplying the value of the reflection coefficient by a roughness factor, which depends on the angle of incidence, the wavelength and the standard deviation of the surface height according to the Rayleigh criterion.

1.4.3 Effects of Multipath Propagation

Multipath propagation results in the spreading of power in delay and angle dimensions. The impact of multipath propagation on the radio signal transmission can be analyzed in both time and frequency

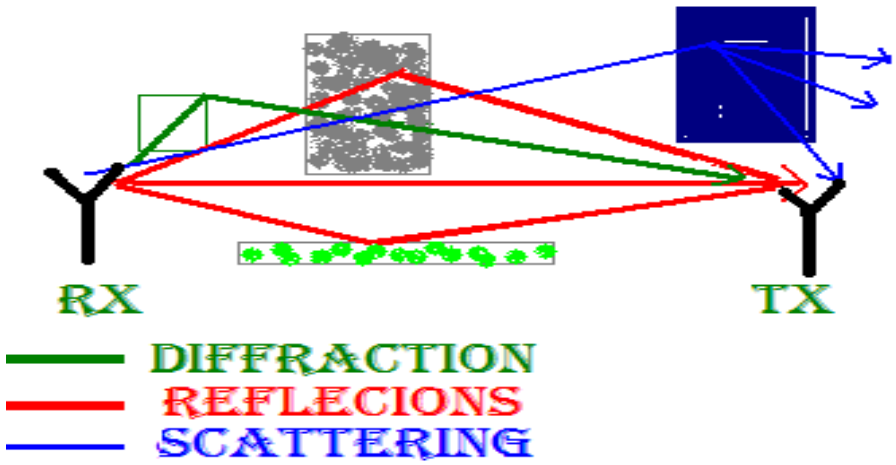

Figure 1.6: Reflections, Diffractions and Scattering schemas.

domains. For the effects observed in the time domain since multipath signals arrive at the receiver with different delays, the received symbols are spread in time. This may cause adjacent symbols to overlap. The phenomenon is called **Inter-Symbol Interference** (ISI). When the data are transmitted at a slow rate, the symbol duration is long compared to the delay spread caused by the channel, and the receiver can easily resolve the transmitted symbols. However, when the data are transmitted at a high rate, the receiver is not able to resolve the adjacent symbols, because they overlap significantly. This is how multipath propagation spreads the signal in time making high bit-rate transmission difficult to realize. Because of time-frequency duality [Bel64], it has also an effect in frequency domain called **Frequency Selectivity** (FS) of the channel. Due to multipath propagation, the channel influences the transmitted signal causing enforcement at some frequencies and suppression (deep fades) at others.

1.4.4 UWB and Capacity

One of the major advantages of the large bandwidth for UWB pulses is to improve channel capacity. Channel capacity, or data rate, is defined as the maximum amount of data that can be transmitted per second over a communications channel. For an AWGN channel the capacity is given by:

$$C = \Delta f \log_2(1 + SNR), \tag{1.4}$$

where SNR represents the signal to noise ratio.

For an UWB channel, in [dLNMDF06] the capacity using channel matrix H is given by :

$$C = \Delta f \log_2(det[1 + HH^H]) \tag{1.5}$$

where C represents the maximum channel capacity, Δf is the bandwidth, and H is the channel matrix constructed using different channel realizations. As shown in equation (1.5), channel capacity C linearly increases with bandwidth Δf.

1.4.5 UWB Receiver

UWB channel is extremely dense and have a high multipath diversity. These multipath components can increase the total signal power if they are combined coherently or decrease it if they are combined in a non coherent way. The multipath components that are not combined coherently lead to interference. In addition, this large number of resolvable multipath components associated with UWB systems increase dramatically the complexity of the receiver. One popular receiver used for UWB systems is called Rake receiver. In this receiver the energy of the signal can be collected across multipath components using different diversity combining techniques [PM96].

Rake receivers

Rake receivers combine different signal components that have propagated through the channel by different paths. This can be characterized as a type of time diversity. The combination of different signal components will increase the signal-to-noise ratio (SNR), which will improve link performance. We will present three main types of rake receivers: I-rake and A-rake, S-rake and P-rake.

1. I-rake and A-rake: The perfect (Ideal) rake receiver structure captures all of the received signal power by having a number of fingers equal to the number of multipath components. The so called ideal rake or all rake (I-rake and A-rake) is such a receiver [Sch93]. The problem with this approach is the need for an infinite number of rake branches, which also means an infinite number of correlators. Consequently, implementation of the A-rake is not possible. The performance close to the performance in AWGN channel can be met by using the maximum ratio combining (MRC).

2. S-rake: A selective rake is practical rake receiver implementation. The S-rake only uses the L_r strongest propagation paths. Information on the channel impulse response is required in order to use the S-rake. The complexity of the S-rake receiver is greatly reduced relative to the A-rake by only selecting those multipath components that have significant magnitude.

3. P-rake: The partial-rake receiver, P-rake, is a simplified approximation to the S-rake. The P-rake involves combining the L_r first propagation paths. The principle behind this approach is that the first multipath components will typically be the strongest and contain the most of the received signal power.

1.4.6 UWB Antennas

On the contrary of conventional narrowband and wide-band systems (CNWS) system analysis, antennas are a critical element in the signal flow of UWB systems. The antenna acts as a filter for the generated UWB signal, and only allows those signal components that radiate to be passed. The antenna is often approximated as a differentiator both at the transmitter and receiver. The basic effect of antennas is that they produce the derivative of the transmitted or received pulse waveform [FSJL95]. This also has the effect of extending the duration of the transmitted and received pulse. This extension of pulse duration decreases the time resolution of the system. The antenna has a greater impact in UWB than in narrower band systems because of the very large bandwidth of an UWB signal. When a very short time domain impulse is used to excite the antenna, after the antenna, the signal is no longer impulse like. Instead the pulse is spread in the time domain.

1.5 Conclusion

In this chapter, we have explored some UWB channel characteristics and properties. The first part of this chapter has dealt with UWB channel characteristics and specifications like channel bandwidth and FCC regulations. We have also presented a short view to illustrate the potentiality of UWB technology. We have shown the impact of propagation mechanisms on channel behavior. Lastly, we have described briefly two important and essential elements in UWB communication systems as the antennas and the receiver.

CHAPTER 2

UWB CHANNEL MODELING: STATE OF THE ART

2.1 Introduction

Unlike narrow and wide bandwidth communication systems, the UWB one behaves differently. Due to ultra large bandwidth of the signal, the physical propagation phenomena are different across signal band (specially upper and lower band). Since 2002, the IEEE working Group for WPAN and the channel modeling subcommittee decided to use some existing channel models such as the modified Saleh-Valenzuela one. Several proposed models are based on this approach. In this chapter, we present a summed up scope of UWB channel models published in the literature. We will also provide comments with respect to their approaches and performances. Specifically, the overview aims to allow the reader of this thesis to connect and compare the existing UWB channel models to each other. We do not include a comprehensive discussion in all areas, since such a thing is already obtainable in several well known references, e.g., [Mol, Mol05]. In this chapter we will also briefly talk about some important contributions published in the last decades before dealing with the following models bellow:

1. A modified S-V clustering channel model for the UWB indoor residential environment [CKL05];
2. A path-loss and time dispersion model for indoor UWB propagation [MASJWR06];
3. A comprehensive model for UWB propagation channels [MBC+05];
4. An UWB channel model based on theoretic information criterion [UH06];
5. An UWB channel based on entropy maximization approach [dLNMDF06];
6. AR models based UWB channel model in frequency domain [TJT02];
7. UWB channel model incorporating frequency dependence [ZAZ06].

Finally, a conclusion is given in the end of this chapter.

2.2 UWB Channel Models

The very large bandwidth of UWB channels can give rise to new effects compared to both narrowband and wide band wireless channel modeling. For example, only few multipath components overlap within each resolvable delay bin (spatial resolution is 3 cm), so that the central limit theorem is no longer applicable, and the amplitude fading statistics are no longer Rayleigh. Besides, there can be

delay bins into which no Multi–Path Components (MPC)s fall [FPM03]. Several works on indoor radio propagation measurements and modeling have been proposed so far in the literature. The main goal of this section is to present some important contributions published in the last two decades that deal with UWB channel sounding so as to focus on the main concepts that make the basis of a propagation channel. In particular, propagation/statistical models usually include the characterization of the following quantities: path loss law, shadowing, multipath delay spread, coherence bandwidth, multipath arrival times, average multipath intensity profile, received amplitude distribution of the multipath components. and so on and so forth.

2.2.1 UWB channel characterization

In this subsection we outline summary of the reported results concerning Power Delay Profile (PDP), Fading, temporal correlation, Arrival Times, and Path Loss (PL).

Power Delay Profile: The UWB measurement results of most measurement campaigns show that the PDP decreases exponentially with excess delay. Another model referred to as double exponential decay model (i.e., two exponential decays one for the clusters and the other for the rays) is introduced to characterize the PDP of UWB channels. The UWB measurements performed in a corridor also show path clustering [KP02].

Fading: The fading margin of UWB is 5 dB [GJRT02]. The effect of the bandwidth on the fading margin is investigated in [RK03]. The results show that when measurement bandwidths of 10 MHz and 1 GHz were used, the fading margins were about 30 to 40 dB and 3 dB, respectively. The measurement results reported in [KP02] show that the path fading can be modeled by a Rice distribution with Rice factor of -9 dB. The results reported in [CSW02] show that deviation of arrival energy from the mean has a Rayleigh probability density function. In [CWM01], the Gamma distribution is reported to give the best fit for the path amplitudes. In [SHA07], the Lognormal distribution gives the best fit for the path amplitudes for both LOS and NLOS cases [SHA07, CKYL05, DMB06].

Correlation: The analysis results in [CWM01] show that temporal correlation between powers does not exceed 0.2 for UWB. In [PCR+02], the spatial correlation for fixed spacing of $s = \frac{\lambda}{2}$ (i.e., s is the spacing and λ is the wavelength) at frequencies 3, 5, and 7 GHz is found to be 0.5, 0.7, and 0.85 respectively, for the LOS case.

RMS Delay Spread (RDS): The RDS seems to follow a Normal distribution. More details and information are given in [GJRT02, KD02, RPCQL03, MASJWR06].

Path Loss: Based on the work presented by Muqaibel et al. in [MASJWR06], the channel measurements and the corresponding statistical analysis indicated that, unlike narrowband signals, UWB signals are immune to multipath fading. The calculated path-loss exponent was as low as 1.27 for a narrow corridor. For LOS and NLOS scenarios the global path-loss exponents were found to be nearly 1.6 and 2.7, respectively. The calculated time dispersion parameters for the measured results indicate high concentration of power at low excess time delays.

Time of Arrival: The arrival times of the multipath components for UWB seem to follow two Poisson distribution [CKL05].

2.2.2 UWB Models for Residential and Commercial Environments

Based on the processing of two large sets of measured data, models for the UWB channel delay profile in indoor environments are presented in [GGS+05]. Measurement sets were carried out for both LOS and NLOS scenarios at center frequency of 5 GHz and two different bandwidths of 1.25

GHz and 6 GHz. For both cases, it is found that the profile for NLOS paths can be modeled as a decaying exponential times, a noise-like variation with lognormal statistics and additionally a strong component at the minimum delay for LOS setting. The simulation results of this model show that it is in agreement with key properties of the measured channels, such as the distribution of τ_{rms} delay spread. In this UWB channel model, the authors do not consider the effects of physical phenomena in the UWB channel context.

2.2.3 A Modified SV Clustering Channel Model for the UWB Indoor

C.-C. Chong et al. propose a new modified SV clustering channel model based on the measurement data collected in various types of high-rise apartments under different propagation scenarios in the UWB frequency band of $3-10$ GHz [CKL05]. A new distribution, namely, mixtures of two Poisson processes is proposed to model the ray arrival times. This new distribution fits the empirical data much better than the single Poisson process proposed in the conventional SV model.

A Modified S-V Clustering Channel Model

Based upon the apparent existence of clusters in the measurement data [CKL05], an UWB channel model which account for the clustering of MPCs is proposed here based on the conventional S-V channel model [SV87]. The clustering CIR can be expressed as follows:

$$h(t) = \sum_{l}^{L} \sum_{k}^{K} a_{l,k} \delta(t - T_l - \tau_{l,k}) \tag{2.1}$$

where L is the number of clusters, K is the number of MPCs within the $a_{k,l}$ is multipath gain coefficient of the k^{th} component in l^{th} cluster, T_l is the delay of the l^{th} cluster and $\tau_{k,l}$ is the delay of the k^{th} MPC relative to the to the l^{th} cluster arrival time.

The proposed channel model relies on two classes of parameters, notably, inter and intra-cluster parameters which characterize the cluster and MPC respectively.

The distributions of the cluster arrival times, T_l and the ray arrival times, $\tau_{k,l}$ are given by two Poisson processes. According to this model, cluster inter-arrival times and ray intra-arrival times are described by two independent exponential probability density functions (PDFs) as follows:

$$p(T_l|T_{l-1}) = \Lambda \exp[-\Lambda(T_l - T_{l-1})], \quad l > 0, \tag{2.2}$$

$$p(\tau_{k,l}|\tau_{k-1,l}) = \lambda \exp[-\lambda(\tau_{k,l} - \tau_{k-1,l})], \quad k > 0, \tag{2.3}$$

where Λ: mean cluster arrival rate and λ: mean ray arrival rate.

The measurement results show that the single Poisson process given in (2.3) doesn't fit the ray arrival times adequately. Thus, authors propose to model the ray arrival times with mixtures of two Poisson processes given by

$$p(\tau_{k,l}|\tau_{k-1,l}) = \beta\lambda_1 \exp[-\lambda_1(\tau_{k,l} - \tau_{k-1,l})] + (\beta - 1)\lambda_1 \exp[-\lambda_2(\tau_{k,l} - \tau_{k-1,l})], \quad k > 0, \tag{2.4}$$

Where β is the mixture probability, while λ_1 and λ_2 are the ray arrival rates. This new model can give a better match to the ray arrival times. Average power of a MPC at a given delay, $T_l + \tau_{k,l}$

$$\overline{a_{k,l}^2} = \overline{a_{0,0}^2} \times e^{-T_l/\Gamma} \times e^{-\tau_{l,k}/\gamma} \tag{2.5}$$

$\overline{a_{0,0}^2}$: expected value of the power of the first arriving MPC. The Γ is cluster decay factor and γ is ray decay factor.

We can conclude that the modified S-V clustering channel model for the UWB indoor residential environment one shows that: Mixture of two Poisson processes was found to give good connection to the ray arrival times when compared to the single Poisson process proposed in the original S-V model. The small-scale amplitude fading statistics can be well-modeled by either the lognormal, Nakagami or Weibull distributions. The parameters of these distributions are relatively invariant across the excess delay and they can be modeled by another Lognormal distribution, respectively [CKL05].

2.2.4 Muqaibel Model's For Indoor UWB Propagation

Based on the time-domain measurements performed using a sampling oscilloscope as receiver and a Gaussian-like pulse generator as transmitter [MASJWR06]. The observations of received signals at different points in a measurement grid confirm the absence of small-scale fading (Definition of signal quality is given in Chapter 4 , Section 4.5.2). Robustness of UWB communication systems, insofar as multipath is concerned, is manifested by small variations in signal quality at various grid locations [MASJWR06]. Also Muqaibel et al. presented a findings about the path-loss and large-scale analysis and time dispersion results. In fact the maximum value returned for path loss exponents is $n_{max} = 3.29$ with variance $\sigma = 1.91$ and the minimum value is $n_{max} = 1.61$ with $\sigma = 1.58$.

In [MASJWR06] it is argued that NLOS scenarios have n path-loss exponents greater than 2 and also have larger σ values compared with LOS scenarios. A verification of path loss exponent is also provided in this work. This shows that in general, there is close agreement between the findings obtained with directive antennas and the results obtained with omni-directional antennas. Time dispersion parameters shed some light on the temporal distribution of power relative to the first arriving components. Delay spreads restrict transmitted data rates and could limit the capacity of the system when multi-user systems are dealt with. The dispersion time of UWB pulses can be presented as the ratio of the average arrival time to the spread of the arrival time. Scatter plots analysis of UWB measured data in [MASJWR06] illustrates that there is no relationship between delay spread and transmitter-receiver (Tx-Rx) separation distance. This is in agreement with results reported in [Rap89] and [SV87] for narrowband systems. On the other hand, when considering the relation between the received energy and the delay spread, lower energy signals might seem to have larger excess delay. Nevertheless, this is because the locations where the received energy is low are usually obstructed and signals arrive at the receiver through many paths. General speaking, received power is not correlated to the excess delay parameters. Also, in [Rap89] and [SV87], scatter plots of RMS delay spread versus path-loss show no correlation.

Muqaibel et al in [MASJWR06], based on channel measurements and the corresponding statistical analysis, indicated that unlike narrowband signals, UWB signals are immune to multipath fading. The calculated path-loss exponent was as low as 1.27 for a narrow corridor. For LOS and NLOS scenarios the global path-loss exponents were found to be nearly 1.6 and 2.7, respectively. The calculated time dispersion parameters for the measured results indicate high concentration of power at low excess time delays.

2.2.5 Molisch et al. UWB channel Model for UWB Propagation Channels

Recently, Molisch et al. [MBC+05] presents a comprehensive statistical model for UWB propagation channels that is valid for a frequency range from $3 - 10$ GHz. It is based on measurements and sim-

ulations in the following environments: residential indoor, office indoor, built-up outdoor, industrial indoor, farm environments, and body area networks. The model is independent of the used antennas. It includes the frequency dependence of the path loss, as well as several generalizations of the S–V model, like mixed Poisson times of arrival and delay dependent cluster decay constants. It was accepted by the IEEE 802.15.4a working group (WG) as a standard model for evaluation of UWB system proposals. The measurements and simulations that form the basis of the model in the different environments cover different frequency ranges (from 3.1 to 10.6 GHz).

Path gain

The frequency-dependent path gain (related to wideband path gain [KL95, Ros99]) in a UWB channel is defined as:

$$G(f,d) = E\int_{f-\Delta f/2}^{f+\Delta f/2} |H(\tilde{f},d)|^2 d\tilde{f} \tag{2.6}$$

where $H(f,d)$ is the transfer function from TX antenna connector to RX antenna connector, Δf is chosen small enough so that diffraction coefficients, dielectric constants, etc., can be considered constant within that bandwidth, d is the distance between transmitter and receiver, and the expectation E is taken over the small-scale and large-scale fading. The total path gain shows random variations (due to shadowing), which are log-normally distributed:

$$G = G_0 - 10n\log_{10}(\frac{d}{d_0}) + S \tag{2.7}$$

where S is a Gaussian-distributed random variable with zero mean and standard deviation σ_S.

Power Delay Profile (PDP)

The impulse response (in complex baseband) of the S-V model is given in general as [SV87]

$$h_{discr}(t) = \sum_{l}^{L}\sum_{k}^{K} a_{l,k}e^{j\phi_{k,l}}\delta(t - T_l - \tau_{l,k}) \tag{2.8}$$

where $a_{k,l}$ is the tap weight of the k^{th} component in the l^{th} cluster, T_l is the delay of the l^{th} cluster, $\tau_{k,l}$ is the delay of the k^{th} MPC relative to the l^{th} cluster arrival time T_l. The phases $\tau_{k,l}$ are uniformly distributed, i.e., for a bandpass system, the phase is taken as a uniformly distributed random variable from the range $[0, 2\pi]$. Deviating from the standard S-V model, the number of clusters L is modeled as Poisson-distributed with probability density function (pdf)

$$pdf_L(L) = \frac{\bar{L}^L \exp(-\bar{L})}{L!} \tag{2.9}$$

The distributions of the cluster arrival times are given by a Poisson processes (see section 2.2.3).

The PDP (mean power of the different paths) is exponential within each cluster

$$E\{|a_k, l|^2\} \propto \Omega_l \exp(-\tau_{k,l}/\gamma_l) \tag{2.10}$$

where Ω_l is the integrated energy of the l^th cluster, and γ_l is the intra-cluster decay time constant.

The cluster decay rates are found to depend linearly on the arrival time of the cluster

$$\gamma_l \propto k_\gamma T_l + \gamma_0 \tag{2.11}$$

For the NLOS case of some environments (office and industrial), the shape of the power delay profile can be different, namely (on a log-linear scale)

$$E\{|a_k, l|^2\} \propto (1 - \chi . \exp(\tau_{k,l}/\gamma_{rise})) . \exp(\tau_{k,l}/\gamma_1) \tag{2.12}$$

Here, the parameter χ describes the attenuation of the first component, the parameter γ_{rise} determines how fast the PDP increases to its local maximum, and γ_l determines the decay at later times.

Small-Scale Fading

The distribution of the small-scale amplitudes is modeled by Nakagami. The m Nakagami parameter is modeled as a lognormally distributed random variable, whose logarithm has a mean m_0 and standard deviation σ_{m_0}. For the first component of each cluster, the Nakagami factor is modeled differently. It is assumed to be deterministic and independent of delay. The parameters of the model are extracted by fitting measurement data to the model described previously. The model for residential environments was extracted based on measurements that cover a range from $7 - 20$ m, up to 10 GHz [CKL05]. For office environments, the model was based on measurements that cover a range from $3 - 28$ m, $2 - 8$ GHz [ea04]. For outdoor, the measurements cover a range from $5 - 17$ m, $3 - 6$GHz [ea04].

The derivation of the model and a description of the simulations (for the farm area) can be found in [ea05]. The model for industrial environments in [Stu96] was extracted based on measurements that cover a frequency range from $3 - 10$ GHz and a distance range from $2 - 8$ m, though the path loss also relies on values from the literature [Rap89]. The tables in [Mol05] summarize the parameters described in this paragraph. Simulations and measurements of the radio channel around the human body indicate that some modifications are necessary to accurately model a body area network (BAN) scenario. Due to the extreme close range and the fact that the antennas are worn on the body, the BAN channel model has different path loss, amplitude distribution, clustering, and inter-arrival time characteristics compared with the other application scenarios within the 802.15.4a context. In the BAN context the path gain can be calculated according to the following formula:

$$G_{dB} = -\gamma(d - d_0) + G_{0,dB} \tag{2.13}$$

The reported values of γ, d_0 and G_0 are 107.8 dB/m ,0.1 m and -35.5 dB/m.

2.2.6 UWB Channel Modeling based on Information-Theoretic Criteria

The main objective of the model selection procedure is to choose the distribution that reducers the discrepancy among all members of the candidate set [DMAS86]. The model selection methodology can be used to characterize multivariate distributions in practice; however, this is hardly feasible because of the large bandwidth and the resulting large number of taps.

In [UH06] Schuster and Bolcskei used Akaike's Information-Theoretic Criteria to determine suitable distributions for UWB channel impulse response taps. Denote the unknown cumulative distribution function (CDF) of the operating model by F, and the set of all CDFs by $\mathcal{M}$. A parametric candidate family $\mathcal{G}^j = \{G^j_{\Theta^j} | \Theta^j \in \mathcal{T}^j\}$ is the subset of $\mathcal{M}$, with individual CDFs G^j_Θ. parameterized

by the U -dimensional vector $\Theta^j \in \mathcal{T}$, with $\mathcal{T}^j \subset \mathrm{R}^U$. In model selection using AIC, The AIC is an approximately unbiased estimator of the expected Kullback-Liebler (KL) distance

$$AIC_j = -2\sum_{n=1}^{N} \log g^j_{\hat{\Theta}}(x_n) + 2U \tag{2.14}$$

with $\hat{\Theta}^j$=arg max$_{\Theta^j \in \mathcal{T}^j} \frac{1}{N} \sum_{n=1}^{N} \log g^j_{\hat{\Theta}}(x_n)$, the Akaike weights are given by

$$\omega_j = \frac{e^{-\frac{1}{2}D_j}}{\sum_{i=1}^{J} e^{-\frac{1}{2}D_i}} \tag{2.15}$$

with $D_j = AIC_j$ – min AIC_i and $i \in J$.

Results

In [UH06] AIC is applied to measurement data to evaluate the different tap amplitude distributions put forward in the UWB literature. The candidate set C, hence, consists of the single-parameter $(U = 1)$ Rayleigh family and the two parameter $(U = 2)$ Rice, Nakagami, lognormal, and Weibull families. The Rice, Nakagami, and Weibull families contain the Rayleigh one as a special case. Rayleigh, Rice, and Nakagami amplitude distributions can be justified from physical principles [VS99]. The Weibull [KD03] and lognormal [BD91], [CWM02a] distributions seem to lack physical support for small-scale fading [VS99].

In [UH06] the analysis demonstrates that even for bandwidths of up to 3 GHz Rayleigh and Rice distributions provide a good fit, although the differences of the Akaike weights for the Nakagami and Weibull distributions are often small, especially in MCI. Consequently, the data do not provide enough evidence to unequivocally select a single distribution. However, the empirical support for Rayleigh and Rice fading, combined with the mathematical tractability of these distributions, leads us to advocate their use. Results about DoF scaling behavior for different captured energy percentage as a function of W is presented. The scaling is approximately linear in all cases. With respect to taps correlation, on average, the correlation is small, but some taps show strong correlation. In the NLOS setting, the correlation is somewhat higher in general.

On the basis of indoor UWB channel measurements in the frequency band from 2 GHz to 5 GHz, the AIC support Raleigh respectively Ricean tap amplitude distributions is founded. This is somewhat surprising, as it is often argued that for large bandwidths the number of partial waves contributing to each tap is not high enough to justify the complex Gaussian assumption by the central limit theorem. The number of significant eigenvalues of the channel impulse response covariance matrix scales approximately linearly with bandwidth. Consequently, the diversity order of the channel shows the same scaling behavior, a common assumption in information-theoretic studies of UWB systems. Nevertheless, it is found that the individual channel taps seems to be correlation between, thus invalidating the discrete-time assumption US.

2.2.7 A Maximum Entropy Approach to UWB Channel Modeling

Recently a new UWB channel model is presented based on the maximum entropy approach [dLNMDF06], the main objective of the model is to delve into how channel uncertainty scales with bandwidth in UWB systems. Equivalently, the number of parameters necessary to predict the wideband channel is determined.

Maximum Entropy Modeling (MEM)

The wireless channel suffers from constructive/destructive interference signaling and therefore yields a randomized channel for which one has to attribute a joint probability distribution for the channel frequency response. The basic idea in the channel model proposed in [dLNMDF06] is based on the response of follow question:

Question: Knowing only certain information related to channel (power, measurements), how to translate that information into a model for the channel?

Response: This question can be answered in the light of the Bayesian probability theory [Jay03] and the principle of maximum entropy.

Entropy Maximization Results

On the basis of the Entropy Maximization it is found that the entropy is a useful measure and its slope decrease characterizes how information scales with bandwidth. The results show that with increasing bandwidth, the model is able to capture the small channel variations. In particular, in wideband schemes, they have shown that it is possible to reproduce the channel frequency behavior with a limited number of AR model coefficients.

2.2.8 Frequency Domain Models

Turin and Taparugssanagorn Models

For the UWB channel the frequency model is given by Turin et al. [TJT02] based on an autoregressive (AR) model. Using AR modeling techniques the parameters of the channel model can be determined from the measured frequency responses.

The AR model relies upon on the previous outputs of the system. The transfer function representation of such a model can be given by:

$$H(z) = \frac{Y(z)}{X(z)} = \frac{b_0}{1 - a_1 z^{-1} - a_2 z^{-2} ...} \tag{2.16}$$

where $X(z)$ and $Y(z)$ denote the z-transforms of the input and output of the AR system respectively. With the assumption of an AR process and non stationary channel, the frequency response at each location is a realization of an autoregressive process of order p given by the equation:

$$H(f_n, x) = W(f_n) - \sum_{i=1}^{i=p} a_i H(f_{n-i}, x) \tag{2.17}$$

where $H(f_n, x)$ is the nth sample of the complex frequency domain measurement at location x and $W(f_n)$ is a complex white noise process. The parameters of the model are the complex constants a_i and p is the order of the process. The z-transformation of (2.18) is given by:

$$G(z) = \frac{1}{1 + \sum_{i=1}^{p} a_i z^{-1}} = \prod_{i=1}^{p} \frac{1}{(1 + p_i z^{-1})} \tag{2.18}$$

where p_i is the ith pole of the transfer function $H(z)$. The coefficients $a_1, a_2, ..., a_p$, σ^2 are obtained by solving the Yule-Walker equations

$$R(0) = -\sum_{k=1}^{p} a_k R(-k) + \sigma^2 \tag{2.19}$$

and

$$R(l) = -\sum_{k=1}^{p} a_k R(l-k), \quad l = 1, ..., N. \tag{2.20}$$

The delay is calculated as $\tau_i = \frac{\arg(p_i)}{2\pi f_s}$ where f_s is the stepping frequency. The order of the process is estimated using AIC and MDL criterion [THK05].

Under the assumption that the UWB channel is non stationary process, an AR models having time-varying coefficients is needed [THK05]. An autoregressive (AR) model with time-varying coefficients is presented in [Gre83]. The AR time-varying model is given by:

$$H(f_n, x) = W(f_n) - \sum_{i=1}^{i=p} a_i(n) H(f_{n-i}, x) \tag{2.21}$$

where $a_i(n)$ is the time function representing the ith time-varying AR coefficient. In [Gre83] the $a_i(n)$ are represented by a family of M time-varying basis functions as follows:

$$a_i(n) = \sum_{j=0}^{m} a_{ij} g_j(n), \tag{2.22}$$

subsisting $a_i(n)$ by its expression in (2.21), we have found:

$$H(f_n, x) = W(f_n) - \sum_{i=1}^{i=p} \sum_{j=0}^{m} a_{ij} g_j(n) H(f_{n-i}, x). \tag{2.23}$$

In vectorial representation, (2.23) becomes:

$$H(f_n, x) + H(f_{n-1}, x) A = W(f_n). \tag{2.24}$$

where $A = [H(f_{n-1})g_0(n), ..., H(f_{n-1})g_m(n), ..., H(f_{n-p})g_0(n), ..., H(f_{n-p})g_0(n)]$ and $A = [a_{10}, ..., a_{1m}, ..., a_{p0}, ..., a_{pm}]$.

It is reported that the goodness of fit achieved using this technique is dependent on the subspace spanned by the chosen basis functions. In this UWB time-varying channel AR model, Legendre function are used to simulate the time-varying AR coefficients. The application of AIC and MDL criterion on measured data depicted that a fifth order process is sufficient to represent the statistic of the channel model. The Table (2.1) summarized the AR model time-varying parameters values. The simulation confirms that the regenerated models are close statistical fits to the real data as well as the time-varying AR model is more accurate than the classical time-invariant AR model due to its less variance. Last result about the AR model that experimenting with higher order models concerns the fact that between the 5 poles found, there are two significant poles which can be interpreted as two significant clusters of multipath in the power delay profile. Based on the results obtained using AR approach to model the UWB channel we can conclude that the AR models are simpler than the time domain models due to their small number of parameters.

Table 2.1: Poles of AR model values

Parameters	p_1	p_2	p_3	p_4	p_5
Magnitude of the largest pole	0.8184	0.8004	around of .5	around of .5	around of .5
Delay of the largest pole	0.04	0.07	–	–	–

Zhang Model

Motivated by the similarities between wireless channel modeling and radar scattering analysis, Zhang et al. proposed a novel exponential UWB channel model incorporating frequency dependence [ZAZ06]. Electromagnetic diffraction mechanism and geometric diffraction mechanism are based on the new exponential model. The impulse response of the modified multipath fading channel in the frequency domain can be described as:

$$H(w) = \sum_{l=0}^{L-1} a_l (\frac{w}{w_0})^{\alpha_l} e^{jw\tau_l} \tag{2.25}$$

where L is the number of multipath signals. a_l and τ_l are respectively random complex amplitude and time delay of each ray. α_l is the frequency dependency factor [ZAZ06]. From this formula, it is obvious that for narrowband systems, frequency dependence can be neglected, as w is close to w_0 and the frequency dependence factor is always 1. The novel spatial-frequency UWB channel model is given by:

$$H(w, x) = \sum_{m=-M}^{M} \gamma_m(w) J_m(k|x) e^{jm(\phi_x \phi + \frac{\pi}{2})} \tag{2.26}$$

where $J_m(.)$ is the order mth first kind of Bessel function and $\gamma_m(w)$ is expressed as

$$\gamma_m(w) = \int_{-\pi}^{\pi} A(w, \phi) e^{-jm\phi} \tag{2.27}$$

where $A(w, \phi)$ the gain of the signal arriving from an angle ϕ measured at the origin. Also, $A(w, \phi)$ could be viewed as the angular frequency dependent fading gain or angular frequency response. It was concluded that the $\gamma_m(w)$ is a complex Gaussian distribution.

The results concerning measured channel bandwidth from 2 to 8 GHz and novel approach based channel reconstruction performed with 3-5 GHz bandwidth, show that the traditional Turin model provides larger deviation between real and simulated impulse response (24.79%) as signal bandwidth increases to 2 GHz, while the exponential UWB channel model with frequency dependence produces much more accurate fit. The novel model is more stable and can also be used to efficiently estimate frequency dependence of each path.

2.3 Conclusion

In this Chapter we have explored some channel models in both time and frequency domains. All proposed UWB channel models are based on measurements and statistical analysis, except those proposed by Schuster et al. [UH06] and the model which is presented by Menouni-Hayar et al.

[dLNMDF06]. These two models are based on channel measurement analysis and information theoretic criteria. The best performances have been proved in all models. We have noted that the presented models do not take into account the physical propagation phenomena except the one presented by Zhang [ZAZ06] which considers the frequency dependence. The proposed models in frequency domain are based on measurements. The AR models are based on Turin and Taparugssanagorn Models. This later is more in agreement with measurements because it takes into consideration the model parameters variation in time domain. We have concluded that those models can reconstruct the channel using a limited number of parameters. Zhang's model in frequency domain is based on the selectromagnetic and geometric diffraction mechanisms. This is an exponential UWB channel model with frequency dependence which provides much more accurate fit.

CHAPTER

3

UWB CHANNEL MEASUREMENTS

3.1 Introduction

The development of channel models for UWB communication systems requires extensive data on UWB signal propagation. The well known experimental and simulation techniques can be used to investigate the propagation of UWB signals in indoor environments. In this thesis the experimental one is used. The advantage of experimental method is that all system and channel parameters affecting the propagation of UWB signals are accounted for without preassumptions. But this method is usually expensive, time consuming, and limited by the characteristics of available equipment. On the other hand, simulation techniques are free from the limitations of experimental approaches but they require more computational time. They also need sophisticated computational resources to carried out simulations.

In CNWS, the information signal modulates a very high frequency sinusoidal carrier; thus, along each propagation path the signal suffers very little distortion because the system elements such as antennas, reflecting objects, diffracting objects in the channel, and so on, have essentially constant electromagnetic properties over the narrow bandwidth of the radiated signal. The only signal degradation is caused by multipath components. On the other hand, in UWB systems, the information signal may suffer significant distortion due to the transmitting/receiving antennas not meeting the necessary bandwidth requirements, and also due to the dispersive behavior of building materials in the propagation channel. Of course, multipath components are also present in UWB channels. But, unlike narrowband signals, UWB signals do not suffer fading due to the destructive interference of multipath components, because the combination of a large number of multipaths results to a more deterministic variable than the combination of a few number of paths. Thus, the behavior of UWB channel in frequency domain is almost similar at all frequencies and no frequency selectivity is observed.

In this chapter, both channel measurement methods in time domain (TD) and in frequency domain (FD) are addressed briefly. Section 3.2 presents frequency domain and time domain measurement techniques. Important axes like advantages and weakness of each technique are presented. The signal analysis using different techniques is illustrated. In addition, an overview of reported UWB measurements in frequency and time domains is presented. The UWB channel propagation measurements conducted at Eurecom institute are detailed in Section 3.3 and Section 3.9.

3.2 UWB Channel Measurement Methods

A basic step required for a communication system simulation is to get precise models of all the elements involved in the system. This includes, of course, the radio channel, as the physical mean of transport for the wireless signal. The essential method to follow in order to complete this task, begins with the knowledge of the radio channel based on a characterization process. This initial process can be performed by several channel measurement campaigns in different environments and covering all the frequency range of interest.

In the literature, two possible domains for performing the channel measurement to characterize UWB radio channel are available. First, the channel can be measured in the FD using a frequency sweeping technique. With FD sounders, a wide frequency band is swept using a set of narrow-band signals, and the channel frequency response is recorded using a Vector Network Analyzer (VNA). This corresponds to $S21$-parameter (i.e, complex transfer function) measurement set-up, where the device under test (DUT) is the radio channel. Second, the channel can be sounded in the TD using channel sounders that are based on impulse transmission or direct sequence spread spectrum signalling.

With impulse based TD sounders, a short pulse is sent to excite the channel and the channel impulse response is measured using a Digital Sampling Oscilloscope (DSO). The corresponding train of impulses can also be generated using a conventional direct sequence spread spectrum (DSSS) based on measurement system with a correlation receiver. The properties of the autocorrelation function (ACF) of the spreading code used as an overlay signal is the basis of the performance of the DSSS sounder . The weakness of using the DSSS technique is that it needs very high chip rates to achieve bandwidths required for UWB.

In this chapter, the frequency and time domain measurement concepts are presented. Theoretically, both techniques lead to the same result if there is a static measurement environment and an unlimited bandwidth [Com].

3.2.1 Channels Measurement in Frequency Domain

With frequency domain sounders, the RF signal is generated, transmitted and received using a VNA which makes the measurement set-up quite simple. The sounding signal is a set of narrow-band sinusoids that are swept across the band of interest. The frequency domain approach makes it possible to use wideband antennas, instead of special impulse radiating antennas. As discussed in chapter 1 (subsection UWB antennas [FSJL95]) UWB antennas have restrictions, for example, with ringing leading to pulse shape distortion. When the FD sounder approach is used, the channel state during the soundings must be static to maintain the channel conditions during the sweep. The maximum sweep time is limited by the channel coherence time. If the sweep time is longer than the channel coherence time, the channel may change during the sweep. For fast changing channels, other sounding techniques are needed. The performance of the frequency domain sounder is also limited by the maximum channel delay. The upper bound for the detectable delay τ_{max} can be defined by the number of frequency points used per sweep and by the bandwidth B_f (frequency span to be swept). The τ_{max} is given by

$$\tau_{max} = \frac{N_{tons} - 1}{B_f} \tag{3.1}$$

and the temporal resolution is given by

$$\delta t = \frac{N_{tons}}{N_{tons} - 1B_f} \tag{3.2}$$

where N_{tons} is the number of frequency tones.

Another possible source of error in the measurement process is the frequency shift caused by the propagation delay when long cables are used, or when the sweep time of the sounding signal is long [OI04]. In frequency-sweep mode, the sounding signal is rapidly swept across the totality of band of interest. For a transmitter and receiver that are in lock step sweeping across the frequency band of interest, very long propagation delays can cause the receiver to take samples at a frequency that is higher than the received frequency. This frequency shift Δf is a function of the propagation time t_{pro}, the frequency span B_f and the sweep time t_{sweep} as

$$\Delta f = t_{pro}(\frac{B_f}{t_{sweep}}) \tag{3.3}$$

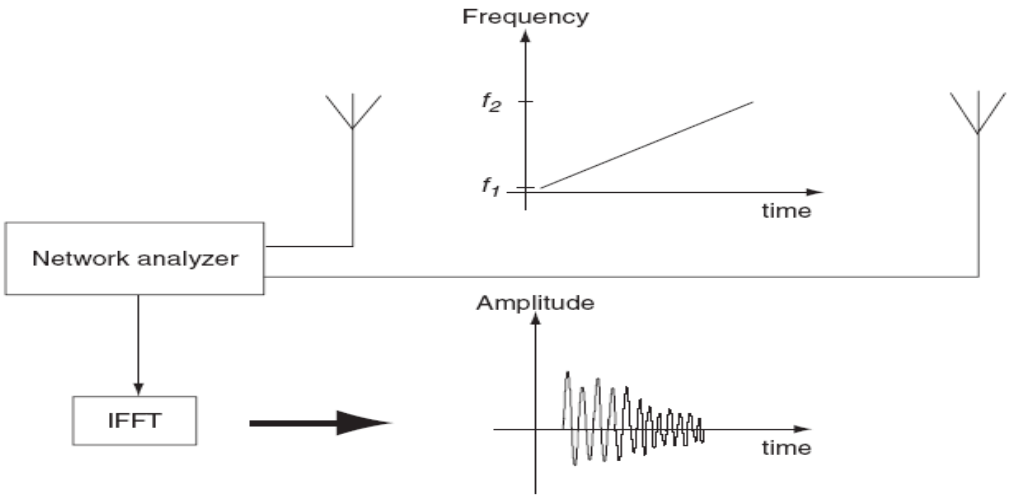

Figure 3.1: Frequency domain measurement.

In general, Δf has to be smaller than the analyzer Intermediate Frequency[1] IF bandwidth to obtain reliable results. The idea used in FD measurements technique is presented in Figure (3.1). This technique of measurement is frequently used because it presents several advantages [GSCea00, OE01, GJRT02, CP02, KD02, HHP02b, Pam02, GGAK03, BDSJea03, DNHea03, AA03, CTS04, Sch04, BWXea04, KWAea04a, KWAea04b, JHH04, CKL04, Dur04, HTK05, SHKD04].

After the channel frequency response has been measured, the time domain representation (Impulse Response) can be achieved by Inverse Fast Fourier Transform (IFFT).

[1] An IF is a frequency to which a carrier frequency is shifted as an intermediate step in transmission or reception. It is the beat frequency between the signal and the local oscillator in a radio detection system.

Windowing

The windowing technique is very used in traditional wide and narrowband channel model approaches, in order to appreciate the main transitions of the power delay profile and to avoid the powerful side lobes caused by the sudden transitions in a frequency domain measurement at the start and stop frequencies, which provoked overshoot and ringing in a time domain response. The window feature is helpful in lessening the abruptness of the frequency domain transitions, and the direct way to do it is just by multiplying the $H(f, d)$ by a Hamming, Hanning, Blackman, Bartlett ... window, and then perform the IFFT process. However, this approach is valid in the power delay profile channel model approach, where only the powerful transitions from multipath have to be taken in consideration. In an accurate characterization of the channel IR, the effect of including a processing window, makes the signal processing to become dirty [JK03]. The reader can be find a complete explication of the windowing process in [JK03].

Signal Analysis Using IFFT

The signal measured using a VNA is a frequency response of the channel. The inverse Fourier Transform is used to transform the measured data from frequency domain to time domain. The IFFT is usually directly applied to the measured data vector. This processing is possible since the receiver has a down-conversion stage with a mixer device. This method is referred to as the complex baseband IFFT, and is sufficient for modeling narrow band and wideband systems. There are two common techniques for converting the signal to the time domain, which both lead to approximately the same results. The first approach is based on Hermitian signal processing, which results in a better pulse shape. The second one is the conjugate approach. It is reported in the literature that the conjugate approach is an easier and more efficient way of obtaining approximately the same pulse shape accuracy. These two approaches are introduced in the following sections.

Hermitian Signal Processing

Using Hermitian processing, the pass-band signal is obtained with zero padding from the lowest frequency down to DC (direct current), taking the conjugate of the signal, and reflecting it to the negative frequencies. The result is then transformed to the time domain using IFFT. The signal spectrum is now symmetric around DC. The resulting doubled-sided spectrum corresponds to a real signal. The time resolution of the received signal is more than twice that achieved using the baseband approach. This improvement in accuracy is important, since one purpose in UWB channel modeling is to separate accurately the different signals paths.

Conjugate Approach

The conjugate method involves the conjugate reflection of the pass-band signal without zero padding. Using only the left side of the spectrum, the signal is converted using the IFFT with the same window size as the Hermitian method. The conjugate result is very likely to be the same as the Hermitian result with zero padding. However, the conjugate method is more efficient in terms of data processing complexity, since the matrix calculations in the post-processing stage become very easier to manipulate due to the smaller memory requirements.

Calibration and Verification

The VNA technique, like all measurement techniques, requires calibration with the same cables, adapters and other components that will be used for the measurements, before the soundings. An enhanced response calibration is required to be able to determine both the magnitude and phase of the transmitted signal [A.99]. In the case of channel measurement using amplifiers, these must be excluded from calibration because they are isolated in the reverse direction. The amplifiers frequency response can be measured independently and their effects can be taken into account in the data post-processing. Long cables and adapters connected to the ports of the analyzer cause a frequency dependent variation in the sounding signal. The deviation is directly proportional to the quality of the used equipments. This variation can, however, be compensated in the calibration procedure. The calibration process moves the time reference points from the analyzer ports to the calibration points at the ends of the cables. When the time references are at the cable ends (at the antenna connectors), the resulting delay profiles only includes the propagation delays that result from the radio channel. Due to their dimensions, delays due to the antennas themselves are insignificant.

A verification of this calibration's impact and their advantages is done by Hovinen et al. [HHP02a]. The performance of the measurement system was verified in a corridor where major delays could be readily calculated from the room geometry [HHP02a].

3.2.2 Channel Measurements in Time Domain

As discussed in Section (3.2.1), the frequency domain channel sounder excludes the measurements of the non-stationary channel. However, movement can be supported to a certain extent if the soundings are made in time domain. The following section introduces time domain sounding systems that can be utilized for UWB channel.

Impulse Measurement

One technique to realize time-domain UWB radio channel measurements is to use very short impulses. The receiver in this case is a Digital Sampling Oscilloscope (DSO). The bandwidth of the sounder depends on the pulse shape and the pulse width used. By modifying the pulse width, the spectral allocation can also be changed. Yet, the simpler the pulse shape, the easier it is to perform the deconvolution during the post-processing, where the channel impulse response is calculated by removing the transmitted pulse waveform from the results. The most exact channel model can be generated if the pulse waveforms used in the sounding correspond to the waveforms of the application. The topology for the time domain measurements is presented in Figure 3.2 [OI04]. The impulse-based measurement system requires an additional antenna to be used for triggering purposes. The sounding distance is still limited due to the probing antenna, which is close to the TX antenna needing to be connected to the DSO. However, the long cable is only needed to transfer the triggering pulse for the sounding pulse, so the high quality (e.g., expensive) cable is not needed. In the modified version, the triggering pulse can also be sent via radio link.

3.2.3 Deconvolution

Channels can be characterized by their transfer function in the frequency domain or by their impulse response in the time domain. If the measurements under investigation were done in the time domain, then a deconvolution process is needed. Deconvolution of the time-domain waveforms can be used to

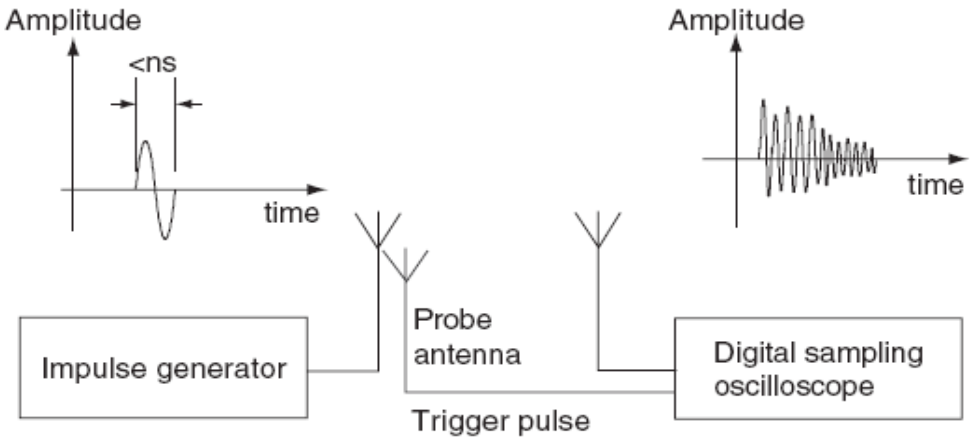

Figure 3.2: Time domain measurement.

determine the impulse response of a linear time-invariant system. In the case that the indoor channel is assumed to be time-invariant if the transmitter and the receiver are static and no motions take place in the channel.

If $h(t)$ is the impulse response of such a channel whose input is $x(t)$, then the output $y(t)$ is given by the convolution integral

$$y(t) = \int_{-\infty}^{+\infty} x(\tau)h(t-\tau)d\tau \tag{3.4}$$

where $*$ denotes the convolution operation. In the frequency domain, convolution transforms into multiplication; that is,

$$Y(jw) = X(jw)H(jw) \tag{3.5}$$

where $Y(jw)$, $X(jw)$ and $H(jw)$ are the frequency-domain representations of $y(t)$, $x(t)$, and $h(t)$, respectively. The process of obtaining $h(t)$ knowing both $x(t)$ and $y(t)$ is called deconvolution. Ideally, deconvolution can also be performed in the frequency domain using the Fourier transform. Thus, from (3.5).

$$H(jw) = \frac{Y(jw)}{X(jw)} \tag{3.6}$$

Due to measurement and signal processing limitations, simple division will result in noise-like error around the zeros of $X(jw)$. Filtering should be used to improve the estimation of the impulse response. A filter that demonstrated quality performance is given by the form [Ria86].

$$H(jw) = F(\lambda, jw)\frac{Y(jw)}{X(jw)}, \tag{3.7}$$

where

$$F(\lambda, jw) = \frac{1}{1+\frac{\lambda}{X(jw)^2}} \tag{3.8}$$

Though this technique is widely used, the assumption that the received pulses through different paths have the same waveform is not justified. This assumption requires that both the transmitter and the receiver antennas have spherical patterns at all frequencies [AMR02].

3.2.4 Overview reported UWB Measurement Campaigns

Many of measurement campaigns and channel modeling efforts have been performed to characterize the UWB channel. Several researchers have performed frequency domain measurements using vector network analyzers. Moreover, a few time domain, direct pulse measurement systems have been used for UWB channel sounding. We have found that the most proposed UWB channel models are extensions of wideband channel models. The TABLE 3.1 presents some UWB channel measurements have been performed using the tow channel methods measurement described above.

Table 3.1: Overview of reported UWB measurements in frequency and time domains

researchers	measurement system	frequency range	environment	Parameters
USC/TDC	DSO: 48.82 ps	BW = 1.3 GHz	outdoor (forest)	τ_m, τ_{rms}, PL
Univ of Oulu [HHP02b]	VNA	2–8 GHz	indoor (university)	Special[2]
TDC [Yan02][PB02]	CS : 3.052ps	1.25-2.75 GHz	indoor	494 PDPs
Intel [PCRH02] [Foe02]	DSO and VNA	2-8 GHz	indoor	2 Ants Rx
IMST [KP02]	VNA	1-11 GHz	Indoor	150x30 1cm
CEA-LETI [KD03]	VNA	2-6 GHz	Indoor	Up to 10 m
AT&T Labs [GJR+04]	VNA	4.3755.625 GHz	Indoor	300,000 PDPs

3.3 UWB Channel Measurement campaigns at Eurecom Institute

3.3.1 Equipment and Measurement Setup

Vector Network Analyzer

The measurement used in this study is a wideband vector network analyzer (VNA) which allows complex transfer function (e.g. S_{21}) parameter measurements in the frequency range extending from 10 MHz to 20 GHz. This instrument has low inherent noise <-110 dBm (measurement bandwidth 10 Hz) and high measurement speed <0.5 ms/point. With a maximum number of frequency tones equal to 2001 for scanned bandwidth of 2 GHz, the measurement characteristics are as follows: Maximum delay Multipath signals with absolute delays up to τ_{max} may be recorded, and the sampling rate corresponds to 1 MHz.

The Antennas

The antennas employed in this study are omnidirectional and are placed in the vertical plane. The antennas are not perfectly matched across the entire band. Omnidirectional antennas radiate equal

amounts of power in all directions. Also known as isotropic antennas, they have equal gain in all directions. The Electrical Specifications of these antennas are [www]:

- Frequency Range: $3.1 - 10.0$ GHz.
- Gain: 4.4 dBi peak at 4.5 GHz.
- VSWR[3] $< 2.0 : 1 :$ across $3.6 - 9.1$ GHz.
- Polarization: Linear.
- Radiation Pattern: Azimuth Omni-directional.
- Feed Impedance: $50\,\Omega$ (Ohms) Unbalanced.

The Mechanical Specification [www]:

- Antenna Element: $0.54 \times 0.63 \times 0.12$ in $13.6 \times 16.0 \times 3.0$ mm
- Assembly PCB: $1.03 \times 0.73 \times .04$ in $26.2 \times 18.5 \times 1.0$ mm
- Area of PCB that is Ground: 0.48×0.73 in 12.2×18.5 mm
- Antenna Element Weight: 0.5 g

The antennas presents a VSWR varying from 2 to 5 for example an efficiency about 82% at 5.2 GHz as shown in figure 3.4.

Figure on 3.3 shows some general characteristics of the used antennas. These characteristics can influence the channel impulse response in frequency domain (or in time domain). The Figure 3.4 shows the $S21$ response of the UWB antenna used on the channel measurements campaigns. The $S21$ presents a flat response over frequency range of interest, this is a very important characteristic of UWB antenna.

Cables

A long cable is connected to the input (receiver port of VNA) and the receiving antenna Figure 3.5. The cable is an **Atem**[4] coaxial cable (model number T303) with characteristic impedance of $50\ \Omega$ (ohm). The Low loss cable is -1.8 dBm at 5 Ghz and -0.8 dBm at 2 GHz. As we work on the frequency domain, the cable frequency characteristics are: the start frequency is $0.040000 GHz, stop frequency is$

3.3.2 Measurement Specifications and Strategy

Measurement Specifications

The VNA records the variation (amplitude and phase) of N tones across the frequency range. These complex data are acquired remotely using the RSIB protocol (PC's serial interface) over an Ethernet network and off line signal processing is done using MATLAB tool. The measurement system is shown in Figure 3.5. The frequency range corresponds to the start and stop frequencies of the sweep

[3] Voltage Standing Wave Ratio.
[4] atelier of transmission électromagnétique

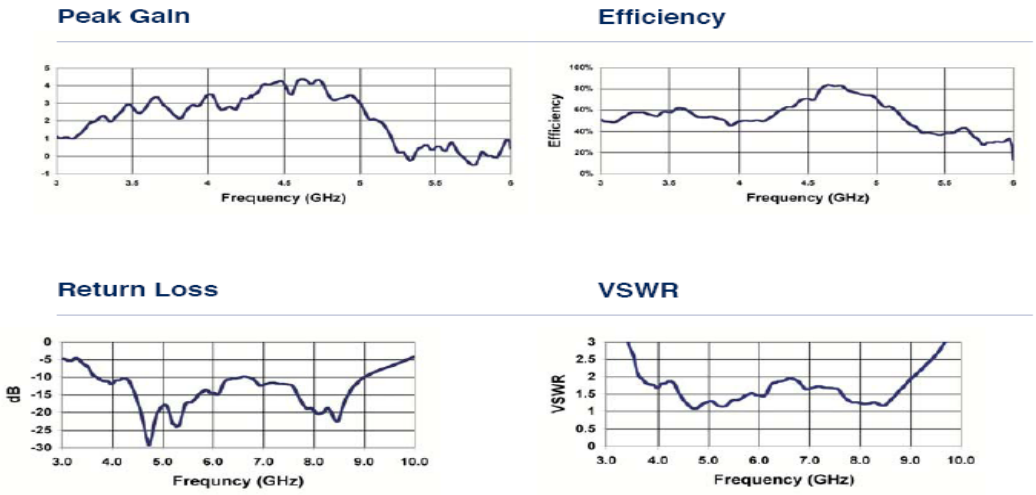

Figure 3.3: Antennas characteristics in frequency domain

cycle programmed in the VNA. The number of samples is the number of tones of the measured vector with frequency range from 3 to 9 GHz, Frequency center $F_c = 6$ GHz, $N_{tons} = 3 \times 2001$, giving a frequency resolution $\Delta f = 1$ MHz. The corresponding time domain resolution is T=167 ps. It is obtained by concatenation of measurements from three sub-bands ($3-5$ GHz, $5-7$ GHz and $7-9$ GHz).

The use of non active elements in the measurement configuration made the calibration operation necessary in order to avoid non desired factors that could affect the collected data. Following the VNA's manual recommendations, the calibration response type was selected , the cables and the connectors were included in this calibration. As we have the channel transfer function $H(f)$ in the frequency domain we use the Inverse Fast Fourier Transform to obtain an approximation of the channel impulse response (CIR) $h(t)$.

Measurement Strategy

Measurements are performed at spatially different locations under both LOS and NLOS scenarios. The experiment area is set by fixing the transmitting antenna on a mast at 1 m above the ground on horizontal linear grid (20 cm) close to VNA and moving the receiver antenna to different locations on horizontal linear grid (50 cm) in 1 cm steps. The height of receiver antenna was also 1 m above the ground Figure 3.5. This configuration targets peer-to-peer applications. Among all positions, we considered both LOS and NLOS configurations. Measurements were carried out at Eurecom's Mobile Communication Laboratory, which is a typical laboratory environment (radio frequency equipment, computers, tables, chairs, metallic cupboard, glass windows,...) with plenty of reflective and diffractive objects, as shown in Figures 3.7 and 3.8. For the NLOS case, a metallic plate is positioned between the transmitter and the receiver. We have recorded a large measurements database of 4000 channel frequency responses corresponding to different scenarios with a transmitter-to-receiver distance varying from 1 meter to 14 meters.

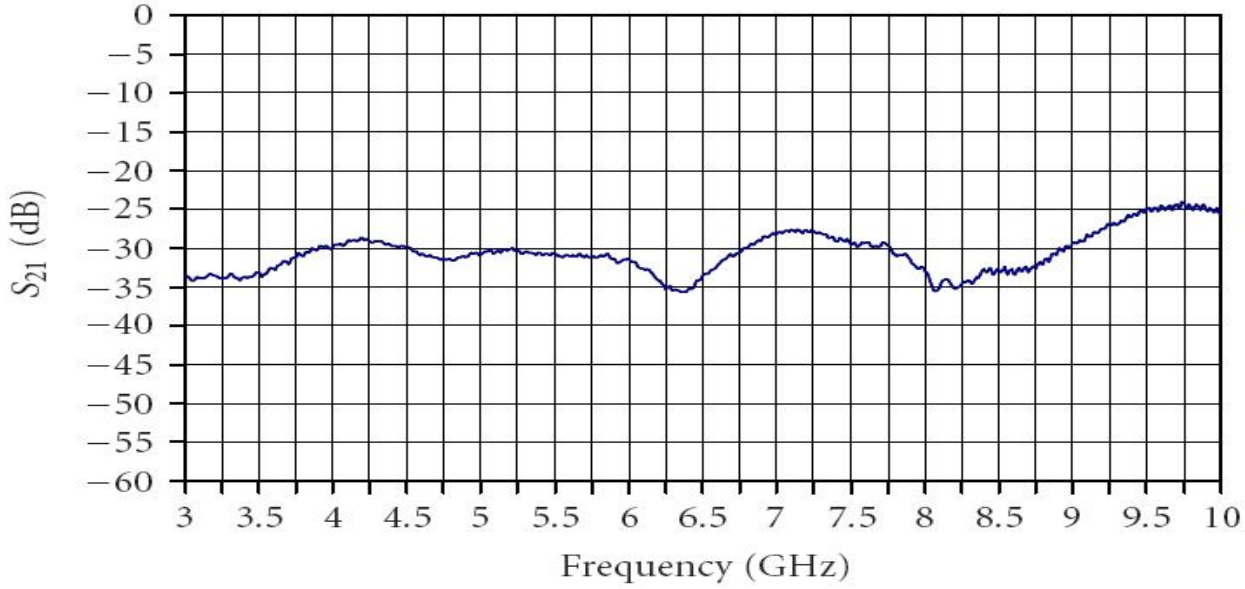

Figure 3.4: S21 Response for the SkyCross UWB Antenna

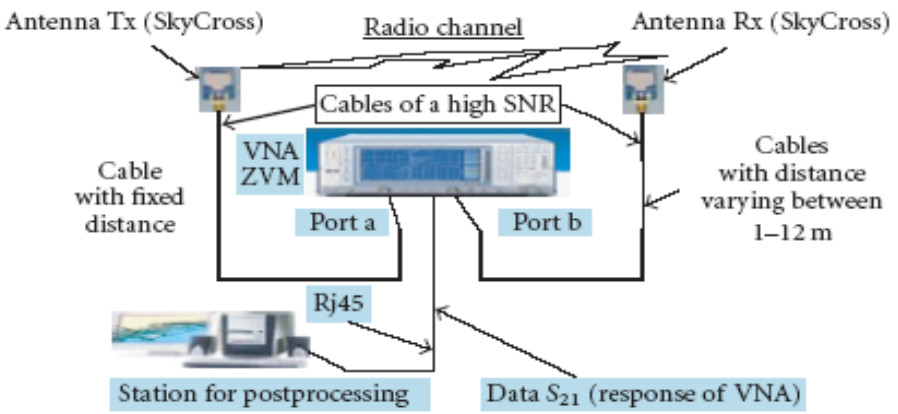

Figure 3.5: The Measurement Setup

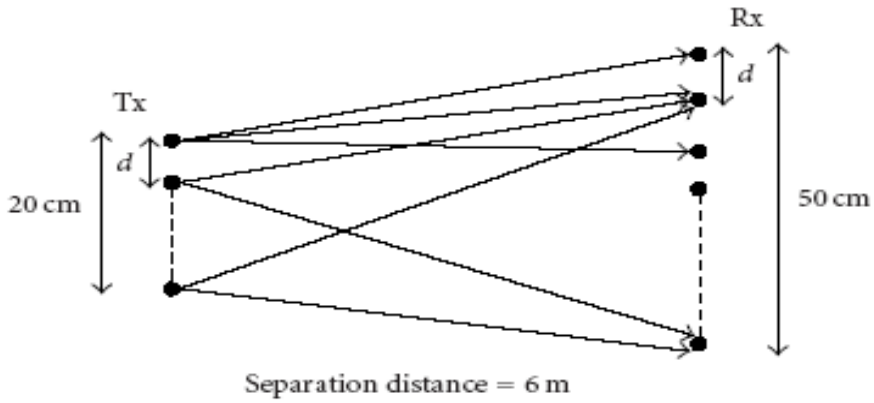

Figure 3.6: Measurement configuration

Figure 3.7: A part of Lab where the UWB channel measurements are conducted

Figure 3.8: The corridor where the corridor channel measurements are conducted

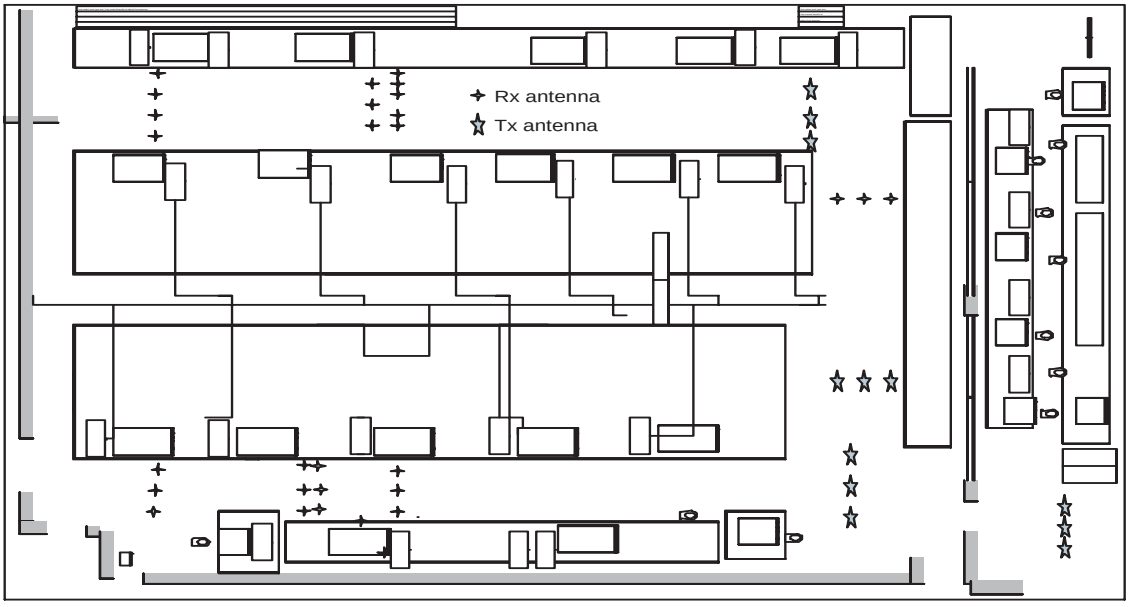

Figure 3.9: Channel Measurement Environment

Measurements were made in both LOS and NLOS situations. We selected the same amount of LOS and NLOS locations and NLOS locations in scenarios I, II, III, IV and V.

3.3.3 Scenarios description

The findings presented in this thesis are obtained from a series of UWB channel measurement companies conducted in different locations. In the following, we present the principal scenarios as follows:

Scenario I

For the LOS and NLOS scenarios, the measurements are performed in Mobile Communication laboratory during the week end (WE) to guarantee "static channel" assumption. This environment is very rich and includes various scatterers (chair, Screen of computer, central processing units, plastic table, vector network analyzer, cable for computer and electrical connection, the walls, the windows of glass, . . .). For NLOS setting, a metallic cupboard is used to obstruct direct paths. Different propagation phenomena occur in this environment such as reflection, diffraction etc...

Scenario II

In this scenario, the measurement are carried out in a corridor configuration (see Figure 3.8). Only a channel measurements in the LOS setting are performed.

Scenario III

This scenario focuses on outdoor LOS measurements. They are made outside Eurecom's buildings. The setup is the same as for previous scenarios. This environment includes different objects width size larger than UWB wavelengths (see Figure 3.10).

Figure 3.10: Outdoor environment of UWB channels measurement

Table 3.2: The Eurecom UWB Database

Scenarios	Distance between Tx and Rx	Setting
Indoor Configuration 1	6 and 12 meters	LOS
Indoor Configuration 1	between 6 and 9 meters	NLOS
Indoor Configuration 2	between 6 and 10 meters	LOS
Indoor Configuration 2	between 6 and 10 meters	NLOS
Indoor Static Configuration 2	between 7 and 8 meters	LOS
Indoor Configuration 2	between 6 and 9 meters	LOS
Outdoor between	6 and7 meters	LOS
Corridor	between 6 and 8 meters	LOS

-LOS: line-of-sight.
-NLOS: Non line-of-sight.
-Configuration 1: The Communications Mobile Laboratory configurations in the 2003.
-Configuration 2: The Communications Mobile Laboratory configurations in the 2004.
-Static: The Measurements are taken as that during the scenario the Tx and the Rx are fixed.

Scenario IV

In this scenario, antennas are fixed for all measurements locations.It focuses on the analysis of the displacement of the antennas. The setup and environment are same as in the scenario I described on 3.3.3.

Scenario V

The aim of this scenario is to investigate if we can create a NLOS setting between the RF laboratory and the corridor. The channel measurements collected from this scenario demonstrated that as the separator wall is not metallic based, the NLOS measurements can not carried out. The antennas are moved and manipulated like in scenario I.

Table 3.2 summarizes all scenarios described above.

3.4 Preliminaries Results

In this Section, we present our first analysis of UWB channel measurement conducted at Eurecom Institute.

3.4.1 Antennas Effects

Radio signal propagation is usually affected by the characteristics of the antennas. For CNWS, the effect of the antenna can be well separated from the channel because the bandwidth is small, i.e. antenna frequency response can be assumed as flat over the frequency band of interest. None the less, this is not the case for UWB systems since the frequency response of the antenna is not flat over the large bandwidth occupied by the UWB signal. Moreover, the statistics of the channel depend on the type of the antenna as well. Figure 3.11 illustrates the effect of a directive and an omnidirectional

antenna on the impulse response of the propagation channel. This implies that the transfer function of the antenna can be expressed as a function of the frequency and the directivity. In general, transfer

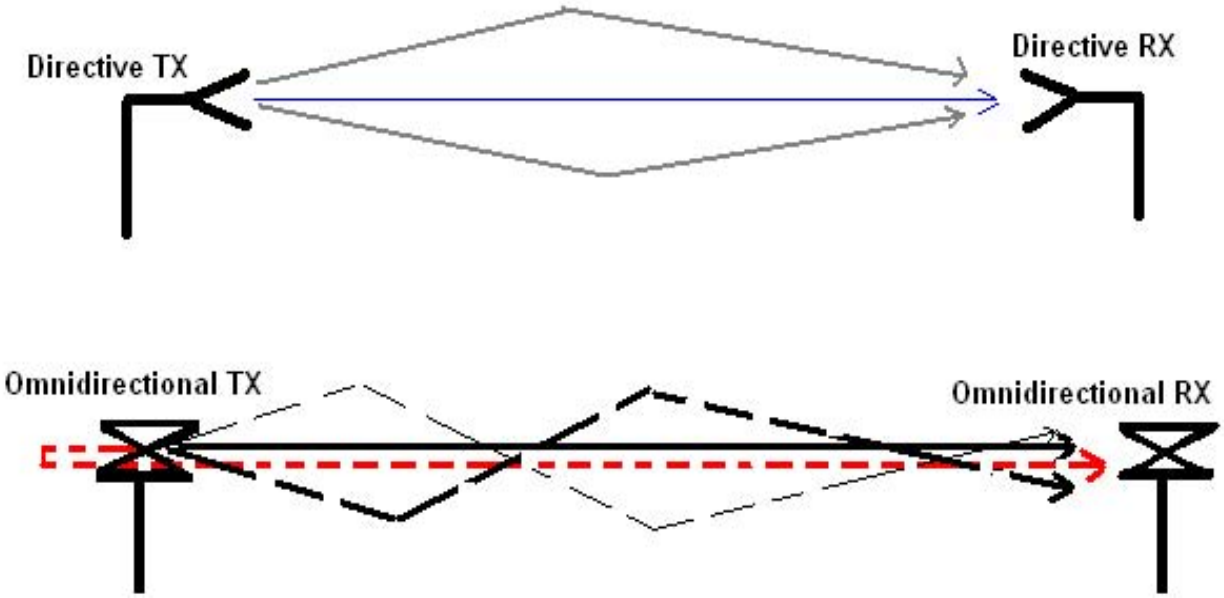

Figure 3.11: The Influence of the antenna type on the channel impulse response.

function of the antenna is given by:

$$H_{ant} = g(f, \theta(f), \phi(f)). \tag{3.9}$$

where $g(.)$ is a function, f is the frequency, ϕ is the azimuth angle and θ is the elevation angle.

According to equation (3.9), the expression of the received signal will be more complicated and is difficult to use in our evaluations. However, if the angular dependencies of the antennas are included in the channel, the result that we will obtain for the impulse response of the channel becomes antenna dependent, but still a general characterization of the channel can be offered for the specific antenna used in the measurements. It means that, if different antennas are used, the results will be not the same. UWB antennas have a significant impact on the measured channel. Just like narrowband antennas, they exhibit an antenna pattern that weights the MPCs arriving from different directions. Furthermore, the antenna itself leads to significant distortions of the arriving signal, i.e., the impulse response of the antenna has a support that is larger than the inverse system bandwidth. This makes the deconvolution of antenna effects and channel effects a highly challenging task [Mol05]. Figure 3.12 shows an example of UWB channel response in frequency domain from Intel UWB channel measurements (6 GHz of bandwidth from 2 to 8 GHz with frequency step sampling 3.75 MHz). From these figures we can observe clearly the antennas effects. In Eurecom UWB channel measurement we haven't corrected the antennas effects because their transfer function in frequency domain are considered flat over frequency band of interest (see Figure 3.4).

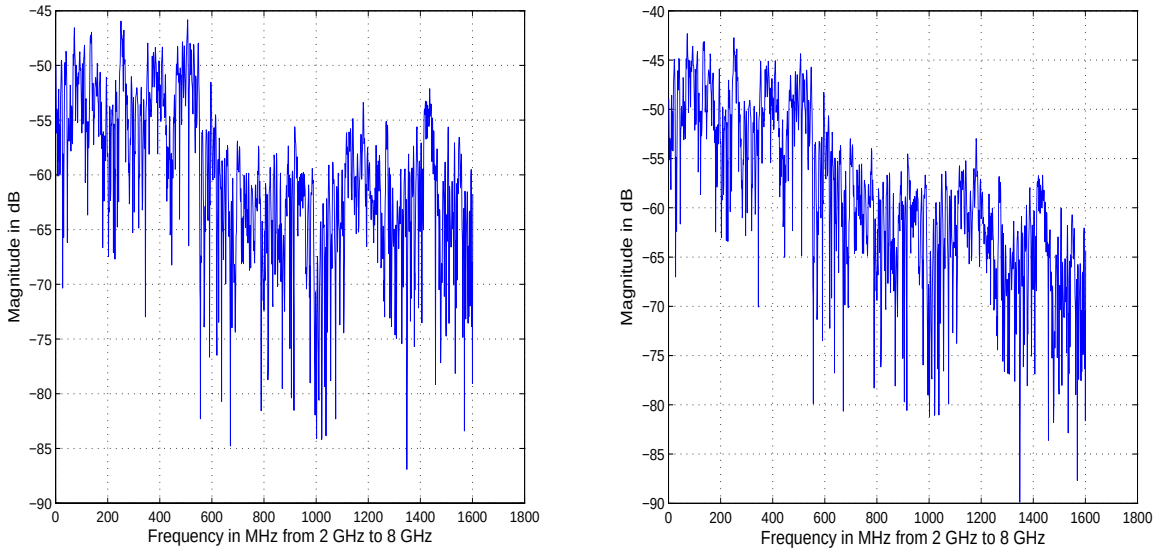

Figure 3.12: Channel frequency response left with antennas correction, right without.

3.4.2 Windowing Effects

In Figures 3.13–3.15 we use complex baseband processing with windowing and without windowing. Before plotting the signal if it is complex we convert it to the equivalent passband signal Figure 3.14. No windowing function was used in Figure 3.14 and we see some low frequency artifacts around 100 ns, more explication about the windowing is given in Section 4.2. Windowing removes this ringing as is evident in Figure 3.15, which shows in blue windowing alone, and in red windowing with power law binning. Binning here is for two samples per bin to represent the lowered resolution in the time domain when using a Hamming window. Note that the red curve is only positive due to the power law processing. Figure 3.16 shows results for interpolative binning which conserves sign information. Caution should be used with interpolative methods on passband signals, as interpolation leads to reducing the highest frequency content. Passband signals may be reduced to noise only by large interpolation factors.

3.4.3 Observed UWB channel behavior

In this part of the chapter some initials observed channel characteristics in time domain and frequency domain will be presented. Figures 3.17, 3.18 present an UWB channel responses in frequency and in time domain respectively (from D. Porrat channel measurements). Figures 3.19, 3.20 show an UWB channel responses in frequency and in time domain respectively (from IMST channel measurements). And the Figure 3.21 presents the channel response in frequency domain (from Intel UWB channel measurements), the channel is with antennas correction. Analysis of these figures (in time domain specially) indicates that most energy does indeed arrive from this direct line-of-sight path, and we remark also a cluster in channel PDP.

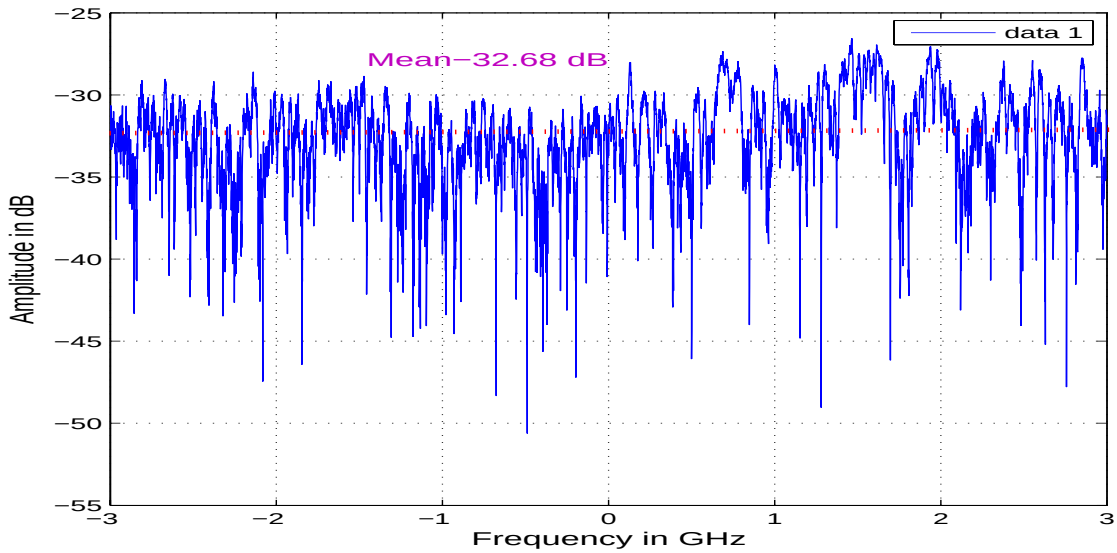

Figure 3.13: Channel frequency in domain LOS case (over 6 GHz).

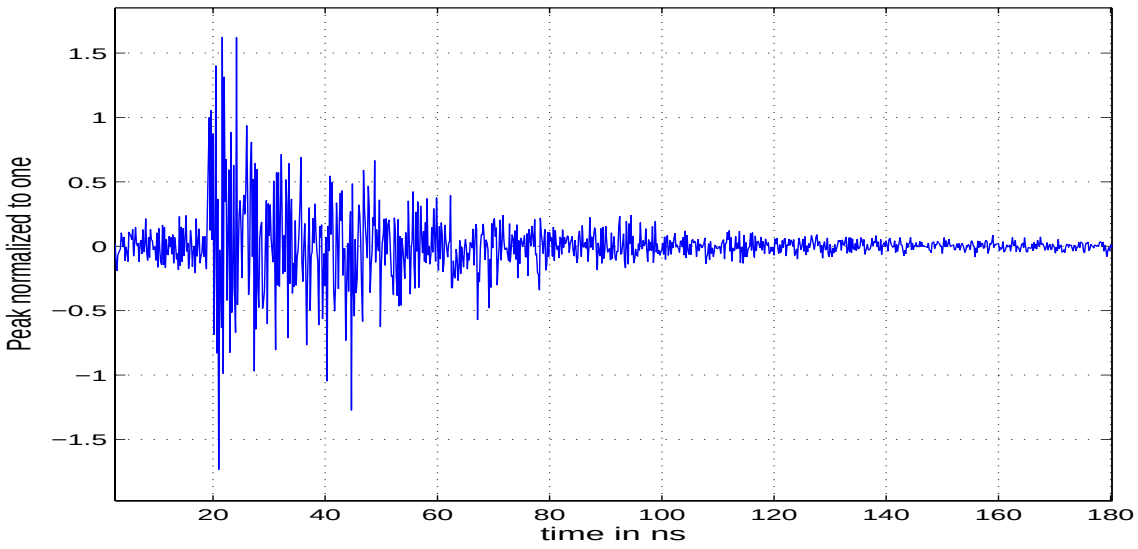

Figure 3.14: Time domain signal without windowing LOS case.

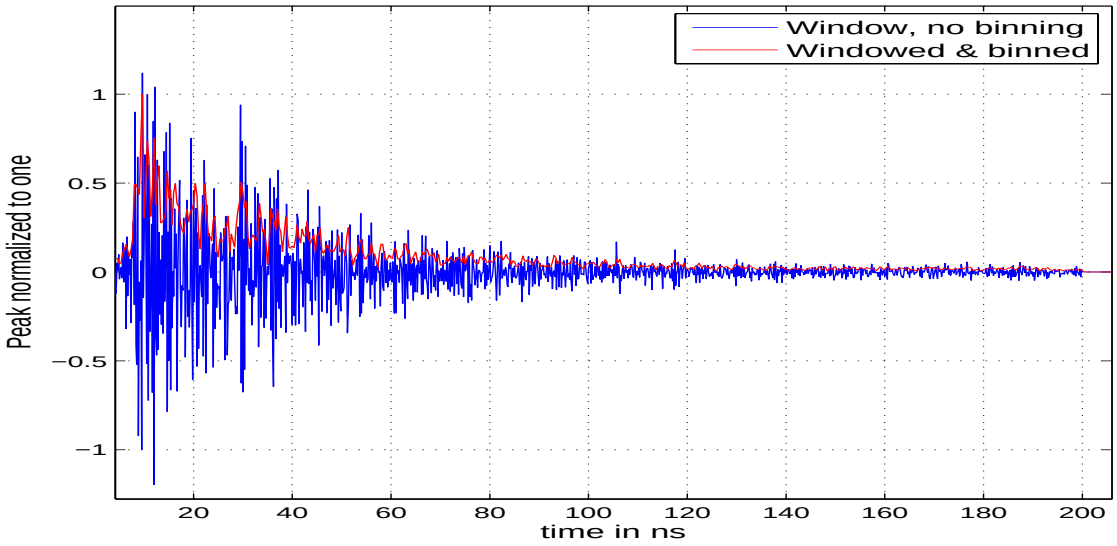

Figure 3.15: Time domain signal with windowing and power law binning LOS case.

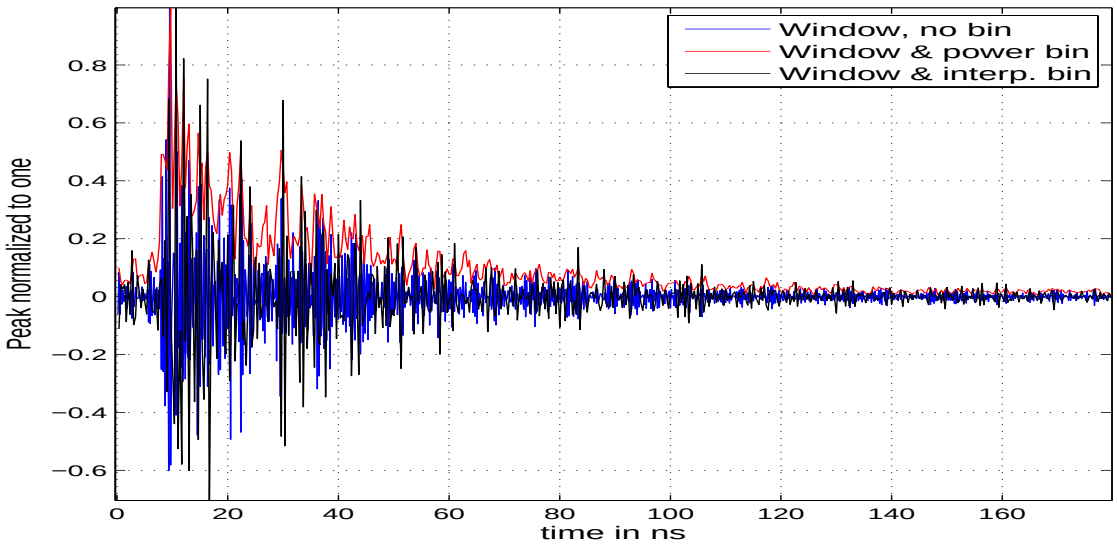

Figure 3.16: Time domain signal LOS case (over 6 GHz).

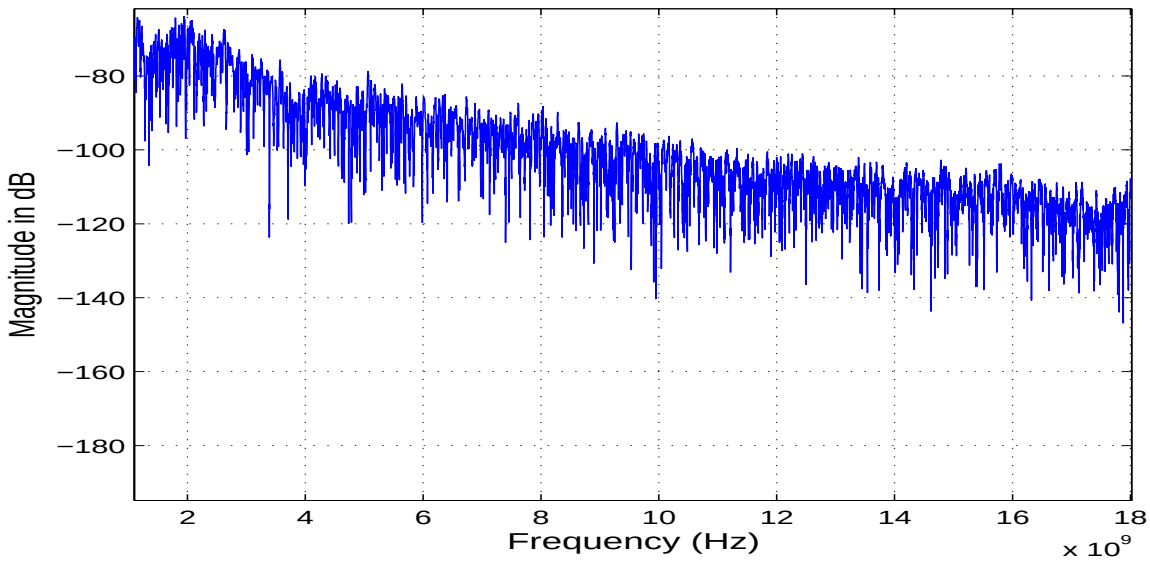

Figure 3.17: Frequency domain signal NLOS case (over 18 GHz).

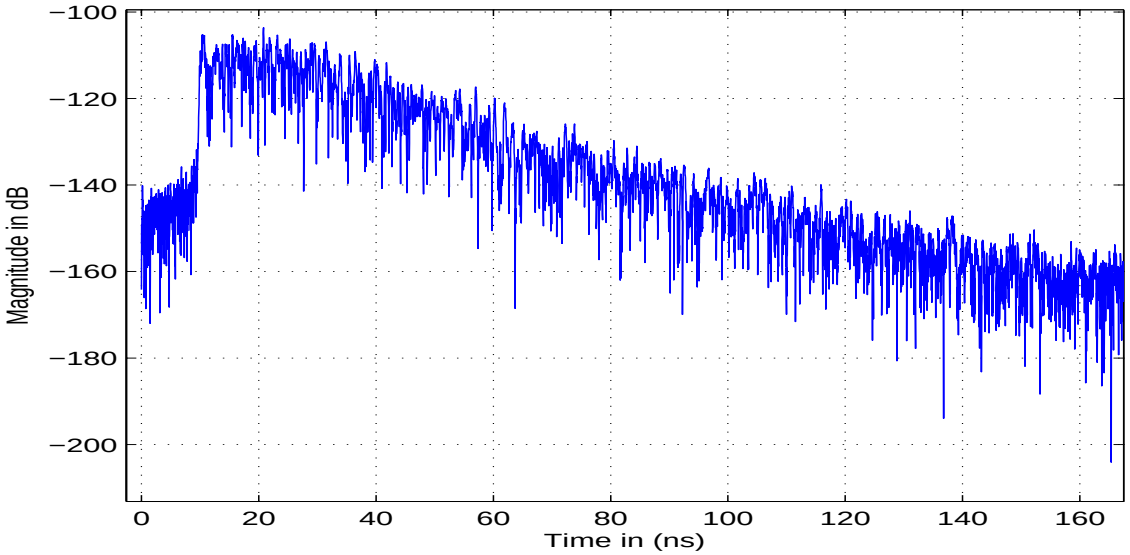

Figure 3.18: Time domain signal NLOS case (over 18 GHz) D. Porrat UWB channel measurments.

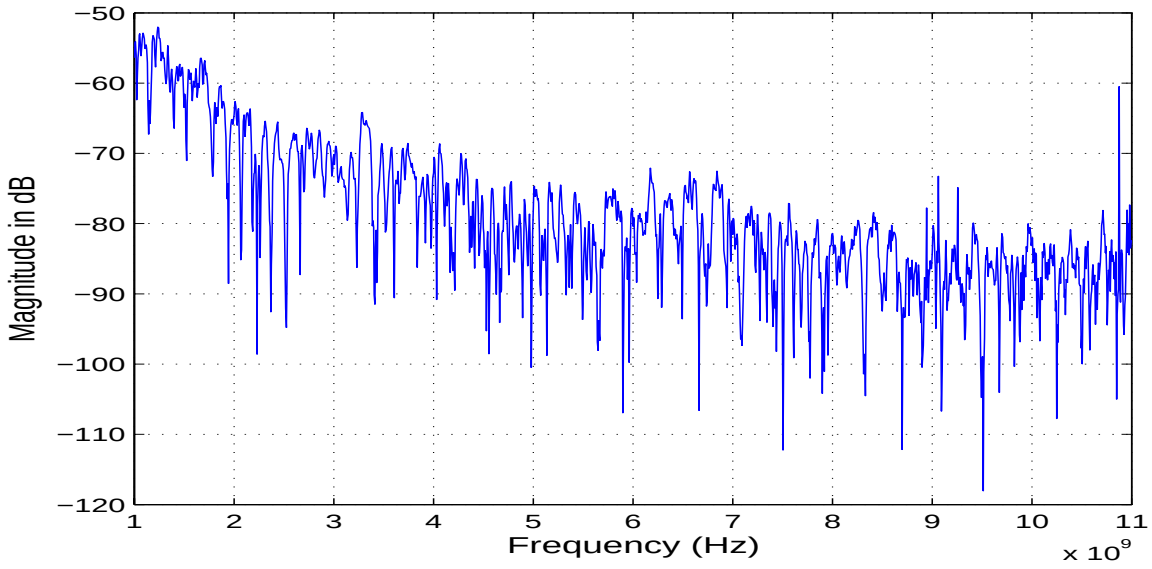

Figure 3.19: Frequency domain signal NLOS case (over 10 GHz) IMST UWB channel measurements.

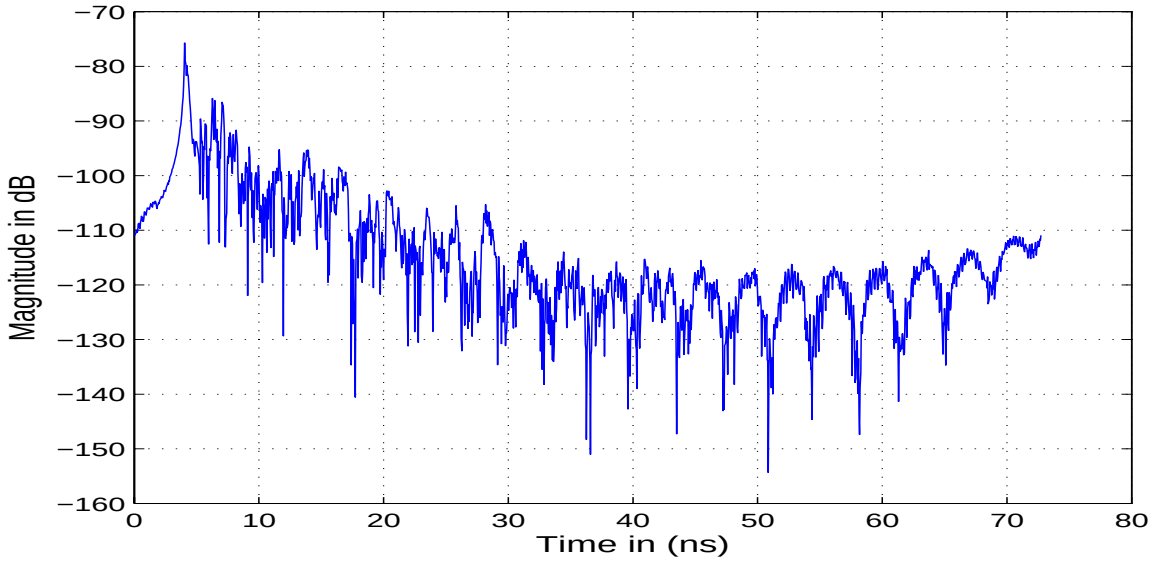

Figure 3.20: Time domain signal NLOS case (over 10 GHz) IMST UWB channel measurements.

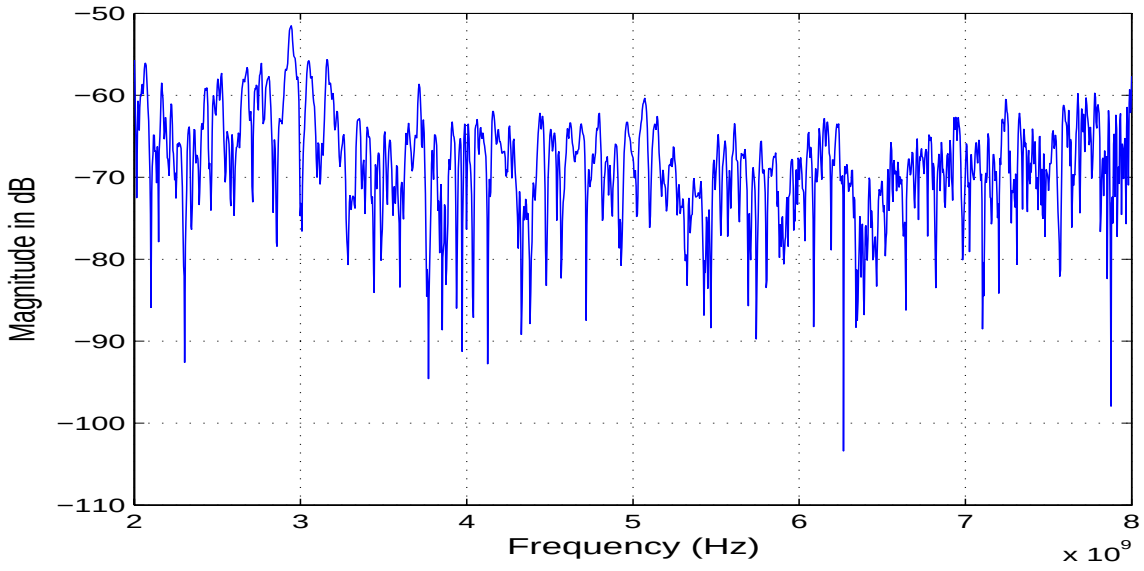

Figure 3.21: Frequency domain signal NLOS case (over 6 GHz) Intel UWB channel measurements.

3.5 Conclusion

In this Chapter, we have dealt with some common channel measurement techniques. In the literature, there are two possible domains for performing the channel measurement to characterize the UWB radio channel. First, the channel can be measured in the frequency domain using a frequency sweeping technique. Second, the channel can be measured in time domain. We have adopted the channel measurement in frequency domain in our channel measurements and characterization. We have also described the environment where the Eurecom channel measurements are conducted. To sum up, in this chapter we have presented a description of UWB channel sounding setup and settings . We have also presented channel measurements constraints and results including the effects of antennas and windowing. The following Chapter aims to present UWB channel large and small scale fading statistics analysis based on the available UWB channel measurement described in this chapter.

CHAPTER

4 UWB CHANNEL: LARGE AND SMALL SCALE FADING STATISTICS ANALYSIS

4.1 Introduction

In any communications systems including narrow Band, Wide Band and UWB systems, the received signal is attenuated, delayed, and distorted (for the UWB systems) version of the transmitted signal affected by the noise present in the propagation environment. The received signal and the transmitted signal are linked to each other via the radio channel. Thus, the evaluation and the designing of communication systems need a channel characterization and modeling. There are two aspects of channel characterization and medeling: small and large scale channel modeling. Large scale channel modeling which, involves modeling the signal attenuation with distance, is generally referred to as path loss. The small scale characteristics include the small-scale fading in a local environment as well as the distortion of the transmitted waveform due to multipath.

The objective of this chapter is not to formulate a channel model for UWB systems, or to provide a universal model for all environments in which UWB devices will operate, but rather to provide a set of tools that can be used to fairly evaluate the performance of different UWB physical layer proposals in real channels such as offices, laboratories and industrial environment. To providing a useful model to fit experimental data, the Nakagami-m model is used. The Nakagami-m distribution offers features of analytical convenience in comparison to other distributions. It is also a generalization of many known distributions like Rayleigh and Rice.

The Chapter is organized as follows: A preliminaries results in time domain are presented in section 4.2. In section 4.3, we present a short analysis of a spatial fading. Section 4.4 will focus on channel large scale statistics and channel behavior in frequency domain. Section 4.6 provides a channel time dispersion characterization in terms of **rms** delay spread and mean excess delay. Conclusion is provided in section 4.7.

4.2 Time Domain Analysis

The channel impulse response is computed from the recovered VNA data in the form of a complex vector of size 6003. Since the time response is obtained using the inverse Fourier transform of the measured frequency response, it is possible to take advantage of a windowing technique to enhance the time response for a particular application (see 3.2.1).

4.2.1 UWB Channel Time Response

Figures 4.1 shows the time response with a rectangular window and the time response with a Hamming window applied to $H(f,d)$ in the LOS case. Figure (4.2) show the time response with a rectangular window and the time response with a Hamming window applied to $H(f,d)$ in the NLOS case.

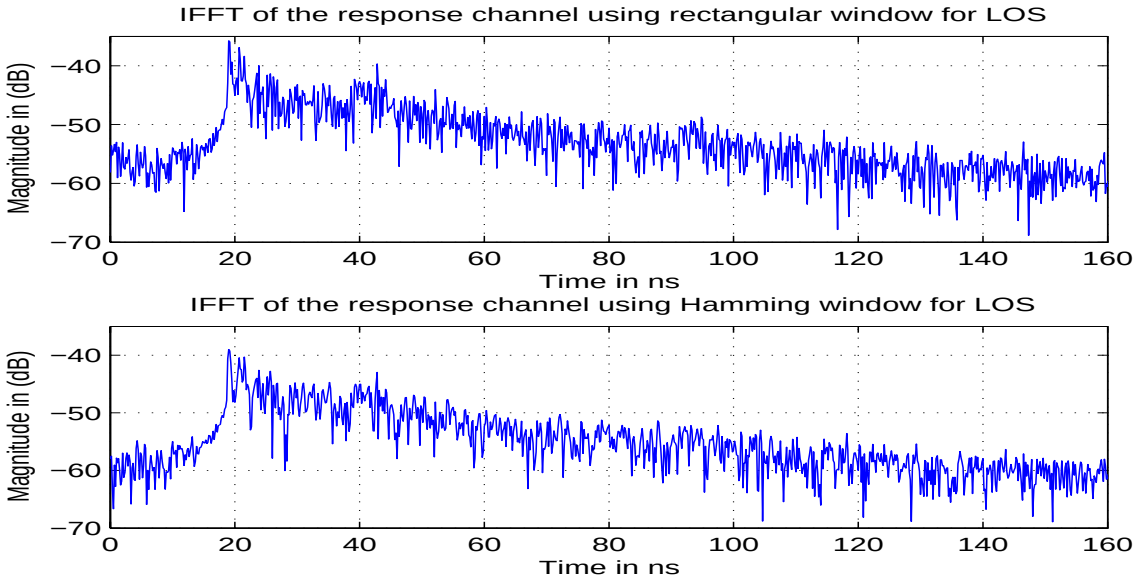

Figure 4.1: IFFT of $H(f)$ using rectangular and Hamming window (LOS).

We can see from the above figures that the effect of side lobes is reduced with Hamming window. The arrival time of the first path can be found by applying a threshold to the peak of the received signal. The 15 dB value gives a good compromise between the measured distance[1] and the true distance figure 4.3. Other works suppose that the arrival time corresponds to 15 dB above the noise floor. The average noise level is approximately 50 dB below the maximum multipath component in the averaged power delay profile (PDP).

4.2.2 UWB Channel Power statistics in Time Domain

To characterize the probability density function of the power variations, we plot on Figures 4.4 (LOS and NLOS) and 4.5 (Corridor/LOS and Outdoor/LOS) the histograms of the measurements data. The power variations are fitted with an analytical probability density function (pdf) approximation, namely a Weibull pdf. The general formula for the Weibull pdf is given by:

$$f(x) = \frac{\gamma}{\alpha}\left(\frac{x-\mu}{\alpha}\right)^{(\gamma-1)} \exp\left\{-\left(\frac{x-\mu}{\alpha}\right)^{\gamma}\right\} \tag{4.1}$$

where α, γ, $\mu \in R$, $\alpha, \gamma > 0$ and $x \geq \mu$, α is the scale parameter, γ is the shape parameter, and μ is the location parameter. It can be observed how the Weibull pdf fits well with the experimental measurements. From our measurements, we obtain the following values summarized in table (4.1).

[1] $d_{musered} = t_0 \times c$, with t_0 time of arrival of first path and $d_{musered}$ is the measured distance.

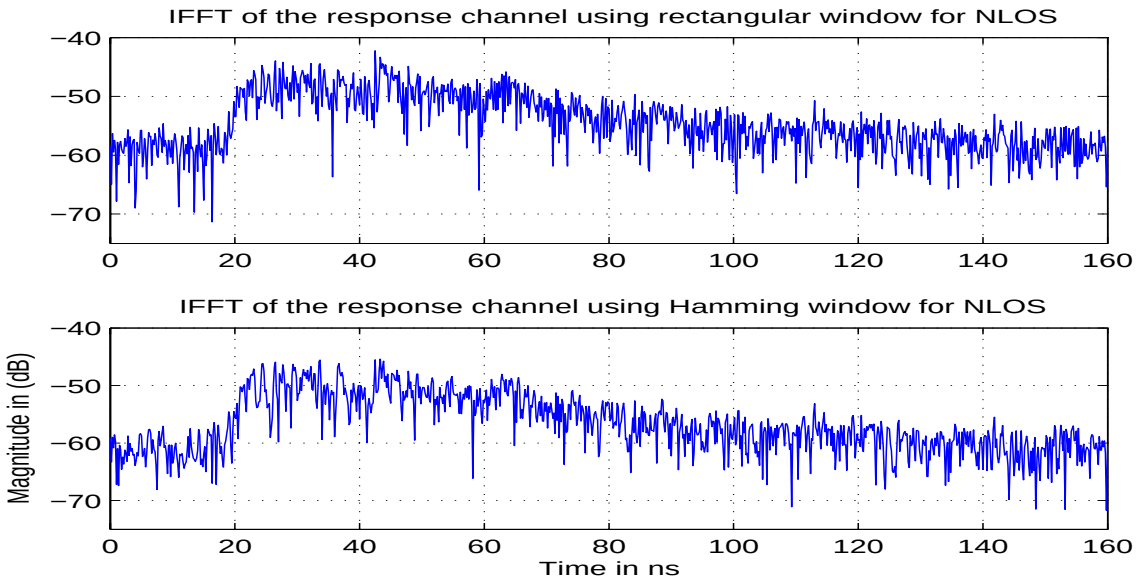

Figure 4.2: IFFT of $H(f)$ using a rectangular and Hamming window (NLOS).

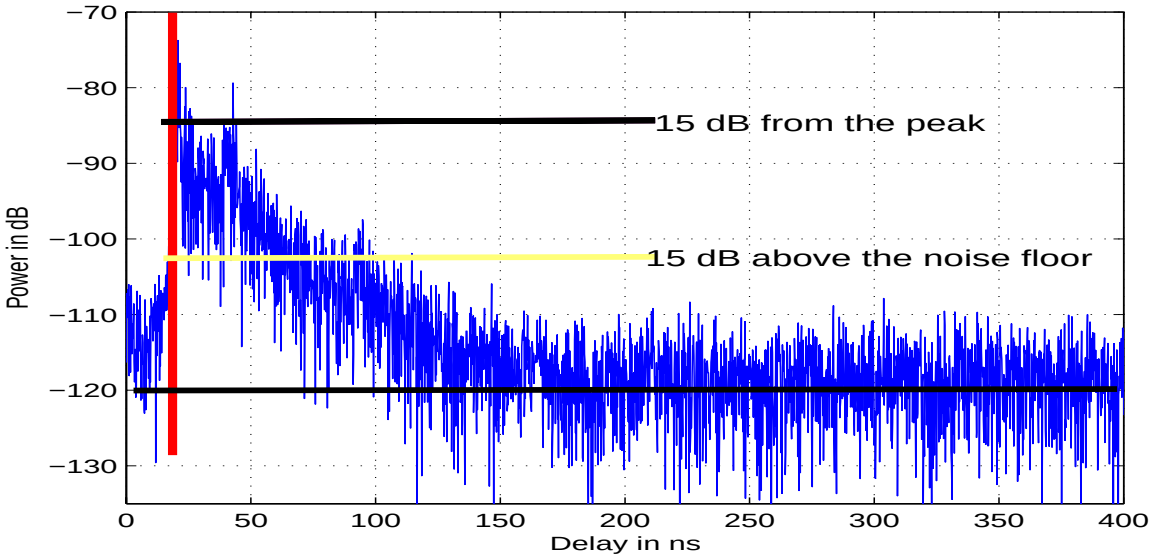

Figure 4.3: Typical impulse response (dB unit).

Table 4.1: pdf shape parameter

Parameter / Setting	LOS	NLOS	Corridor	Outdoor
γ	6	4	5	6.5
α	26	26	28	28.5
μ	-23	-21	-22	-21

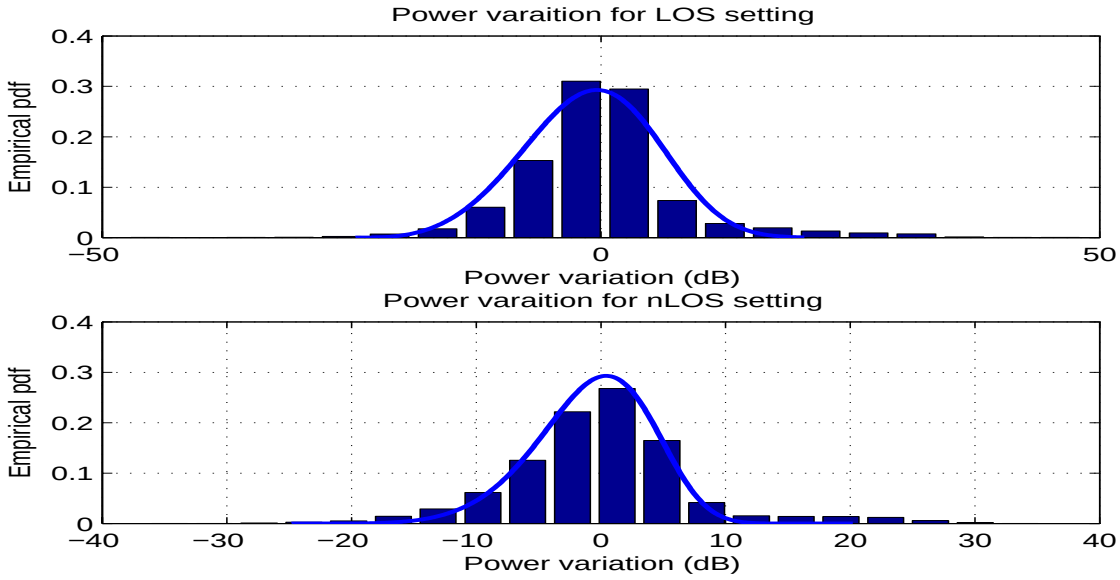

Figure 4.4: PDF of the power variations (LOS) and LOS.

4.3 Spatial Fading

The average received power is estimated from the measured frequency response using the following equation [CFAT06a]:

$$P(d) = -10\log_{10}\{\sum_{m=1}^{m=M}\sum_{n=1}^{n=N}|H(t_m, f_n, d)|^2\}. \tag{4.2}$$

where N is the number of frequencies tons and M is the number of frequency response snap shots over time at d meters. Figures 4.6 and 4.7 present, for the LOS and NLOS cases, the received signal and the cumulative distribution function of the received signal energy, respectively.

These figures show that the variation of received signal is small (less than 1.5 dB for LOS, and 2 dB for NLOS). This result confirms the robustness of UWB communication systems, insofar as multipath is concerned, which is manifested by small variations of the received signal at various grid locations.

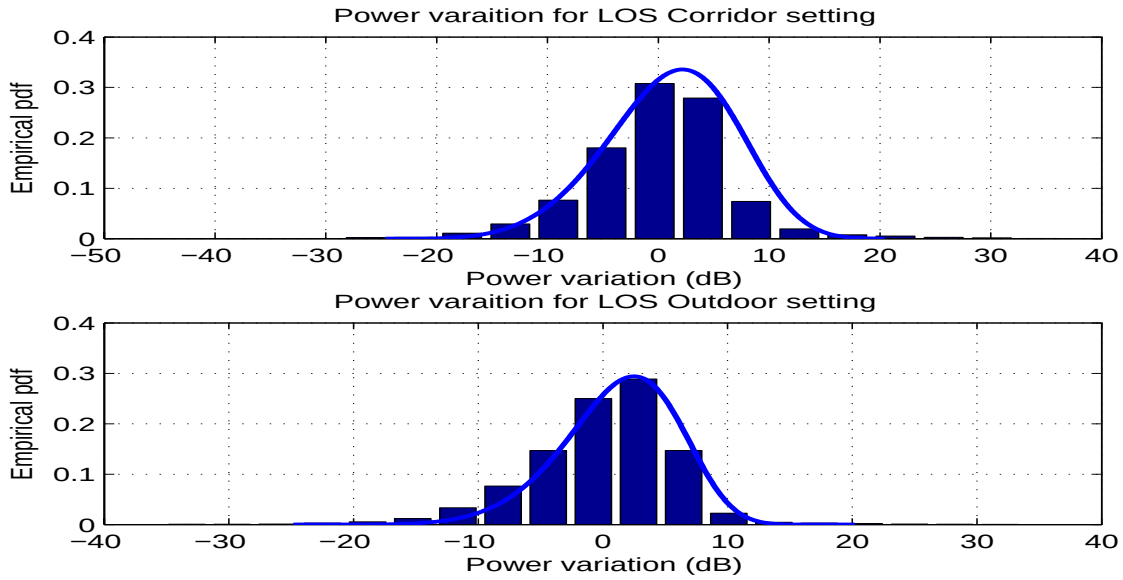

Figure 4.5: PDF of the power variations Corridor (LOS) and Outdoor (LOS).

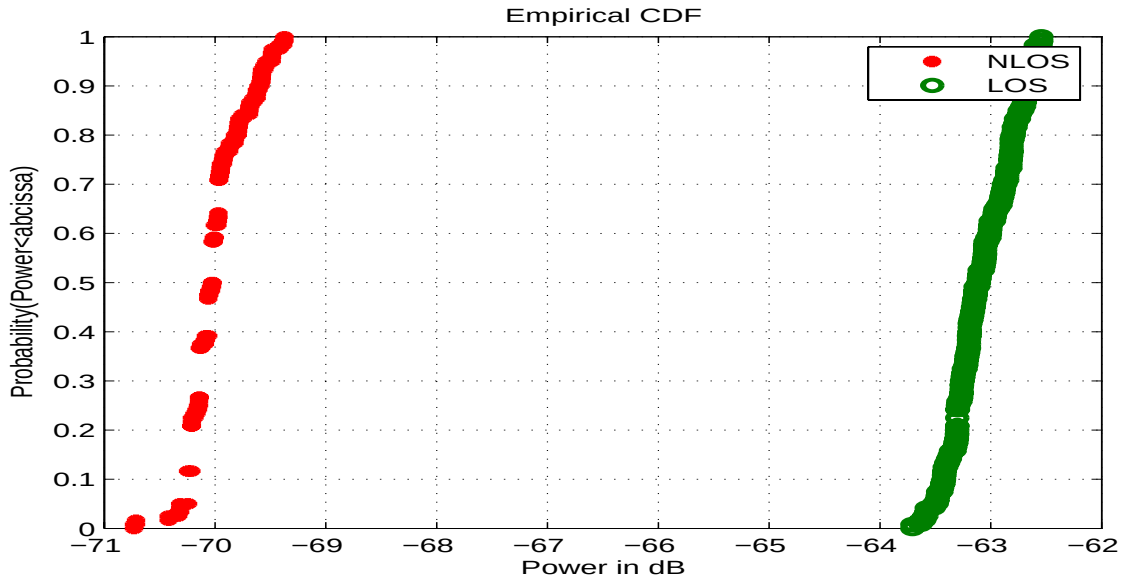

Figure 4.6: Cumulative Distribution Function of the received signal in LOS and NLOS.

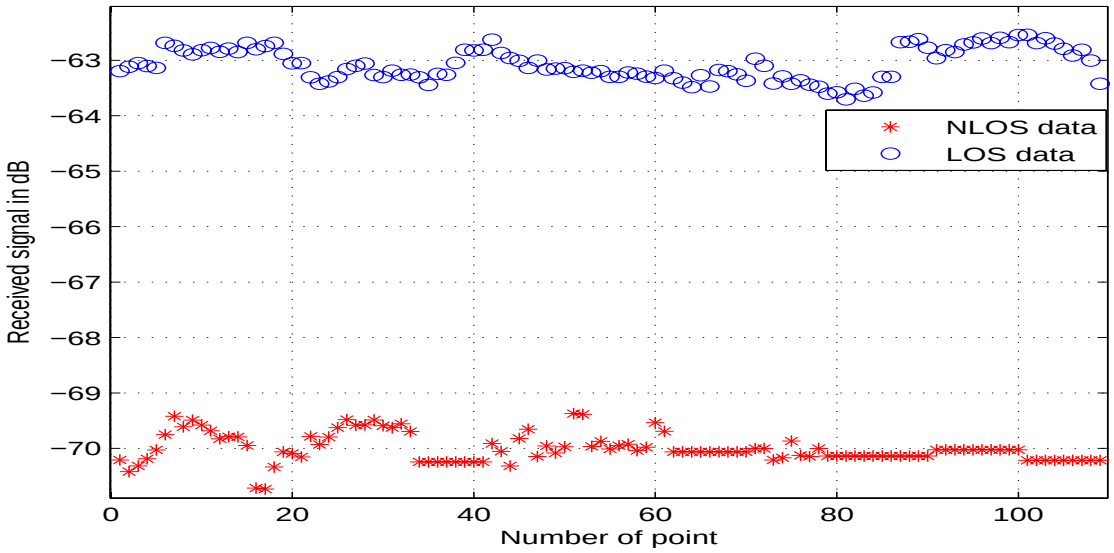

Figure 4.7: Received signal for the Indoor LOS and NLOS cases.

4.4 Frequency Domain Analysis and Large-Scale Fading

4.4.1 path loss Analysis Definition

The path loss (PL) defines the relationship between transmitted power (P_{TX}) and received power (P_{RX}) in a far-field RF link. This relation was first given by Harald Friis (1946):

$$P(f,d) = \frac{P_{RX}}{P_{TX}} = \frac{G_{TX}G_{RX}\lambda^2}{(4\pi)^2 d^2} \tag{4.3}$$

In this formula, $G_{Rx} =$ and G_{Tx} are the receive and transmit antenna gains (respectively), d is the distance between the antennas, λ is wavelength. The upshot of Friis's Law is that the far-field power rolls off as the inverse square of the distance $(1/d^2)$. Near-field links do not obey this relationship. Near field power rolls off as powers higher than inverse square, typically inverse fourth $(1/d^4)$ or higher.

For UWB systems in several works it is reported that the path loss modeling can be simplified by assuming that the frequency dependence and the distance dependence can be treated independently of each other:

$$P(f,d) = PL(f) \cdot PL(d) \tag{4.4}$$

4.4.2 Path Loss and Distance Dependency Analysis

The path loss $PL(d)$ can be calculated directly from the measured channel function transfer $H(f,d,t_n)$, where t_n, d, and, f, is the time when the H is taken, the distance between transmitter and the receiver, and, the frequency, respectively. The spatial path loss, PL^k_{sp} at local point k and TX-RX separation distance d is given by:

$$PL_{sp}^{k}(d) = \frac{1}{M \times N} \sum_{m=0}^{m=M-1} \sum_{n=0}^{N-1} |H_k(f_m, t_n; d)|^2. \tag{4.5}$$

with $k = 1, ...K$.

where $H_k(f_m, t_n; d)$ denotes the n^{th} channel function transfer snapshot at frequency f_m and at local point k in a distance d. Here, K is the total number of spatial points at each local point, M is the total number of channel function transfer snapshots over time, N is the total number of frequency points over bandwidth, and d is the TX-RX separation distance in meters. The local path loss, $PL_{l_c}(d)$ is computed by averaging the corresponding set of spatial path losses (in order to normalize the fading effects) and can be expressed as follows

$$PL_{lc}(d) = \frac{1}{K} \sum_{k=0}^{m=K-1} PL_{sp}^{k}(d) \tag{4.6}$$

The PL in dB as function of the distance is given by [GJR+04]

$$PL(d) = PL_0 + 10 \times nlog_{10}\frac{d}{d_0} + S; \quad d_0 < d \tag{4.7}$$

where $PL(d)$ represents the received power at a distance d, computed relative to a reference distance d_0 ($d_0 = 1m$), and PL_0 is the free-space PL in the far-field of the antennas at a reference distance d_0. PL_0 is the interception point and is usually calculated based on the mid-band frequency. n is the PL exponent and S is the shadowing fading parameter. The PL exponent is obtained by performing least squares linear regression on the logarithmic scatter plot of averaged received powers versus distance in Equation (4.7).

Using our measurements database, we have obtained $n = 1.4$ for LOS case (NLOS channel measurements at different RX-TX separation distance are not available).

These results show that indoor UWB LOS radio channel can have path loss exponent less than the free space loss $n = 2$. This can be explained by the fact that the indoor UWB radio channel has a dense multipath which contribute, if combined coherently, to increase the received power.

In [MASJWR06] the reported path-loss exponent was as low as 1.27 for a narrow corridor. For LOS and NLOS scenarios the global path-loss exponents were found to be nearly 1.6 and 2.7 respectively. In [CKYL05] the reported values of n for TX-RX separation ranging from 1 to 20 m are 1.18, 2.18, 2.48 and 2.69 for LOS (three-bedroom apartment), NLOS (three-bedroom apartment), LOS (four-bedroom apartment) and NLOS (four-bedroom apartment) respectively. Table 4.2 summarizes path loss exponents results published in the literature.

4.4.3 Path Loss and Frequency Dependance

In the literature there is a point of dissimilarity, whereas some authors say that there is no correlation between the path loss and channel frequency bandwidth, others say that there is a correlation and they have even proposed a function which connects the path loss to the frequency (Kunisch and Alvarez models [KP02] [AA03]). Most of the measurement results in the literature reported that narrowband model can be used to approximate the PL for UWB systems, leading to independency between path loss and frequency [GGAK03], [RPCQL03]and [DMB06], except two published works in references [AA03] and [KP02]. Still, a major difference between narrowband and UWB channels is that for UWB channels the received power shows a general decay trend with increasing frequency [KP02].

Table 4.2: The reported values on path loss exponent based on previous measurement campaigns

Researchers	mean value of the path loss exponent n	RX-TX distance (m)
Virginia Tech (office) [App]	1.3-1.4 (LOS) 2.3-2.4 (NLOS)	5-49 (LOS) 2-9 (NLOS)
AT&T [GJR+04]	1.7 /3.5 (LOS/NLOS)	1-15 (LOS/NLOS)
U.C.A.N. [AVL+03]	1.4/3.2(soft)/4.1(hard) LOS/NLOS/NLOS	4-14 (LOS/NLOS)
France Telecom [PPV03]	1.5 / 2.5 (LOS/NLOS)	2.5-14 (LOS) 4-16 (NLOS)
CEA-LETI [KD03]	1.6 (lab)1.7(flat) LOS	1-6, 1-8 (LOS)
CEA-LETI [KD03]	3.7 (office/lab/NLOS) 5.1 (flat/NLOS)	2-20,7-17(NLOS)
Intel [RPCQL03] (Resident.)	1.7/4.1 and 1.5/3.6 (LOS/NLOS)	1-11 (LOS) 4-15 (NLOS)
IKT, ETH Zurich [ZAS+03]	2.7- 3.3 (on body) 4.1 (around the torso)	.5 to 1.5
Cassioli/Molisch/Win [CWM02a]	2.04 (d<11m) -56+74$\log(d)$ (d>11)	8-11 and 11-13(NLOS)
Oulu Univ. [Ha02]	1.04,1.4,1.8 LOS 3.2, 3.3, 3.9 NLOS	1-30 (LOS) 4-14 (NLOS)
Whyless [KP02]	1.58/1.96 LOS/NLOS	2.5-16 (LOS/NLOS)
Time Domain [Yan02]	2.1 (LOS/NLOS)	2-21 (LOS/NLOS)
DARPA NETEX [DMB06]	1.3/2.3 (LOS/NLOS)	Distances less than 10m.

In frequency domain analysis two parameters are often used: the frequency range which is determined by the measured range (in our case we have covered the 3 to 9 GHz frequency band), and the frequency decaying factor noted δ. Several research studies [AA03], [KP02] and [CKL05] have showed that the frequency dependency of the path loss is characterized by this factor. Two models of path loss frequency dependence are mainly used:

$$PL(f) \propto k.e^{-\delta_1 f} \tag{4.8}$$

$$\sqrt{PL(f)} \propto f^{-\delta_2} \tag{4.9}$$

The model of equation (4.8) and (4.9) are presented in [AA03] and [KP02] respectively. For our measurements we used the two models to fit the variations of the path loss as a function of frequency. Using non-linear least square fitting with the measurements data, we have found the values of δ_1 and δ_2 summarized in Table 4.3. As Figure 4.8 and 4.9 show we can notice that no correlation between path loss and frequency.

Table 4.3: path loss δ_1 and δ_2 parameters

	LOS	NLOS	Corridor	Outdoor	Static	lab LOS 9 meters
δ_1 (Alvarez)	1.1	1.3	0.9	1.2	1.1	1.3
δ_2 (Kunisch)	2.4	2.8	2.5	1.3	2.1	2.5

4.4.4 Shadowing

Due to variations in the surrounding environments, PL observed at any given location will deviate from its average value [Rap02]. This phenomenon is called shadowing and has been reported by many measurements [GJR+04, DVB+04, CKYL05] to follow a lognormal distribution. In the Equation , shadowing fading parameter is given by the term S that varies randomly from one location to

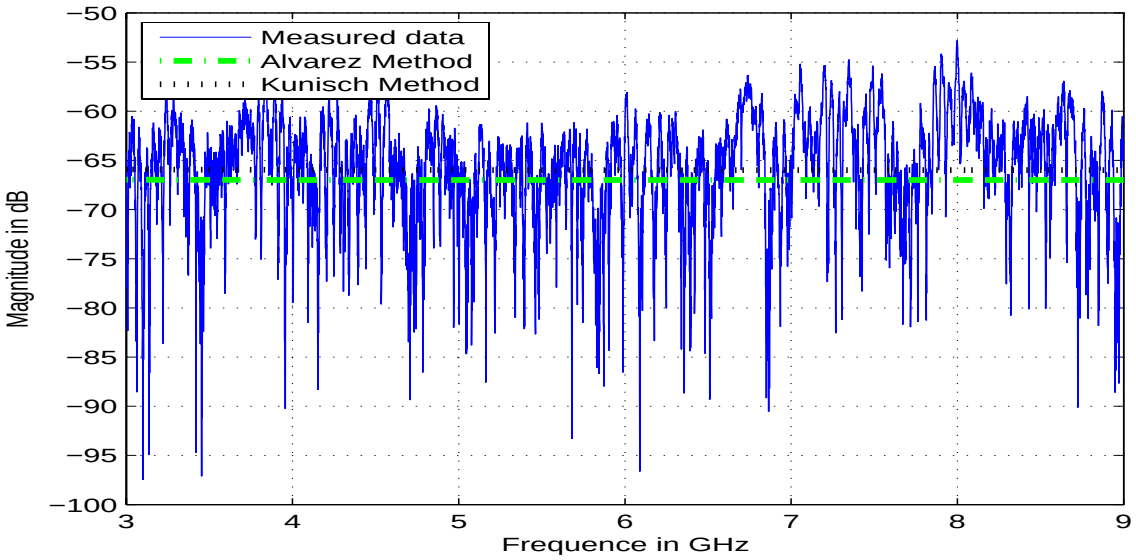

Figure 4.8: Path loss as a function of frequency (LOS).

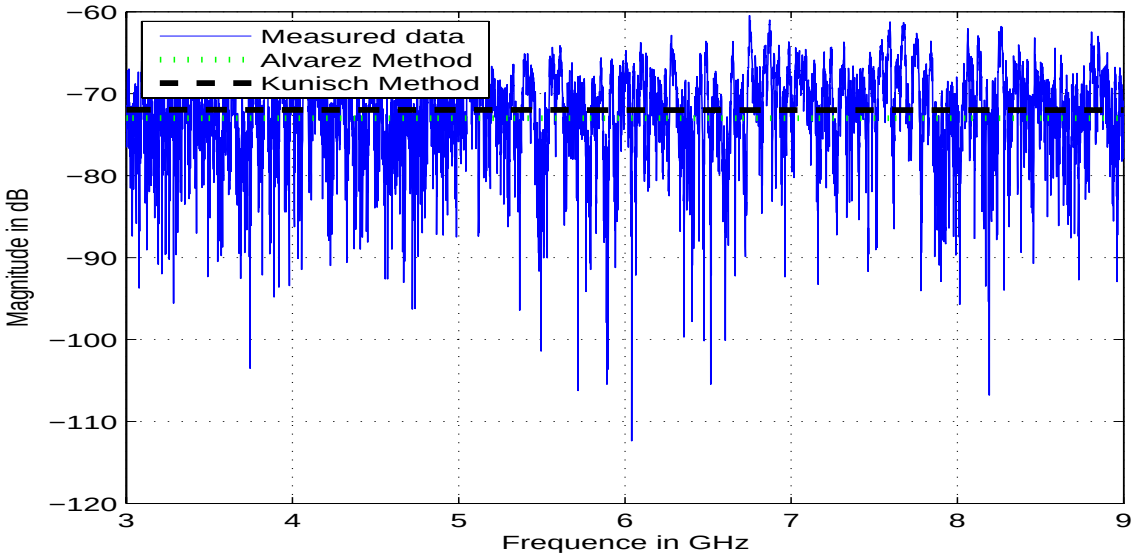

Figure 4.9: Path loss as a function of frequency (NLOS).

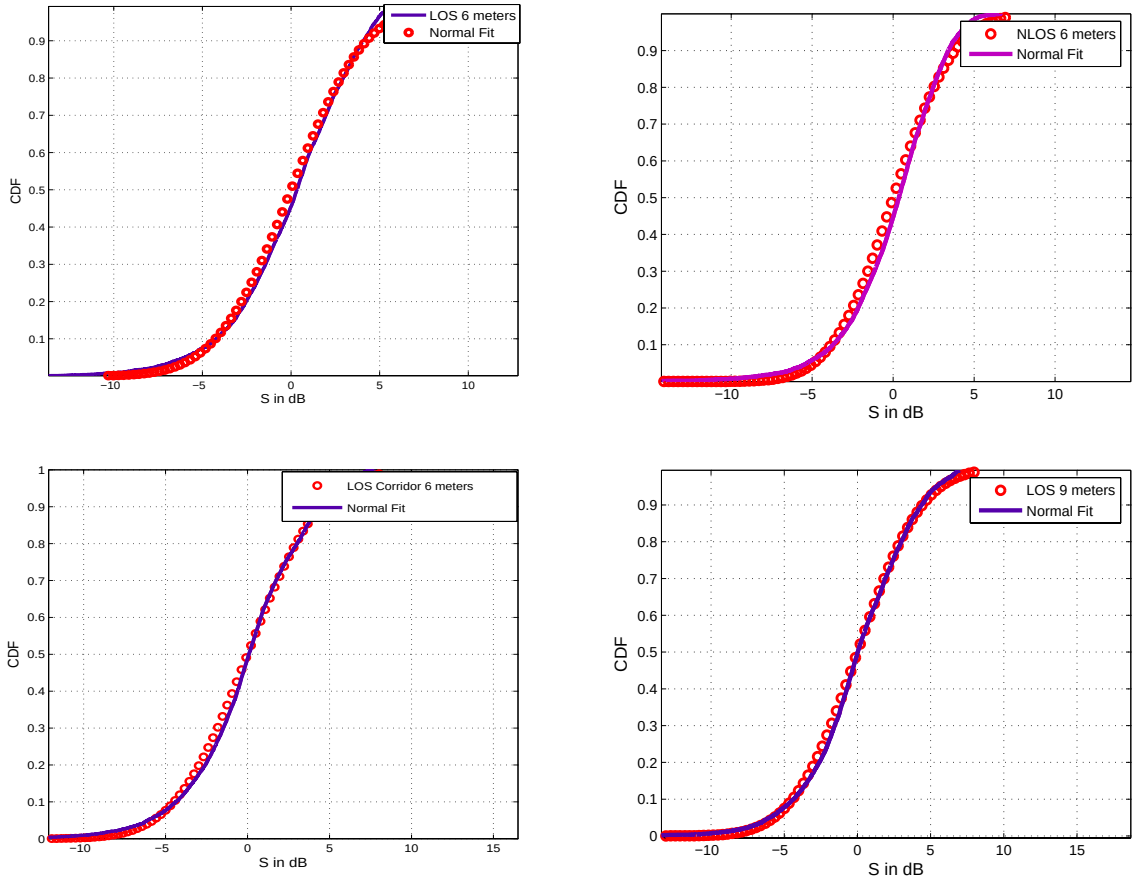

Figure 4.10: Cumulative distribution functions (CDFs) of shadowing fading fit to lognormal distribution under the LOS and NLOS scenarios for different channel settings.

another. It is a zero-mean Gaussian distributed random variables in dB with standard deviation σ_s which is also in dB. Different values of σ_s are obtained, ranging from 0.93 to 4.69 dB (see Table I in [CKYL05]) which are strongly dependent on the measurement environments and scenarios. The Figure 3 in [DMB06] shows the CDF of the deviation of the measured received power from the calculated average. The curves in general fit a log-normal distribution fairly well, although the NLOS scenarios exhibit some deviation from this distribution. The same results about shadowing is reported in [CKYL05]. We note that the log-normal shadowing assumption is used in [MASJWR06]

Figure 4.10 shows the cumulative distribution functions (CDFs) of the shadowing fading random variable S under the LOS and NLOS scenarios for different settings. The statistical analysis of S gives $\sigma_S = 1.1$, and the cumulative distribution of the deviation between the fitted and measured data is plotted versus the normal CDF on 4.10. These curves show that for all settings the shadowing fading fit a lognormal distribution well.

4.4.5 Power Variation and Frequency Fluctuations

Figures 4.11, 4.12, 4.13 and 4.14 show the pdf of the path loss fluctuations with respect to the two models of equations 4.3 and 4.4.

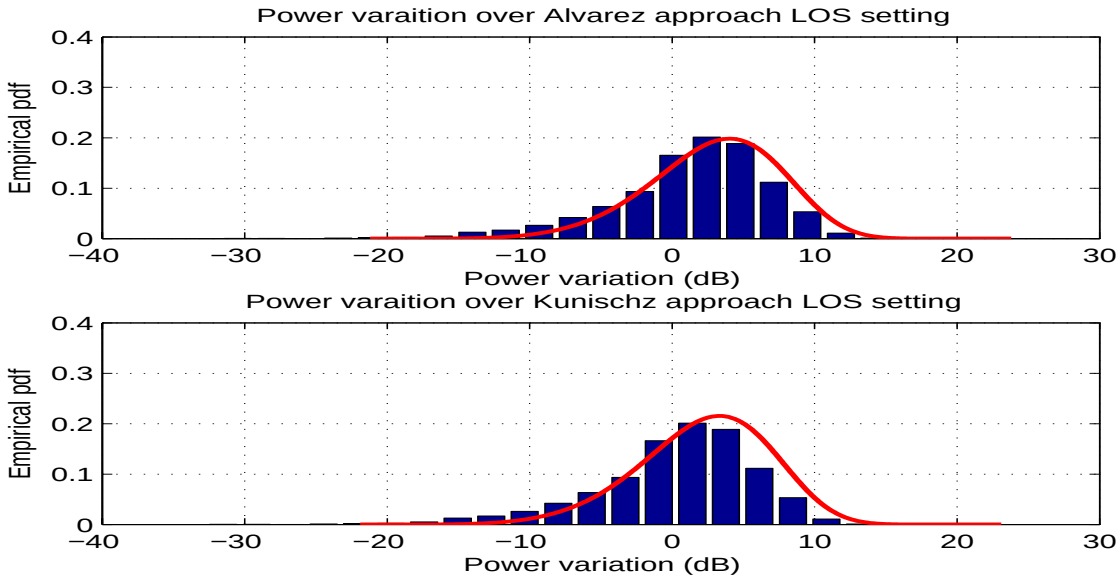

Figure 4.11: PDF of path loss fluctuations for Alvarez's and Kunisch's model LOS.

It can be observed how the Weibull pdf fits well with the experimental measurements. The model of equation (4.9) is adopted by the IEEE 802.15.4a standard [Mol05].

The pdf shape parameter of path loss fluctuations values are summarized in table (4.4).

4.4.6 Path Loss and Central Frequency Analysis

In order to assess the relationship between the central frequency and channel behavior in frequency domain, we evaluate the path loss versus central frequency using the following equation

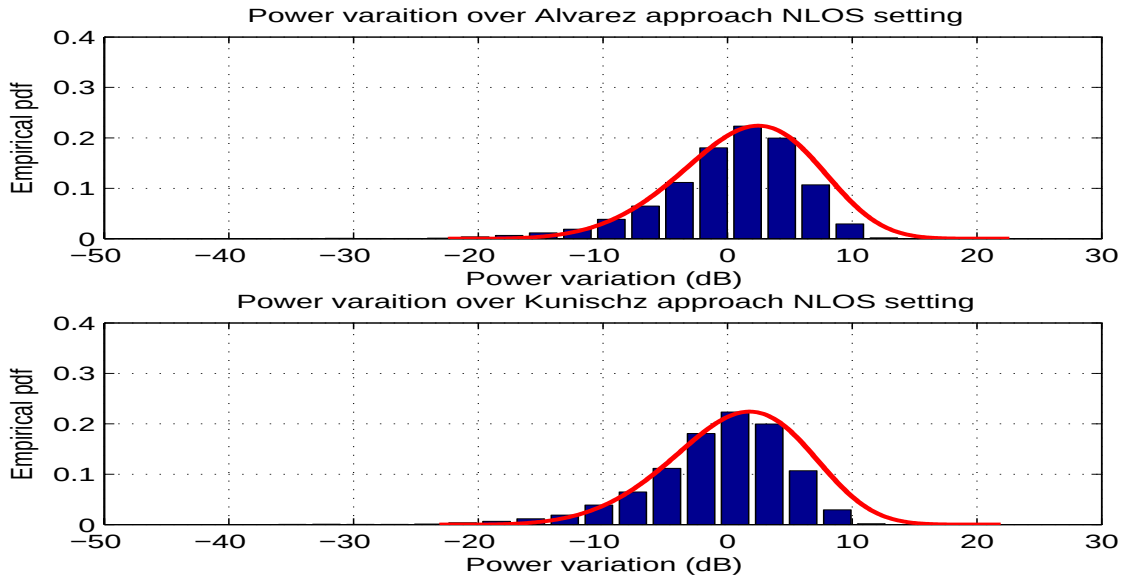

Figure 4.12: PDF of path loss fluctuations for Alvarez's and Kunisch's model NLOS.

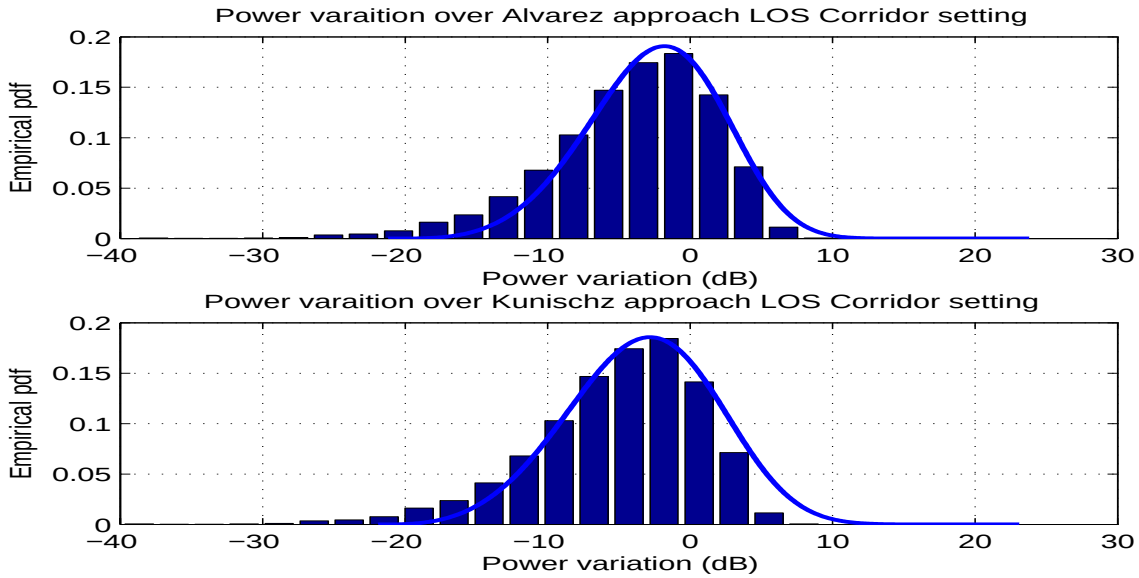

Figure 4.13: PDF of path loss fluctuations for Alvarez's and Kunisch's model: Corridor.

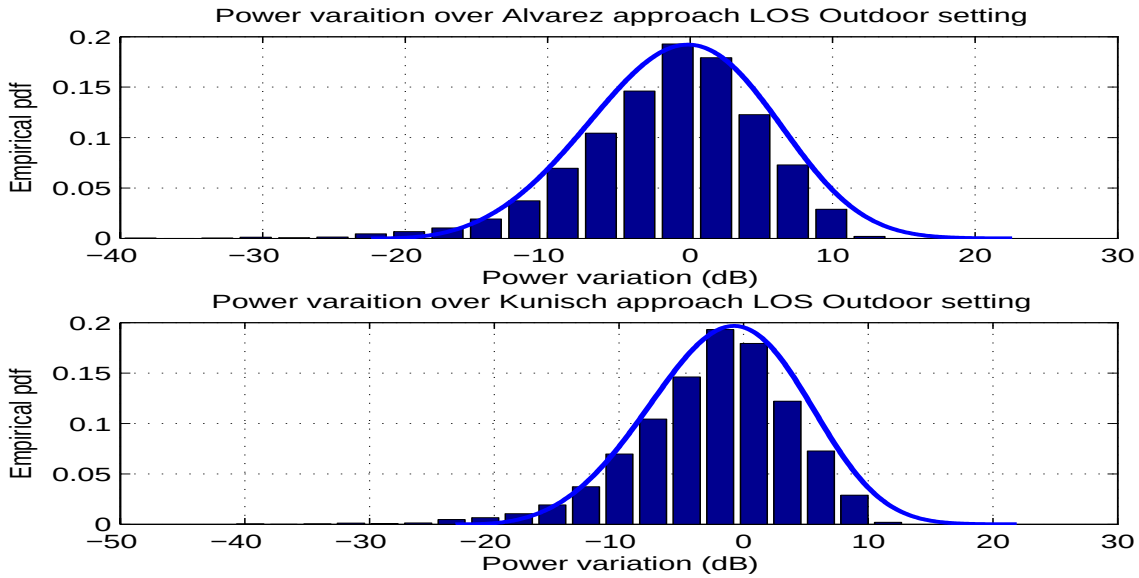

Figure 4.14: PDF of path loss fluctuations for Alvarez's and Kunisch's model: Outdoor.

Table 4.4: pdf shape parameter of path loss fluctuations

	Weibull density function parameters			
	Alvares's Model		Kunisch's Model	
Settings/Parameter	γ	α	γ	α
LOS	6	26	6	26
NLOS	5	26	5	26.1
Corridor	9	26	9	26
Outdoor	9	26	8	26
Static	9	26	8	26
LOS Lab (9 meters)	9	26	8	26

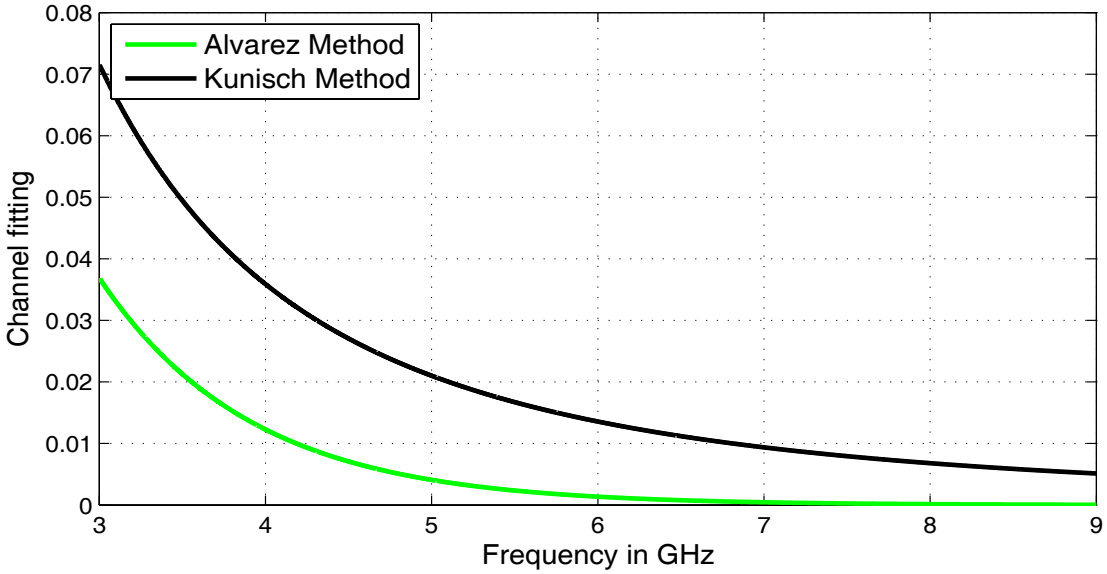

Figure 4.15: path loss channel fitting versus frequency for Corridor case (6 metres).

$$PL(f_c, B) = \frac{1}{MN} \sum_{m=1}^{m=M} \sum_{f_i=f_c-B/2}^{f_c+B/2} |H(f_i, t_m, f_c)|^2 \tag{4.10}$$

where f_c and B are respectively, the central frequency and the bandwidth. In our these parameters are fixed ($B = 500$MHz, $3.1\,\text{GHz} < f_c < 8.6\,\text{GHz}$ and $M = 120$). Figures 4.16 and 4.17 show this relationship for indoor LOS and indoor NLOS settings respectively. We conclude that the general trend of path loss behavior increases with central frequency.

4.5 Small-Scale Fading and Signal Quality

4.5.1 Small scale effects

The Indoor, Outdoor and Corridor UWB propagations constitute a channel with multiple paths. Many obstacles and objects are present (walls, electric wires, cables and metallic bar, glass windows, etc.) and they, more or less, act as reflective surfaces for the radio waves. Small scale variations in the channel response are caused by the combination of the multiple paths when the movement range of the receiver or the transmitter (or obstacles in between) is about a few signal's wavelengths. Large scale variations are caused by the losses in open space and the shadowing due to static obstacles or walls when the movement range is about a hundred times of the signal's wavelengths. The received signal at a given location is a function of the signal at the transmitter and the impulse responses of the channel and the antennas (in our analysis the antennas responses are included in the channel impulse response). To study the small scale effects[2], we focus on wireless channels that are commonly

[2]The non-linear effects are neglected in the UWB channel

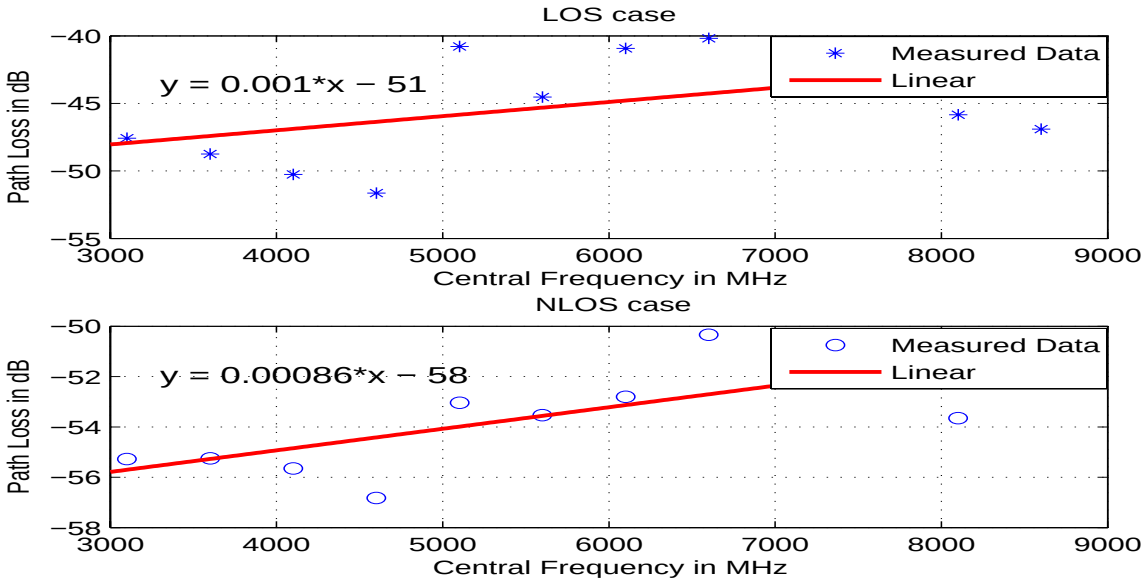

Figure 4.16: path loss versus central frequency: LOS and NLOS.

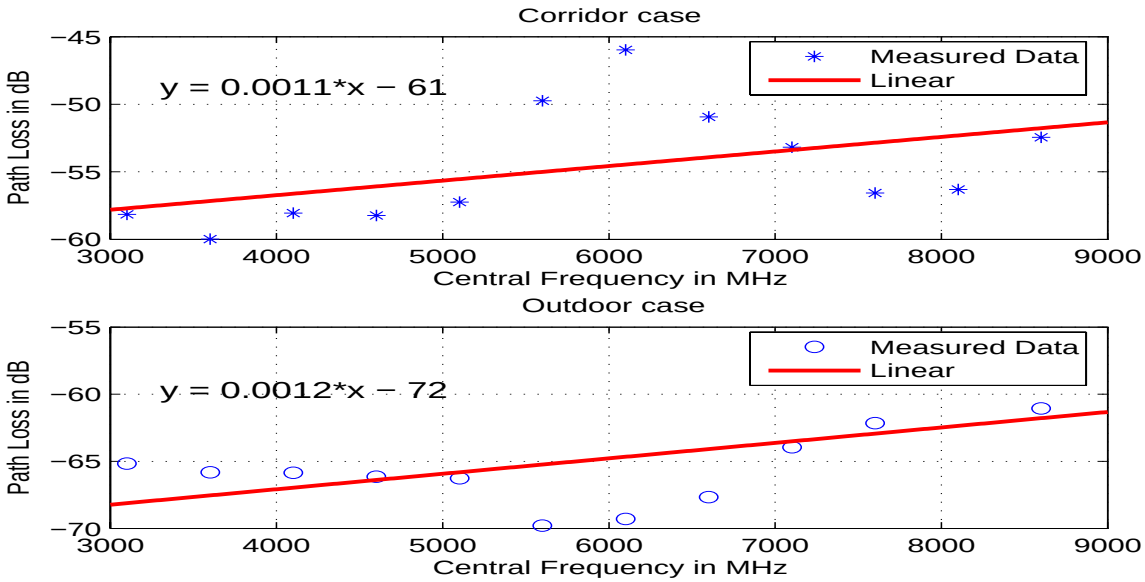

Figure 4.17: path loss versus central frequency: Corridor and Outdoor.

described by a linear filter where the received signal is given by:

$$r(t) = s(t) * h(t) + z(t) \tag{4.11}$$

where $s(t)$ is the transmitted signal, $h(t)$ is the CIR, and $z(t)$ is complex valued additive white Gaussian noise. The CIR can change as a function of time (or as a function of spatial variation) due to the motion of the transmitter or receiver and/or changes in the physical channel itself. If the channel is assumed to be static over the interval of observation, a time invariant model for the channel can be used:

$$h(t) = \sum_{l=0}^{L-1} a_l \delta(t - \tau_l) e^{-j\theta_l} \tag{4.12}$$

In [KWAea04a], it is stated that for an indoor channel the energy that falls within a certain delay bin is m-Nakagami distributed. In order to analyze if this is the case for our measurements, we have checked the fit of a set of channel realizations ($|hi|$ $(i = 1, 2, ...70)$) to the m-Nakagami distribution using the m-estimates given by the inverse normalized variance (INV) estimator [MA00],

$$\hat{m}_{INV} = \frac{\mu_2^2}{\mu_4 - \mu_2^2} \tag{4.13}$$

where

$$\mu_k = \frac{1}{L} \sum_{l=1}^{l=L} |h_l|^k \tag{4.14}$$

For our channel measurements, the good fit for the distribution is given by m close to 1 (figures 4.18

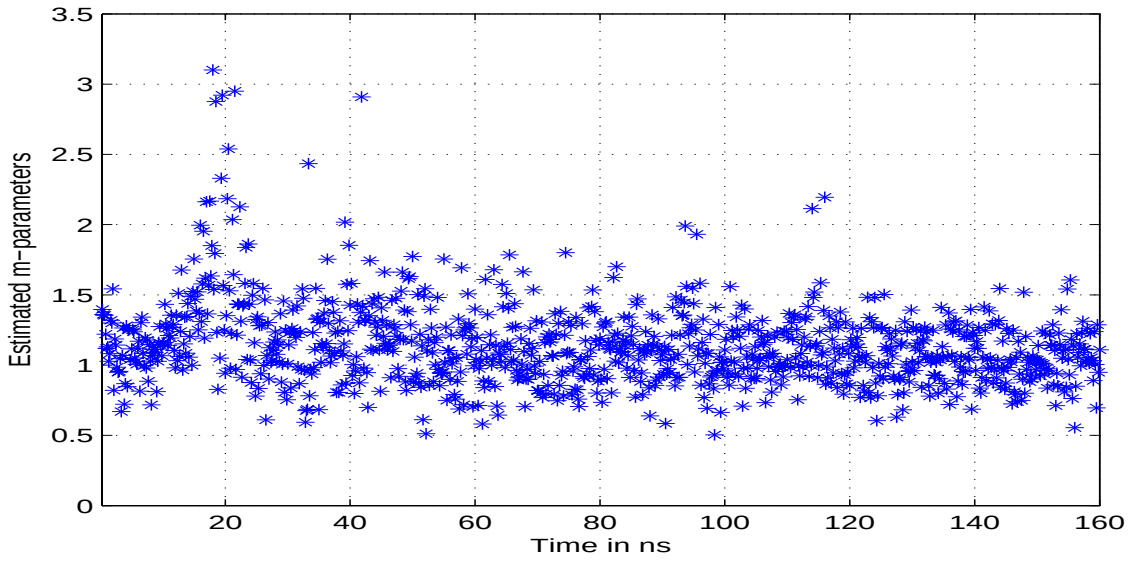

Figure 4.18: The m-parameter estimates for each delay bin of a 6 meters LOS.

and 4.19). The only exception is for the first components (before 20 ns) in each cluster which can show a high specular contribution. For the NLOS scenario the estimated parameter value is $m \simeq 1$

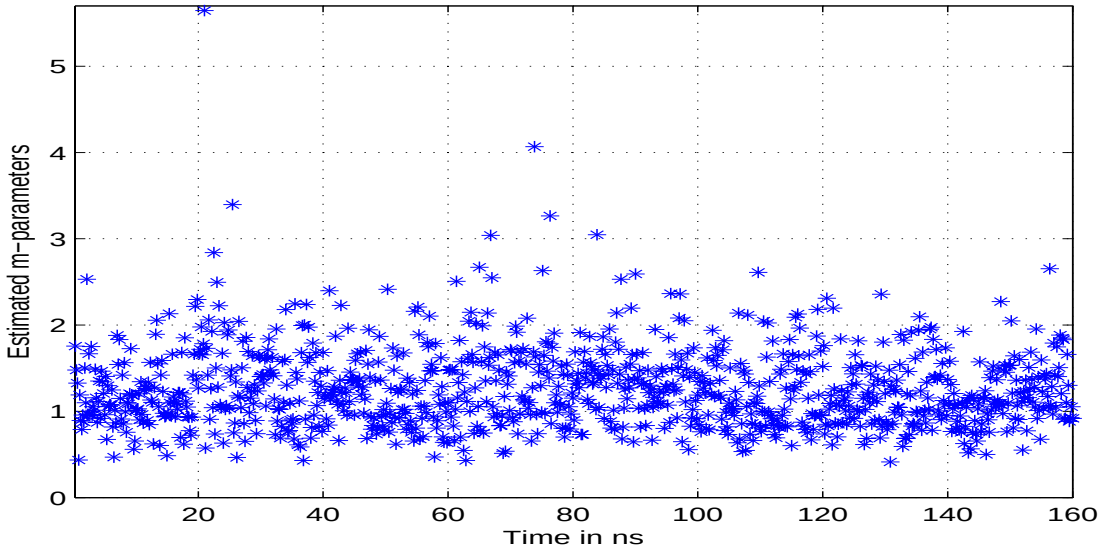

Figure 4.19: The m-parameter estimates for each delay bin of a 6 meters NLOS.

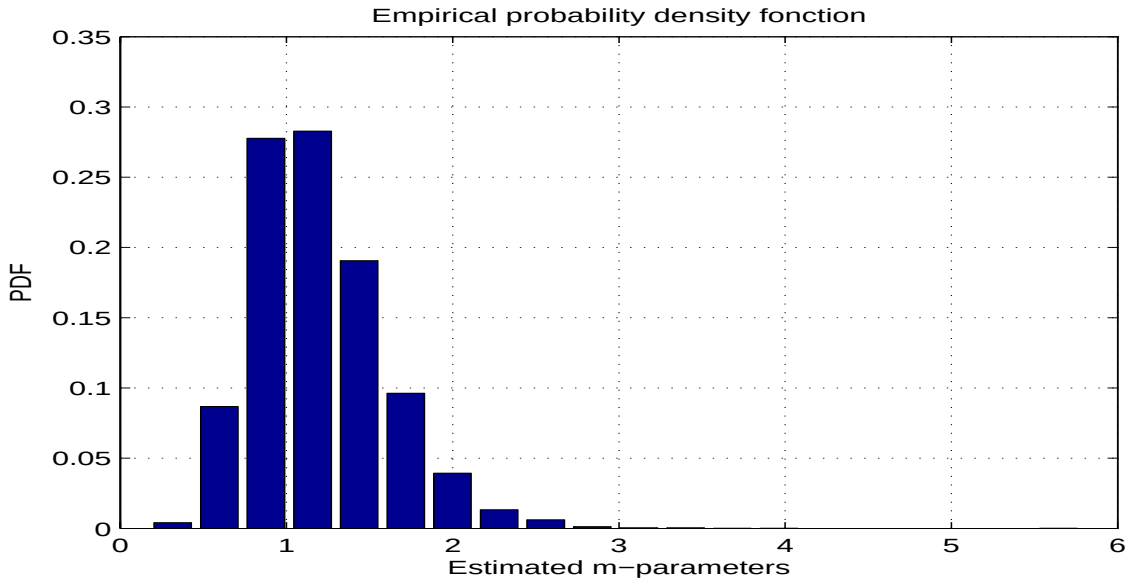

Figure 4.20: PDF for the m-parameter estimated for each delay bin in NLOS.

figure 4.20. The Nakagami model was first observed and used by Nakagami to the fading effects for short distance communications, who formulated a parametric gamma distribution-based density function to describe the experimental data he obtained [Saa03]. The table 4.5 presents different m-Nakagami value for different measurements location. Based on the analysis of the m values and it's distribution we conclude that the small fading corresponds to a Rayleigh distribution ($m = 1$).

Table 4.5: Estimated m-parameters

Parameter / Setting	LOS	NLOS	Corridor	Outdoor
$\tilde{m}$	1.093	1.13	1.09	.97

4.5.2 Signal Quality Analysis

In narrowband communication systems, small-scale fading describes the fluctuation due to constructive and destructive interference of the multipath components at the receiver when sub-wavelength changes are made in the receiver position. Such a definition can be extended to UWB communications as the constructive and destructive interference of the multipath components at the receiver due to a change in its position in the order of the sub-spatial width of the transmitted pulse. To quantify the variation of the received power for small-scale variations, let us consider the signal quality as defined by [MASJWR06]: The signal quality is defined as

$$Q = 10\log 10(\frac{E}{E_0}) = 10\log 10(E) - 10\log 10(E_0) \tag{4.15}$$

where E is the received signal energy given by

$$E = \int_0^T r^2(t)dt \tag{4.16}$$

where $r(t)$ is the received signal at Rx. E_0 is the energy measured at a reference location distance from the transmitter ($d_0 = 1$ m). The cumulative distribution functions (CDF) for the signal quality for some measured grids (3 locations; LOS 6 meters, LOS 9 meters and NLOS 6 meters) are shown in Figure 4.21. This result confirms the robustness of UWB communication systems against fading, as far as multipath is concerned, manifested by small variations in signal quality at various grid locations [MZW98].

4.5.3 Fading of Primary Path

In this subsection we want to examine the relationship between the bandwidth and fading. The Figure 4.22 shows that increased bandwidth reduces the fading experienced by the primary (strongest) multipath component. Concerning the average power of primary path the Figures 4.23 and 4.24 show for NLOS and LOS cases the evolution of the fraction of total energy found in the primary path versus the channel bandwidth. We have observed that increasing bandwidth allows to reduce the fading effects and also the average power of paths. We can explain all this by the fact that when bandwidth increases the number of paths increase and the energy is spread into other multipath. As bandwidth increases, the energy per resolvable multipath component decreases. For large bandwidths, the energy is spread into a large number of paths.

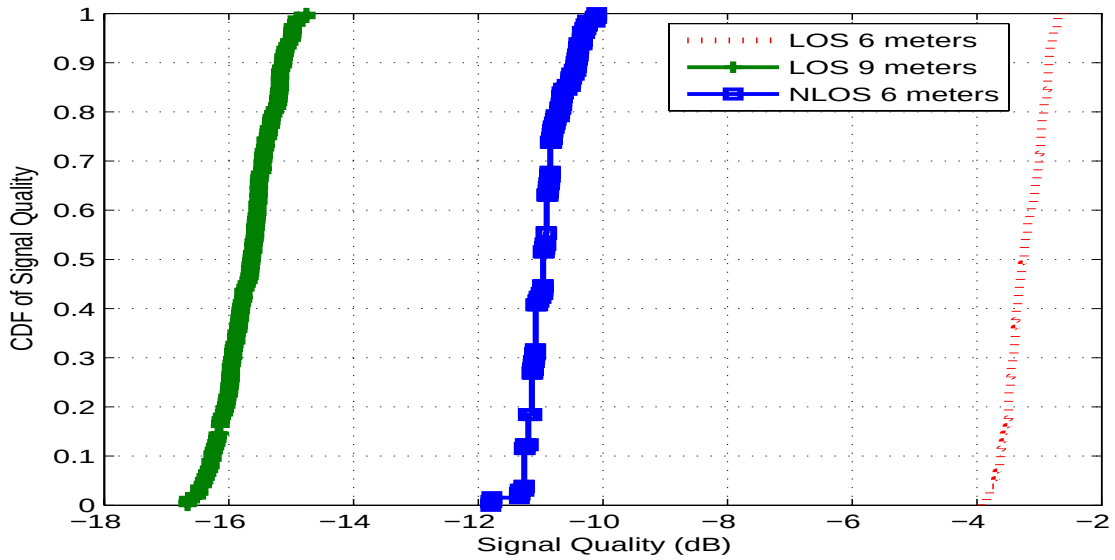

Figure 4.21: CDF of the signal quality based on 130 spatial sample points.

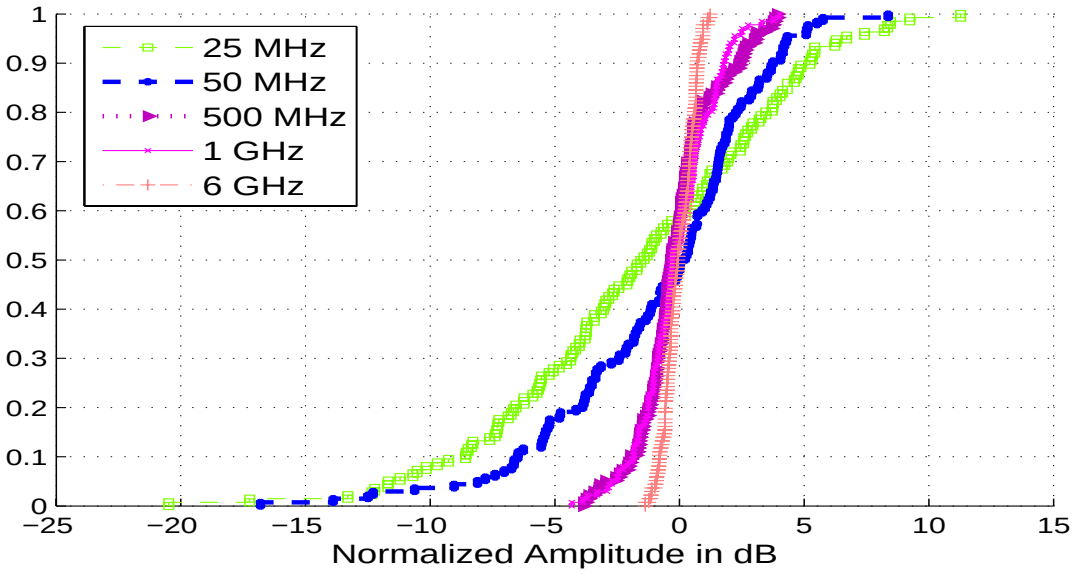

Figure 4.22: CDF of Normalized Amplitude.

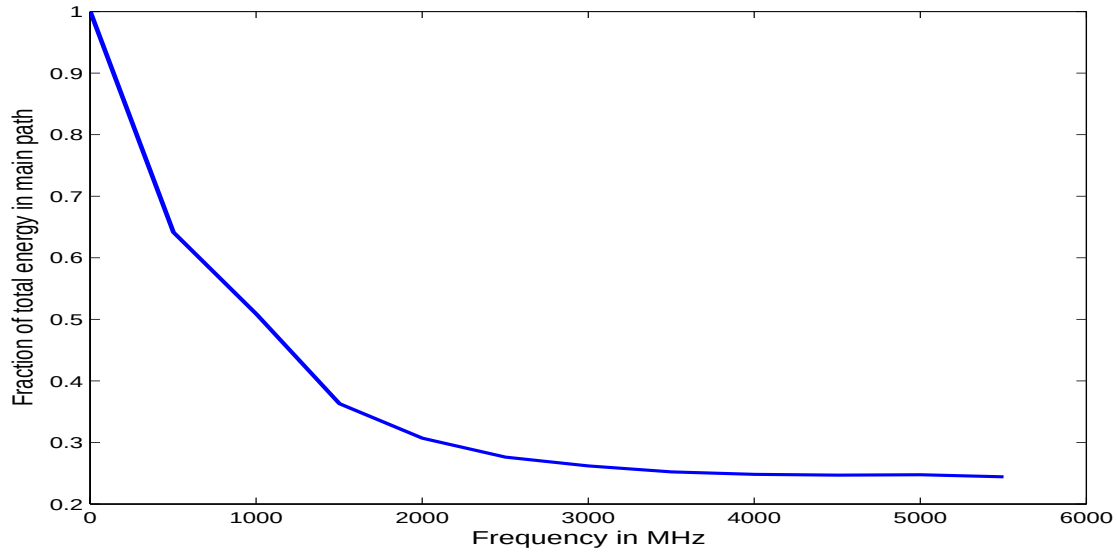

Figure 4.23: Fraction of total energy in the primary path NLOS case.

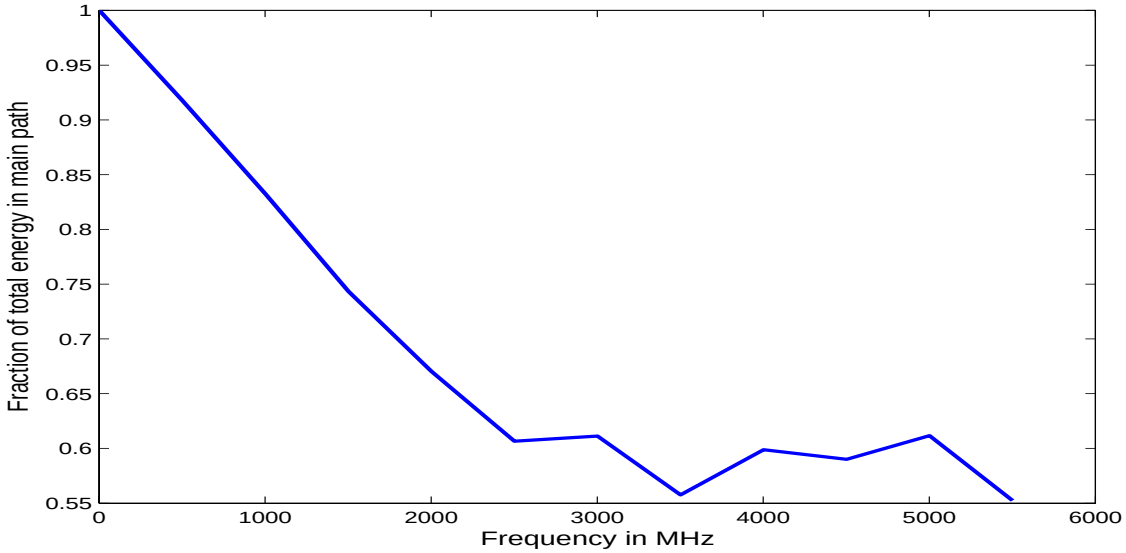

Figure 4.24: Fraction of total energy in the primary path LOS case.

Table 4.6: Results about small scale reported in previous measurement campaigns for LOS case

Researchers	τ_{rms}	τ_m	N_{paths}
Virginia Tech(Office)	5.41	5.19	24
TDC [Yan02][PB02]	5.27 (0-4m)	4.95 (0-4m)	24
CEA-LETI [KD03]	14-18	4-9	Not found
CEA-LETI [KPDR](1)	11.45 (home)	6.53 (home)	3.4 (hoe)
CEA-LETI [KPDR](2)	10.07 (office)	6.42 (office)	2 (office)
AT&T [GJRT02]	4.7	2.3	
AT&T [SSGT02]	4.7		
Intel [PCRH02, Foe02]	9	4	7
802.15 model [Foe02]	5.3	5.1	24

4.6 The Dispersive Properties of UWB Channel

4.6.1 Mean Excess Delay and Time Delay Spread

The dispersive properties of UWB channel can be considered as extension of the large scale study of the channel. The are two parameters to be characterized and analyzed. These parameters are the mean excess delay τ_m and delay spread τ_{rms}. The mean excess delay τ_m and τ_{rms} delay spread are two important parameters used to characterize the temporal dispersive properties of the multipath channels. This is useful to estimate the performance and potential for ISI. These values tend to increase with large Tx/Rx separation distance. The mean excess delay τ_m is defined as the first moment of the power delay profile (PDP) and is defined as:

$$\tau_m = \overline{\tau} = \frac{\sum_{l=0}^{L-1} \tau_l |a_l|^2}{\sum_{l=0}^{L-1} |a_l|^2}. \tag{4.17}$$

with $P(a_l) = a_l^2$

where a_l, τ_l and $P(a_l)$ are the gain coefficient, delay and PDP of the l^{th} multipath component. The τ_{rms} delay spread, $P(\tau_{rms})$ is the square root of the second central moment of the PDP and is defined to be:

$$\tau_{rms} = \sqrt{\overline{\tau^2} - \tau_m^2} \tag{4.18}$$

where the $\overline{\tau^2}$ is given by

$$\overline{\tau^2} = \frac{\sum_{l=0}^{L-1} \tau^2 |a_l|^2}{\sum_{l=0}^{L-1} |a_l|^2}. \tag{4.19}$$

τ_{rms} is seen to be the second centralized moment of the normalized power delay profile.

Typical values for the τ_{rms} delay spread for indoor channels have been reported to be between 10 and 50 ns, and mean values between 20 and 30 ns for 5 to 30 m antennas separation distance were reported in [HT94], Tables 4.6 and 4.7 present an illustaration of reported results in the literature for the RMS delay spread, τ_{rms}, the mean excess delay, τ_m, and the number of paths N_{paths}.

In addition, the multipath delay spread has been found to increase with increasing separation distance between the receiving and transmitting antennas, and the mean increases with the threshold

Table 4.7: Results about small scale reported in previous measurement campaigns for NLOS case

Researchers	τ_{rms}	τ_m	N_{paths}
Virginia Tech(Office)	13.7	16	72
USC [CSMZ99] [CSW02]	45-74	59-126	
TDC [Yan02][PB02]	8.78 (0-4m)	10.04 (0-4m)	36.1 (0-4m)
TDC [Yan02][PB02]	14.59 (4-10m)	14.24 (4-10m)	61.6 (4-10m)
CEA-LETI [KD03]	14-18	17-23	
CEA [KPDR]	14.78 (4-10m)	16.01 (4-10m)	46.8 (4-10m)
CEA [KPDR]	17.64 (10-20m)	18.85 (10-20m)	75.8 (10-20m)
AT&T [GJRT02]	9.3 (-15 dB)	10.3 (-15 dB)	48 (-15 dB)
AT&T [GJRT02]	11.5 (-30 dB)	12.4 (-30 dB)	82 (-30 dB)
AT&T Ghassemzadeh$_2$002	8.5		
Intel [PCRH02, Foe02]	15	17	35
802.15 model [Foe02]	8/14.3	10.4/14.2	36/62

level (TL) [J.F01]. In [CDC05] Ciccognani et al. is presented an accurate analysis of the time dispersion parameters, showing for both LOS and NLOS scenarios a strong dependence of the mean excess delay on the SNR detected at the receiver side. A very slight correlation instead has been noticed between the RMS delay spread and the path loss, mainly related to the shadowing effects [CDC05]. The RMS delay spread has been shown to decrease considerably when using directional antennas as opposed to using omnidirectional antennas [DHG].

Tables 4.8 and 4.9 present the main values of τ_m and τ_{rms} that obtained in Eurecom measurements for different channel settings [SHKA05a].

Another important parameter which can be used as an effective measure of the time dispersion is the ratio $\rho_{\tau_m/\tau_{rms}} = \tau_m/\tau_{rms}$. Indeed, lower values of this ratio indicate that a higher power level is concentrated at small values of the excess delay (the concentration of the energy in the direct path). The measurement environments and the characteristics of the probing signals considerably influence the statistics of the time dispersion parameters and even the correlation between them. For instance, the existence of a clear LOS path between the transmitter and the receiver reflects on the ratio of the average arrival time to the spread of the arrival times [DJ99].

As we argued above the ratio of the mean excess delay to the τ_{rms} delay spread can be used as a measure of the time dispersion for UWB signals particularly, if $\rho_{\tau_m/\tau_{rms}} = 1$, the multipath delay profile decays exponentially. This situation corresponds to two multipath components with equal power where the second path is $2\tau_m$ away from the first component. High concentration of power when the excess delay is small is reflected by $\rho_{\tau_m/\tau_{rms}} < 1$. When energy arrives at the mid point of the power delay profile and not at the earliest part then $\rho_{\tau_m/\tau_{rms}} > 1$ [MASJWR06].

From the Figures 5.4 and 5.5, initial observation of the Average Power Delay Profiles (APDPs) show that the clustering phenomenon exists in both LOS and NLOS scenarios with more number of clusters under the NLOS scenario. These multiple clusters are due to the multiple order reflections, scattering and diffraction that occurred in the environment [SHKA05a]. Figures 4.29 and 4.30 show the $\rho_{\tau_m/\tau_{rms}}$ behaviors for LOS and NLOS cases respectively. From these figures we conclude that a high concentration of energy is observed in the first paths of the PDP in the LOS case and in the mid

Table 4.8: Table of Averages Delay Statistics in the time domain, With Windowing

Scenarios Parameters	τ_{rms} in ns (TL: 20 dB)	τ_m in ns (TL: 20 dB)	NP_{10dB}
LOS CM1 (6 meters, grid)	6.8179	4.8366	25
LOS CM2 (6 meters, grid)	13.769	17.699	24
NLOS CM1 (6 meters, grid)	15.186	24.285	52
NLOS CM2 (6 meters, grid)	13.769	17.7699	53
LOS CM2 (9 meters, grid)	12.033	35.065	26
LOS CM2 (6 meters, Fix)	7.6730	6.4861	20
LOS CM1 (7 meters, grid)	7.16	35.06	25
LOS Corridor (7 meters, grid)	9.7673	5.2105	25
LOS Outdoor (6 meters, grid)	3.5867	2.6735	17

Table 4.9: Table of Averages Delay Statistics in the time domain, Without Windowing

Scenarios Parameters	τ_{rms} in ns (20 dB)	τ_m in ns (20 dB)	NP_{10dB}
LOS CM1 (6 meters, grid)	8.9	6.6	27
LOS CM2 (6 meters, grid)	8.5	8.47	x
LOS CM2 (7 meters, grid)	7.71	38.5	
NLOS CM1 (6 meters, grid)	12.6	27.3	24
NLOS CM2 (6 meters, grid)	13.1	20.4	54
LOS CM2 (9 meters, grid)	24.48	40.3	26
LOS CM2 (6 meters, Fix)	9.19	5.9	
LOS Corridor (7 meters, grid)	19.46	26.01	26
LOS Outdoor (6 meters, grid)	4.44	3.26	18

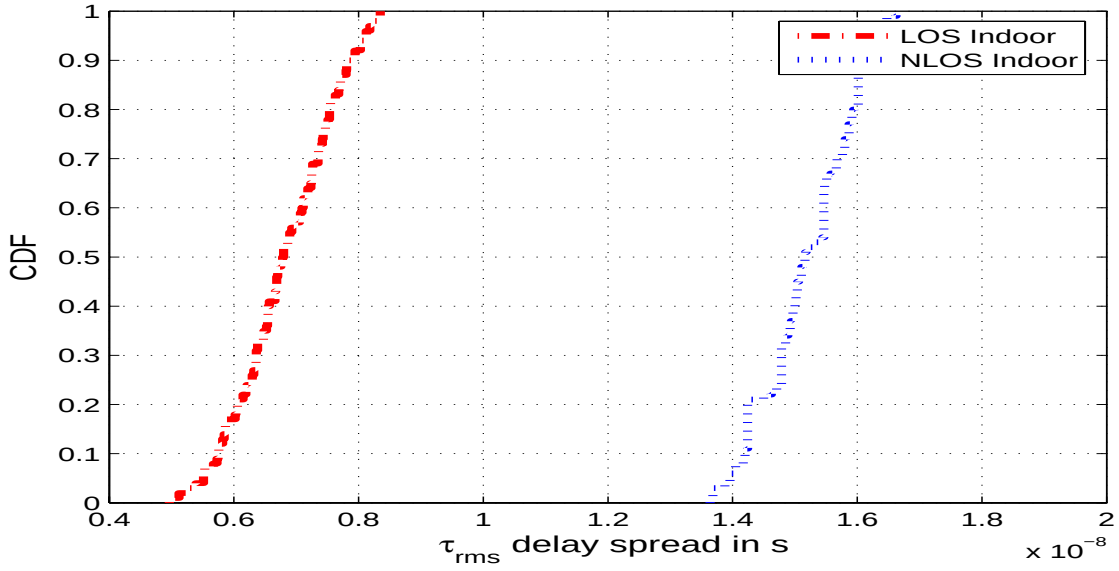

Figure 4.25: RMS Delay Spread CDFs for LOS and NLOS

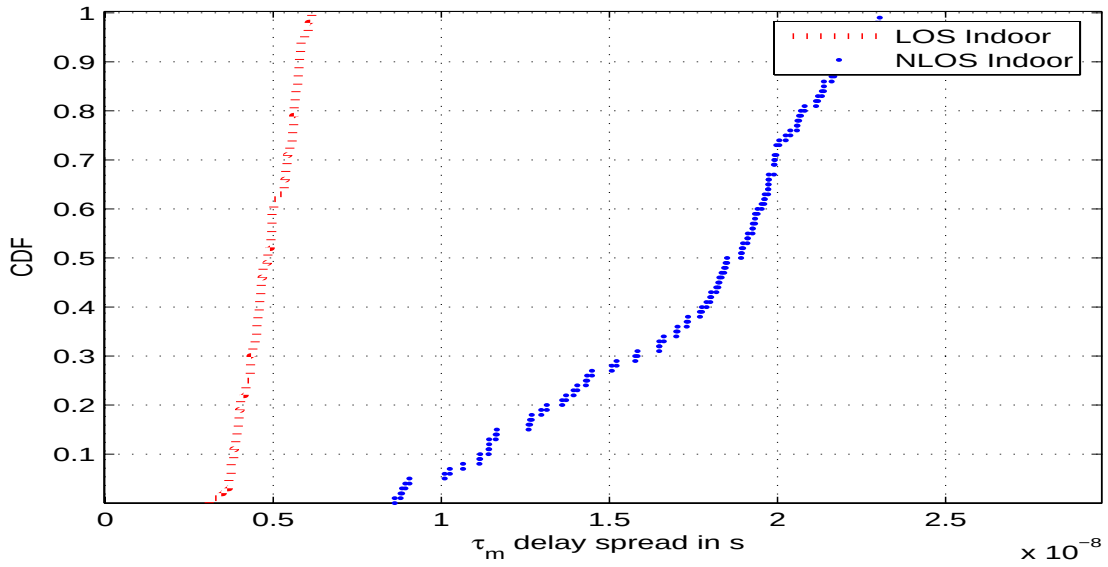

Figure 4.26: Mean excess delay CDFs for LOS and NLOS

paths of the PDP in the NLOS case.

4.7 Conclusion

We have investigated UWB propagation channels under different sittings (LOS, NLOS indoor, corridor,...), and analyzed a statistical model that describes the behavior of the channel. We found out that the power variation and the path loss can be well described by a Weibull distribution model. Also, we have observed that there was no correlation between the path loss and the frequency bandwidth of interest. This can be explained by the form of antenna's $S21$ parameter response. On the other hand, a distance frequency dependency is shown for LOS case. Moreover, a correlation between the central frequency and path loss is indicated for most measured data, we have found that for large bandwidth values, energy is spread into a large number of paths. Finally, The calculated time dispersion parameters for the measured results indicate high concentration of power at low excess time delays for all the considered scenarios.

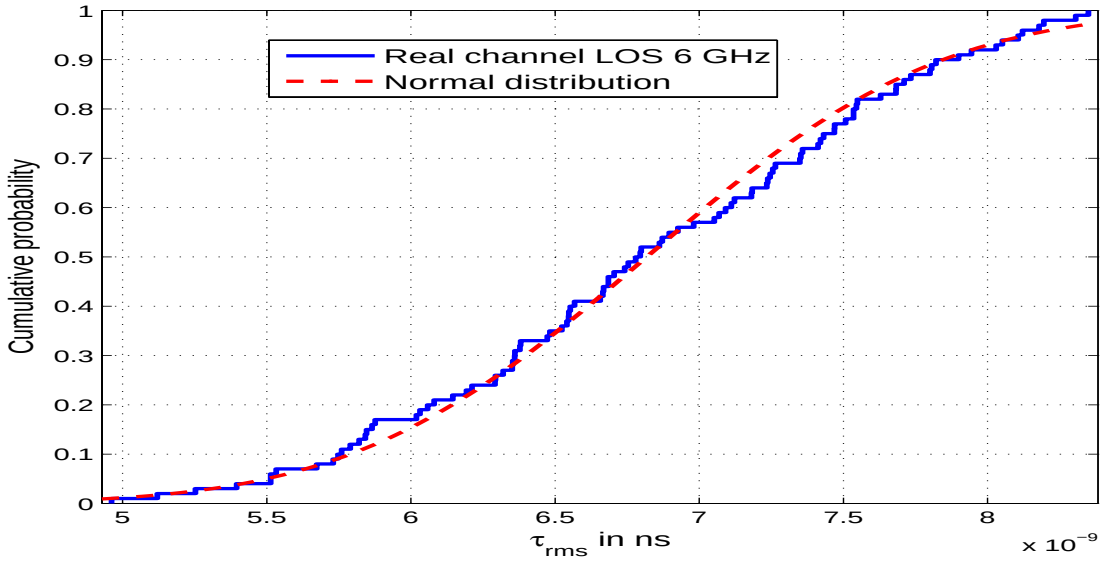

Figure 4.27: CDF of τ_{rms} fit to normal distribution under the LOS setting.

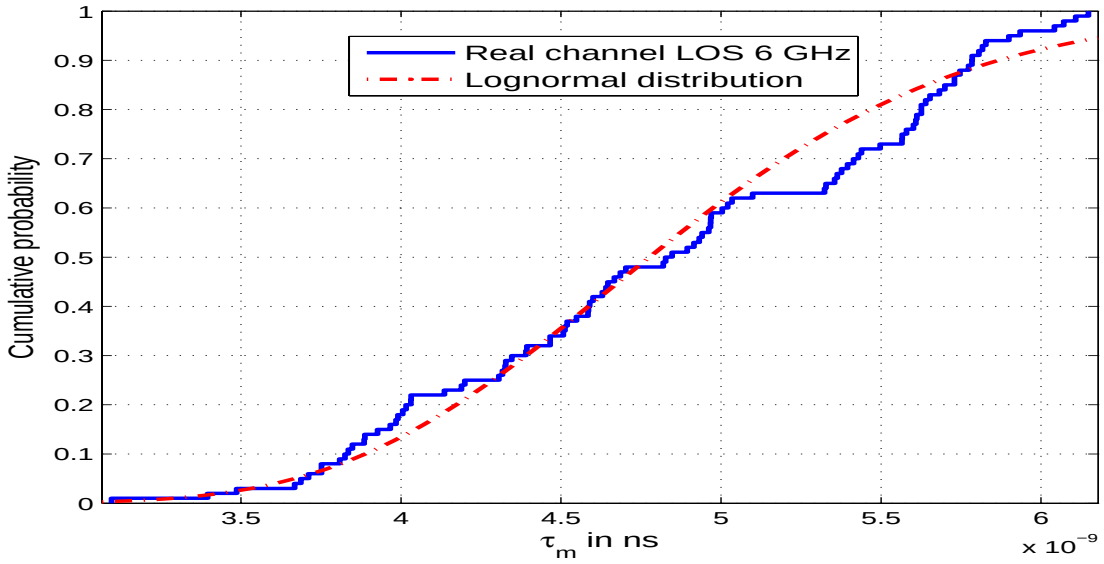

Figure 4.28: CDF of τ_m fit to normal distribution under the LOS setting.

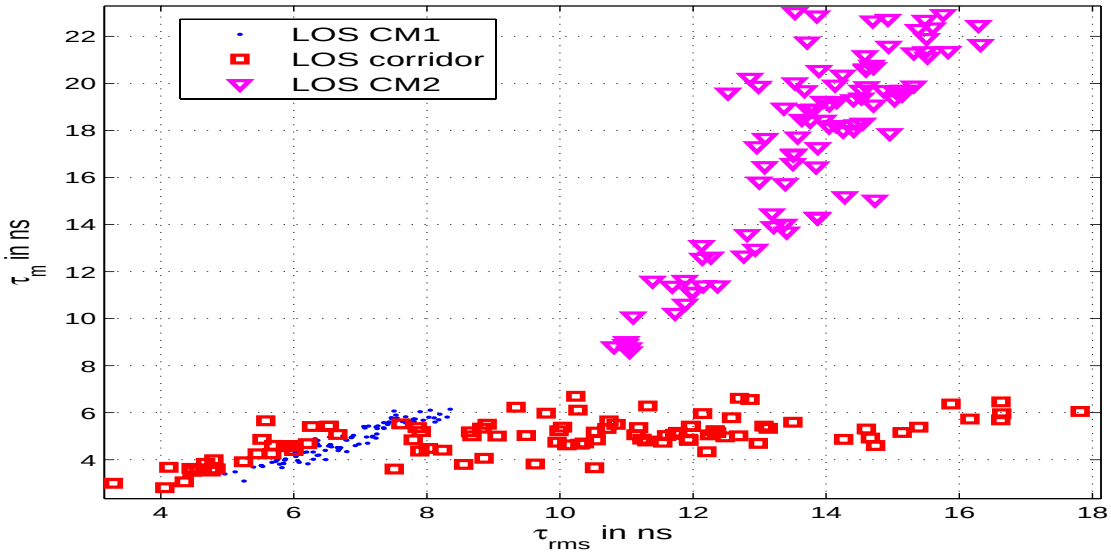

Figure 4.29: Ratio of τ_m to τ_{rms} for LOS cases.

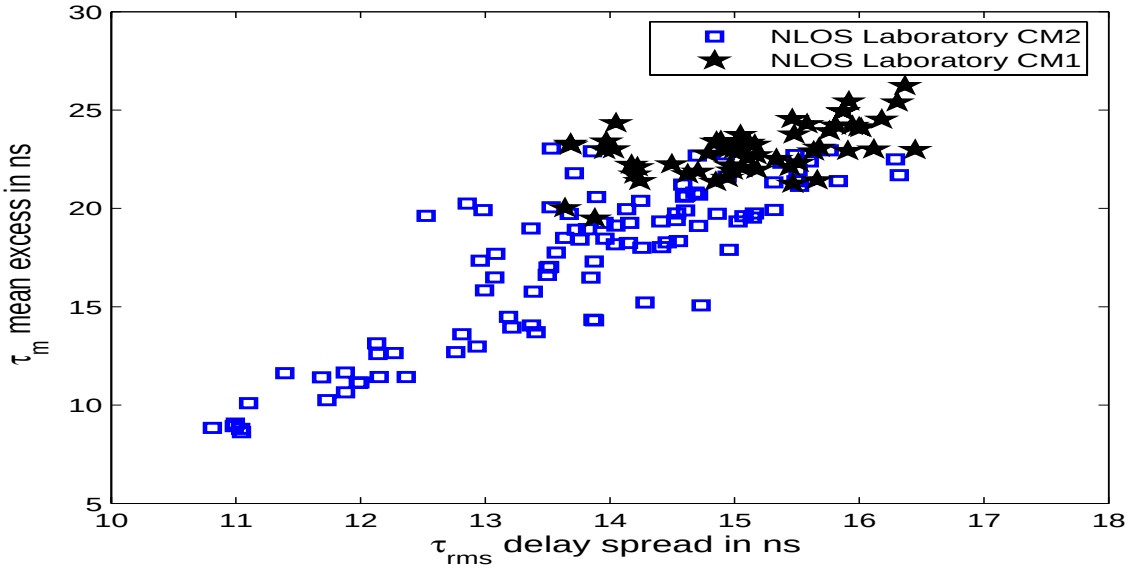

Figure 4.30: Ratio of τ_m to τ_{rms} for NLOS versus threshold of SNR.

CHAPTER

5

UWB CHANNEL AND SUB-SPACE ANALYSIS

5.1 Introduction

From a communication-theoretic perspective, the number of resolvable multipath components reflects the number of independent DoF in the channel [SA99], [SV02], which in turn governs fundamental performance limits. When the channel coefficients corresponding to the resolvable multipath are perfectly known at the receiver (coherent regime), the DoF reflect the level of delay-Doppler diversity afforded by the channel [SV02]. On the other hand, when the channel coefficients are unknown at the receiver (non-coherent regime), then the DoF reflect the level of uncertainty in the channel. The UWB communication systems are defined by a large channel bandwidth. The question is how the number of DoF evolves with channel bandwidth.

The capacity of multipath channel in the limit of infinite bandwidth is identical to the capacity of the AWGN channel

$$\lim_{B\to\infty} \log_2(1+\frac{P}{BN_0}) = \frac{P}{N_0}\log_2(e) \tag{5.1}$$

where P is the received power and N_0 is the one sided noise spectral level. Golay shows that this capacity, with non fading channels, can be approached by On-Off keying (pulse position modulation) with low duty cycle [Gol49]. Also, Telatar and Tse in 2000 show that: With spectrum signals over multipath channels, the data rate is inversely proportional to the number of channel paths [TT00]. In the direct sequence spread spectrum without duty cycle system the throughput tends to zero in the limit if the number of multipaths increases. The question here is that: **How does the number of multipaths increases with the channel bandwidth?**

When the bandwidth increases, the temporal resolution increases too, this allows to discover the hidden paths, but beyond a given bandwidth all the independent paths are resolved (the new resolvable paths are mostly dependent to the ones already resolved). Physically the growth of number of multipaths with channel bandwidth can be explained as follow: The number of multipaths increases with the bandwidth because the reflection (due to constitutive parameters) and diffraction mechanisms are frequency and bandwidth dependent. To evaluate the number of paths in a given environment that corresponds a sitting (LOS or NLOS) for a given bandwidth, we use DoF (representing the number of independent paths) that is based on the eigen decomposition of channel covariance matrix (to extract the independent components in the channel i.e., independent paths.

This Chapter aims at characterizing the second order statistics of indoor UWB channels using channel sounding techniques. These are based on a eigen-decomposition of the channel autocovariance matrix, which leads to an analysis of the growth in the number of significant DoF of the channel process as a function of the signaling bandwidth as well as the statistical correlation between different propagation paths. We show empirical eigenvalue distributions as a function of the signal bandwidth

for both line-of-sight and non line-of-sight situations. Furthermore, we give examples where paths from different propagation clusters (possibly arising from reflection or diffraction) show strong statistical dependence. The expected bandwidths of these systems are one the order of gigahertz, which has significant implications both for systems design and implementation. The goal of this Chapter is to determine the result of these extremely large system bandwidths on the second order statistics of the propagation channel as it is seen by the underlying system. We are primarily interested in assessing the growth in the number of DoF needed to characterize the channel as a function of the system bandwidth empirically and using the *Akaike information criterion* AIC and the *Minimum Description Length* MDL. We are also interested in the product of RMS delay spread with bandwidth to address DoF scaling behavior for both LOS and NLOS cases. To assess the channel uncertainty, the channel entropy is also evaluated.

5.2 UWB Eigenanalysis

The classical approach [H.H93a] [HD94] [H.H93b] used for the characterization of the selectivity of multipath fading channels, is based on root mean square (rms) delay spread T_d. This parameter or equivalently the *coherence bandwidth* B_c[1] defined as

$$B_c = \frac{k}{T_d} \tag{5.2}$$

where $0 < k < 1$ is a constant is widely used as a measure of channel frequency selectivity. This approach is considered right when the signal bandwidth comprises a small number of coherence bandwidths. In other words, the coherence bandwidth varies over cellular or PCS communications paths because the multipath spread T_d varies from path to path. But in wide band or UWB channels, this study will show that the coherence bandwidth can only be viewed as a local measure and does not give an accurate description of channel selectivity. Similar ideas for channel bandwidths on the order of tens of megahertz were also suggested in [DSY00].

5.2.1 Eigen-Decomposition of Covariance Matrix

The radio-propagation channel is randomly time-varying due to variations in the environment and mobility of transmitters and receivers. It is classically represented, following the work of Bello [Bel63, Bel64] by its input delay-spread function $h(t, \tau)$ called also, by abuse of language, the time-varying Channel Impulse Response (CIR). The variable t in the CIR notation represents the time-varying behavior of the channel caused by the mobility of either the transmitter, the receiver or the scatterers. The second variable τ represents the delay domain in which we characterize the channel regarding the most important arriving paths. We consider for each measurement a fixed position at the transmitter and the receiver sides, and a static environment (at least during the time-frame of one measurement). We are thus considering a static channel and we can then simplify the notation of the CIR by dropping its dependence on t. In what follows, $h(\tau)$ is simply replaced by $h(t)$.

[1]Definition: Coherence bandwidth is a statistical measurement of the range of frequencies over which the channel can be considered "flat", or in other words the approximate maximum bandwidth or frequency interval over which two frequencies of a signal are likely to experience comparable or correlated amplitude fading. If the multipath time delay spread equals D seconds, then the coherence bandwidth W_c in hertz is given approximately by the equation: $W_c = \frac{1}{2\pi D}$

Let $\mathbf{h(t)} = [h_{W,1}(t), h_{W,2}(t), ..., h_{W,N}(t)]$ be the channel process obtained from measurements for N different antenna configurations, where $h_{W,i}(t)$ is expressed as

$$h_i(t) = g_i(t) + n_i(t), i = 1..N, \tag{5.3}$$

where $n_i(t)$ is zero-mean additive white Gaussian noise with power spectral density equal to σ_n^2 at all frequencies in the bandwidth of interest. We neglect any non-linear perturbation caused by measurement elements (e.g. VNA amplifiers), which were treated in a more general setting in [MMH+02]. We include the frequency response of the antenna as part of the channel response as argued in the previous section, and moreover, the linear response of the equipment is assumed to be perfectly accounted for in the calibration of the measurement apparatus. The noise process, resulting from thermal noise in the receive chain of the VNA and the noise generated by device itself, is assumed to be white in the band of interest. We therefore have that $\mathbf{g}(t) = [g_1(t), g_2(t), ..., g_N(t)]$ are the observations of the noise-free channel process corresponding to N observation positions. Due to the rapid variation of the wave's phase (from 0 to 2π over one wavelength), we can assume that the received electric field at each position represents a zero-mean process, and thus $g(t)$ is taken to be zero-mean. We remark that this does not rule out the possibility of LOS propagation as will be treated shortly.

The VNA provides samples of the observed channel process in the frequency domain, $H(k\Delta f)$, where Δf is the frequency separation, in our case 1 MHz. Furthermore, it is a filtered version of the channel response, where the filter corresponds to an ideal bandpass filter of bandwidth W centered at $f_c = (f_{\max} - f_{\min})/2$, as shown in figure 5.1. After removing the carrier frequency f_c, we denote the complex baseband equivalent filtered channel by $h_W(t)$. By sampling the frequency response in the VNA we obtain an aliased version of $h_W(t)$ denoted by $\tilde{h}_W(t) = \sum_k h_W(t - k/\Delta f)$. The time-domain samples obtained by performing an inverse discrete Fourier transform (IDFT) on the vector $\mathbf{H} = \begin{pmatrix} H(0) & H(\Delta f) & \cdots & H((N-1)\Delta f) \end{pmatrix}^T$ are samples of $\tilde{h}_W(t)$ at sampling frequency W Hz. We note that the choice of frequency separation Δf has an impact on how closely $\tilde{h}_W(t)$ approximates $h_W(t)$ in the interval $[0, 1/\Delta f)$. In our case the choice of $\Delta f = 1$ MHz guarantees that the approximation will be very accurate since the typical delay spread of the considered channels is less than 100 ns and therefore time-domain aliasing will not distort the channel measurement. For this reason we assume in what follows that the measurement equipment provides perfect samples of $h_W(t)$.

Our approach to characterize the UWB propagation channel is based on the analysis of the channel subspace and the eigen-decomposition of the covariance matrix, $\mathbf{K_h}$, of the samples of $h_W(t)$, denoted by the vector $\mathbf{h} = \begin{pmatrix} h_W(0) & h_W\left(\frac{1}{W}\right) & \cdots & h_W\left(\frac{p-1}{W}\right) \end{pmatrix}^T$, where p is the length of the channel used for statistical analysis with $0 \leq p \leq \frac{1}{\Delta F} - \frac{1}{W}$. This allows us to estimate the number of DoF characterizing $h_W(t)$ [SP78]. A similar approach for estimating the (finite) unknown number of Gaussian signals using a finite set of noisy observations is described in [MT85][Wil94]. These techniques amount to determining the finite dimension of the signal subspace.

In order to estimate the true covariance matrix $\mathbf{K_h}$, we use statistical averages based on observations from (20×50) positions. The sample covariance matrix is a maximum-likelihood estimate, under the assumption of a large number of independent channel observations [And84] which arise from the different transmitting and receiving antenna positions as explained earlier. The separation between positions on the grids must be large enough to obtain sufficient variation of the wave's phase, $\Delta\phi$ [2], in order to extract all the DoF of the channel. On the other hand, the separation must be small

[2] $\Delta\phi = \frac{2\pi d}{\lambda}$ is the wave's phase variation between two positions, d is the corresponding distance and λ is the wavelength varying from 3 to 10 cm for a UWB channel bandwidth ranging from 3 to 10 GHz

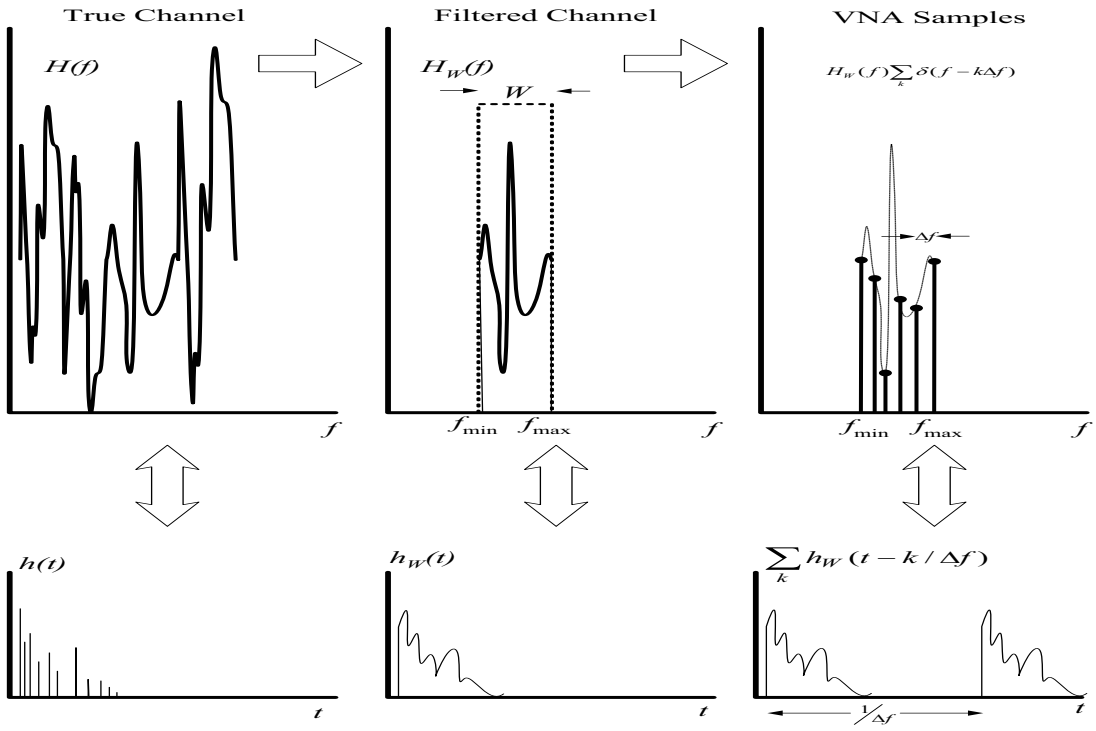

Figure 5.1: Channel Representations

enough to ensure that the distance between transmitter and the receiver (6 m in our primary measurement scenario) remains virtually constant. If both constraints are satisfied we can assume that $\mathbf{K_h}$ will depend solely on the slowly-varying parameters (distance, arrival angles, scatterers, geometrical settings,...) and thus will not vary significantly across the set of the total transmitter and receiver positions. The covariance matrix of measured channel samples, $\mathbf{h}$, is written as

$$\mathbf{K_h} = E[\mathbf{h}\mathbf{h}^H] = E[\mathbf{g}\mathbf{g}^H] + \sigma_n^2\mathbf{I} \tag{5.4}$$

where $\mathbf{g}$ is a vector of samples of the noise-free channel process, and $\mathbf{I}$ is the identity matrix. The maximum-likelihood covariance matrix estimate computed from N statistically independent channel observation with length p and $p < N$ is given by [And84]

$$\mathbf{K}_\mathbf{g}^N = \mathbf{K}_\mathbf{h}^N = \frac{1}{N}\sum_{i=1}^{N}\mathbf{h}_i\mathbf{h}_i^H, \tag{5.5}$$

The assumption of $p < N$ holds in our case since we ensure that the length of sampled CIR is less than 1000 samples which represents the total number of channel observations for one scenario. For small d/λ, the assumption of independent observations and thus that the channel samples are spatially decorrelated is justified in an indoor MIMO setting in [SW02]. In the context of our measurements, the multiple transmitter/receiver grid can equivalently be seen as a large(50×20) MIMO system.

The covariance matrix is Hermitian and positive definite. For this reason, a unitary matrix $\mathbf{U_h}$ exists such that the Karhunen-Loève (KL) expansion gives

$$\mathbf{K}_\mathbf{h}^N = \mathbf{U_h}\Lambda_\mathbf{h}\mathbf{U}_\mathbf{h}^H = \sum_{i=1}^{N}\lambda_i(\mathbf{h})\psi_i(\mathbf{h})\psi_i^H(\mathbf{h});\ \mathbf{U}_\mathbf{h}^H\mathbf{U_h} = \mathbf{I}_N, \tag{5.6}$$

where $\lambda_1(\mathbf{h}) \geq \lambda_2(\mathbf{h}) \geq ... \geq \lambda_N(\mathbf{h})$, $\psi_i(\mathbf{h})$ is the i^{th} column of $\mathbf{U_h}$ and $\mathbf{I}_N$ is the $N \times N$ identity matrix with N number of samples. $\lambda_i(\mathbf{h})$ and $\psi_i(\mathbf{h})$ are the i^{th} eigenvalues and eigenvectors of $\mathbf{K}_\mathbf{h}^N$, respectively. Decomposing (5.6) into principal and noise components yields

$$\begin{gathered}\mathbf{U}_{s,\mathbf{h}} = [\psi_1(\mathbf{h}), \psi_2(\mathbf{h}), ..., \psi_p(\mathbf{h})];\\ \lambda_1(\mathbf{h}) \geq \lambda_2(\mathbf{h}) \geq ... \geq \lambda_L(\mathbf{h});\\ \mathbf{U}_{n,\mathbf{h}} = [\psi_{L+1}(\mathbf{h}), \psi_{L+2}(\mathbf{h}), ..., \psi_N(\mathbf{h})];\\ \lambda_{L+1}(\mathbf{h}) \geq \lambda_{L+2}(\mathbf{h}) \geq ... \geq \lambda_N(\mathbf{h}).\end{gathered}$$

where $\mathbf{U}_{s,\mathbf{h}} \perp \mathbf{U}_{n,\mathbf{h}}$. $\mathbf{U}_{s,\mathbf{h}}$ defines the subspace containing both signal and noise components, whereas $\mathbf{U}_{n,\mathbf{h}}$ defines the noise-only subspace. L is the number of significant eigenvalues which also represents the channel DoF [MT85], in the sense that any set of observations can be characterized by a set of approximately L independent random variables which excite L modes (their corresponding eigenvectors). In our case, the eigenvectors correspond to the samples of the eigenfunctions characterizing the propagation environment. They convey information regarding the statistical correlation between paths arriving at different time instants, since if in a particular eigenvector, ψ_i, we find several significantly-spaced high-energy samples (paths), the same random variable with variance $\lambda_i(\mathbf{h})$ excites these samples and thus they exhibit statistical correlation.

5.2.2 Characterization of the Total Received Energy

Following the eigen-decomposition, we can define the normalized total received energy in an observation as $X = \mathbf{h}^H\mathbf{h}/\overline{\mathbf{h}^H\mathbf{h}}$ where the average channel energy is denoted by $\overline{\mathbf{h}^H\mathbf{h}}$. We must distinguish two important cases, namely the presence or lack of a line-of-sight path in the received wavefront. In general we may express the filtered impulse response of the channel, assuming a discrete set of scatterers, as

$$h_W(t) = A_0 e^{j\phi_0}\text{sinc}(W(t-t_0)) + \sum_{i>0} A_i e^{j\phi_i}\text{sinc}(W(t-t_i)) \tag{5.7}$$

where A_0 represents the strength of the line-of-sight component, and $A_{i>0}$ the random amplitudes of scattered components, and t_i are the delays of each component. For a particular channel sample we obtain

$$h(n) = A_0 e^{j\phi_0}\text{sinc}(W(n/W-t_0)) + \sum_{i>0} A_i e^{j\phi_i}\text{sinc}(W(n/W-t_i)) \tag{5.8}$$

In the characterization of the energy of the channel, $\mathbf{h}^H\mathbf{h}$, the phase offset of the direct path can clearly be neglected, and thus we can assume that ϕ_0 is zero, even if it is truly a random quantity. Moreover, for a dense multipath environment, each $h(n)$ can be approximated by a Gaussian random variable with mean $A_0\text{sinc}(W(n/W-t_0))$ as is classically assumed [W.C74]. We can thus express the channel-energy moment generating function as

$$G_X(s) = E\left[e^{sx}\right] = \int_{-\infty}^{+\infty} e^{sx} f_X(x)dx = L(f_X(x))|_{s=-s} \tag{5.9}$$

L is the Laplace transform operator and $f_X(x)$ is the probability density function (pdf) of variable X. We can see from last equation that $G_X(s)$ and $f_X(x)$ are Laplace transform pairs with $s = -s$. $G_X(s)$ can also be expressed as follows using the covariance matrix $\mathbf{K}_h$

$$G_X(s) = \frac{e^{\mathbf{m}^H(\mathbf{I}-s\mathbf{K}_h)^{-1}\mathbf{m}}}{\det(I-s\mathbf{K}_h)} \tag{5.10}$$

where the vector $\mathbf{m}$ has components $m(n) = A_0\text{sinc}(W(n/W - t_0))$ [SBS66]. We will assume that $\mathbf{K}_h$ is characterized by L significant eigenvalues, $\lambda_i(\mathbf{h}) : i = 1..L$, which are positive. Furthermore, we constrain our treatment of the channel energy to the non-line-of-sight case since no attempt was made to estimate the LOS component strength, A_0, from our collected data. It is easily shown using the initial value theorem [OWY83] that the probability density function of the normalized channel energy can be approximated around the origin as

$$f_X(x) \approx \frac{x^{(L-1)}}{(L-1)!}\frac{1}{\det(K_{\mathbf{h}})} = \frac{x^{(L-1)}}{(L-1)!}\frac{1}{\prod_i \lambda_i(\mathbf{h})}, \text{for} 0 \leq x << \min(\lambda_i(\mathbf{h})) \tag{5.11}$$

This indicates that around the origin X behaves as an Erlang-L [3] variable with parameter $2\sigma^2 = \sqrt[L]{\prod_i \lambda_i(\mathbf{h})}$. The approximate cumulative distribution function can be expressed in terms of the incomplete Gamma function, or in terms of the Marcum-Q function, $Q_L(0, x)$, as

$$\begin{aligned} F_X(x) &= \gamma\left(\frac{x}{2\sigma^2}, L\right) = 1 - Q_L\left(0, \frac{\sqrt{x}}{\sigma}\right) \\ &\approx \frac{1}{\Gamma(L+1)}\left(\frac{x}{2\sigma^2}\right)^L, \quad 0 \leq x \leq \prod_i \lambda_i(\mathbf{h}) \\ &= \frac{x^L}{\Gamma(L+1)\prod_i \lambda_i(\mathbf{h})}. \end{aligned} \tag{5.12}$$

The above approximations can be found in [Shn89]. Since the approximation is valid for small X, we are characterizing the region of the CDF in its lefthanded tail. From the above expression we see that we can use the slope of log(cdf) to gain insight regarding the number of significant DoF for a particular average channel strength. This can also be seen equivalently as determining the inherent diversity-order of the channel [PM96].

The Figures 5.2 (resp. 5.3) show the cumulative distribution function of the total received energy over a UWB channel of 6 GHz bandwidth in comparison to a flat fading Rayleigh channel with the same average received energy for LOS (resp. NLOS). The measurements were conducted in a typical office environment. The CDF corresponding to the UWB channel is very close to a step function, which proves that the received energy is effectively constant irrespective of channel realization. The physical explanation for this behavior comes from the fact that the large bandwidths considered here (more than 500 GHz) provide a high temporal resolution and allow the receiver to resolve a large number of paths of the impinging wave front. Providing that the channel has a high diversity order (i.e. in indoor communications), the total channel gain is slowly varying compared to its constituent components. Variations in the received signal power will typically be caused by shadowing rather than fast fading as it is shown in the previous chapter. Based on the observation of UWB channel energy behavior, we are interested on a sub space channel analysis. This allows to evaluating the number of multi-paths or the UWB channel independent versus the channel bandwidth.

[3] The Erlang-L probability density function of variable X is given by $f_X(x) = \frac{x^{L-1}}{(2\sigma^2)^L\Gamma(L)}e^{-\frac{x}{2\sigma^2}}, x > 0$ and L aninteger

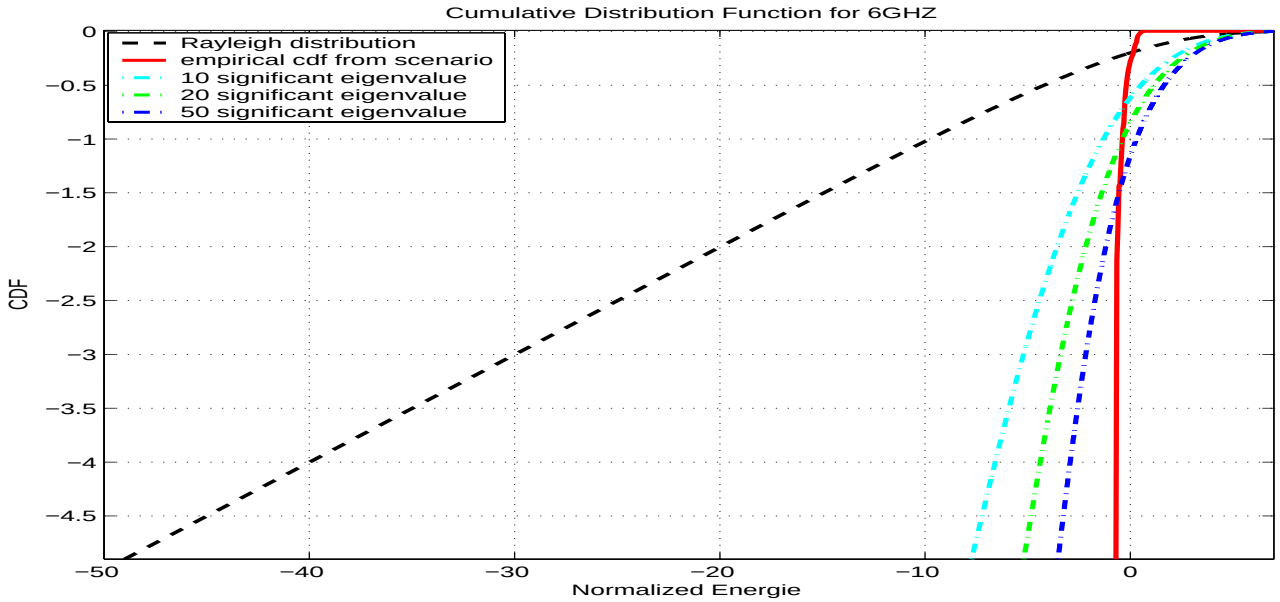

Figure 5.2: Cumulative Distribution Function of the energy in UWB channel LOS case

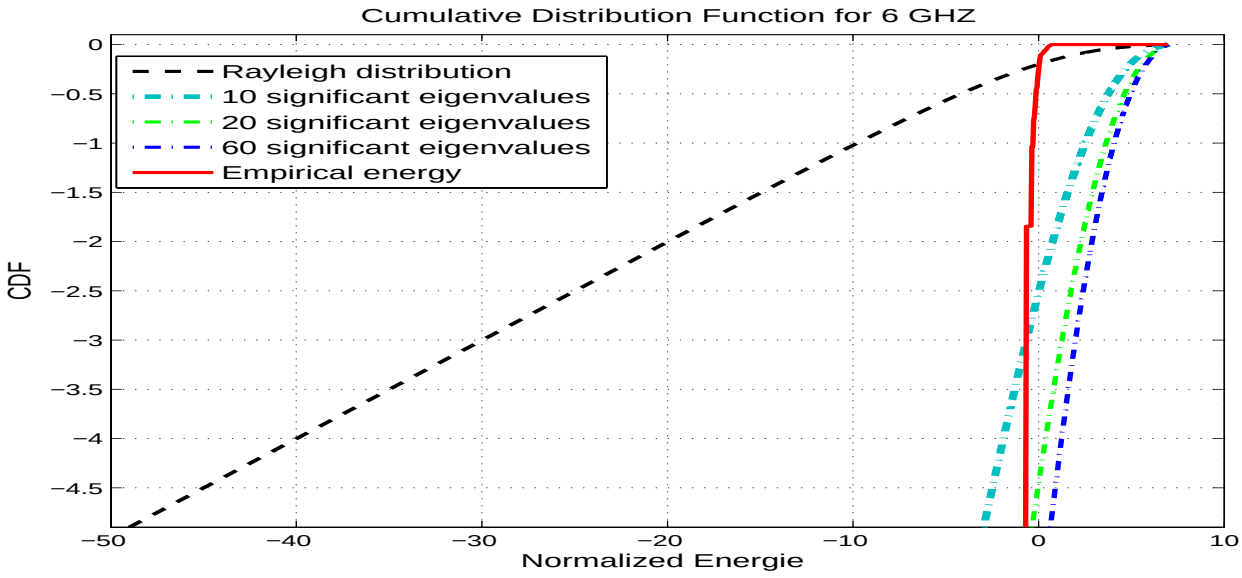

Figure 5.3: Cumulative Distribution Function of the energy in UWB channel NLOS case

5.2.3 Empirical Measurement Results

Empirical Distribution of Eigenvalues For Indoor UWB Channels

The empirical results presented in this Section are obtained from the LOS/NLOS 6m scenarios described earlier. The sampled CIR is calculated from 6003 samples of the frequency response using IFFT, limited to 1000 samples for the computation of the sample covariance matrix, $\mathbf{K}_{\mathbf{h}}^{N}$. In figures 5.4 and 5.5 we show the sample mean power delay profile ($\mathrm{diag}(\mathbf{K}_{\mathbf{h}}^{N})$) for the LOS and NLOS cases. We see that the LOS is characterized by two dominant clusters, one of which is around the LOS path

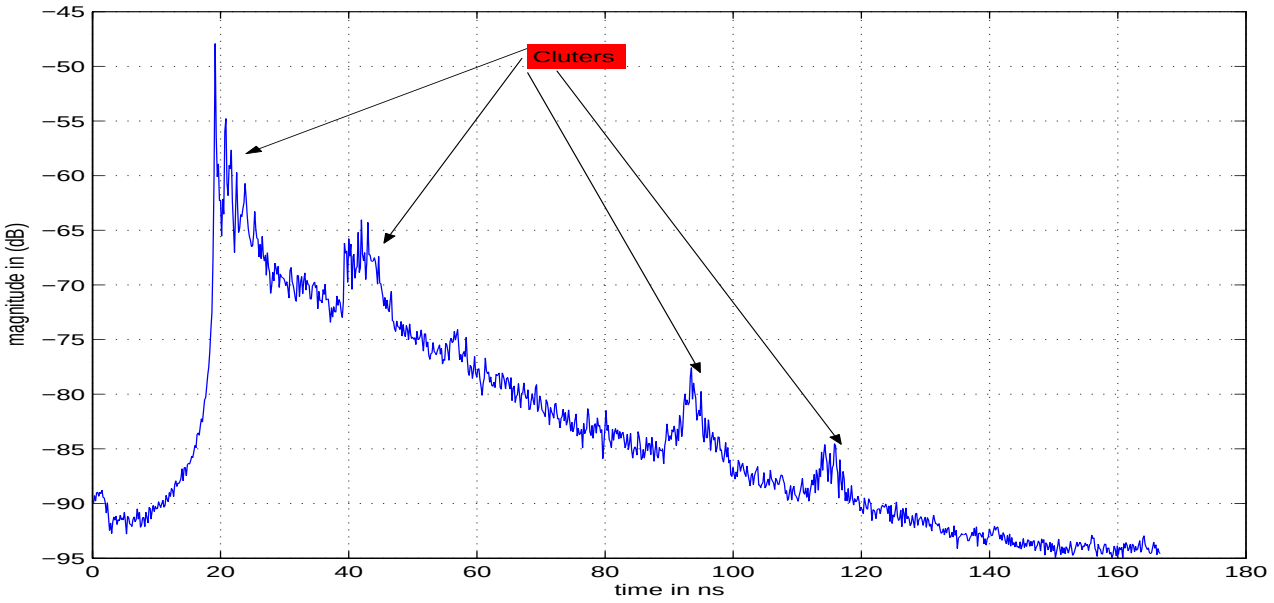

Figure 5.4: Power Intensity Profile in LOS situation

that is clearly visible. Secondary scatterers comprise significant energy non the less. In the NLOS case there is dense scattering for short delays and the same secondary cluster as the LOS scenario, resulting surely from multiple reflections in the room.

In figures 5.6[4], 5.7[5] and 5.8 we plot, for the LOS (for low and high frequency range) and NLOS measurements, the fraction of the captured energy for M considered eigenvalues defined by:

$$E_M = \frac{\sum_{i=1}^{M} \lambda_i(\mathbf{h})}{\sum_{i=1}^{N} \lambda_i(\mathbf{h})}. \tag{5.13}$$

where N is the total number of eigenvalues. We remark in both plots, for the narrowband cases, that the majority of the channel energy (more than 90%) is confined in small number of significant eigenvalues whereas in the wide bandwidth case, the channel energy is spread over a large number of eigenvalues (i.e. DoF). The results are obtained for a sampling rate, in the frequency domain, of 1 sample per megahertz. This sampling resolution was verified to be sufficient to capture all channel DoF and at the same time minimize the effect of time domain aliasing as mentioned previously. Actually, figure 5.9 shows that increasing the sampling rate from 1 sample per 2 megahertz to 1 sample per megahertz does not modify channel eigenvalue distribution.

[4]Low frequency in the band of interest from 3 GHz to 6 GHz.
[5]High frequency in the band of interest from 6 GHz to 9 GHz.

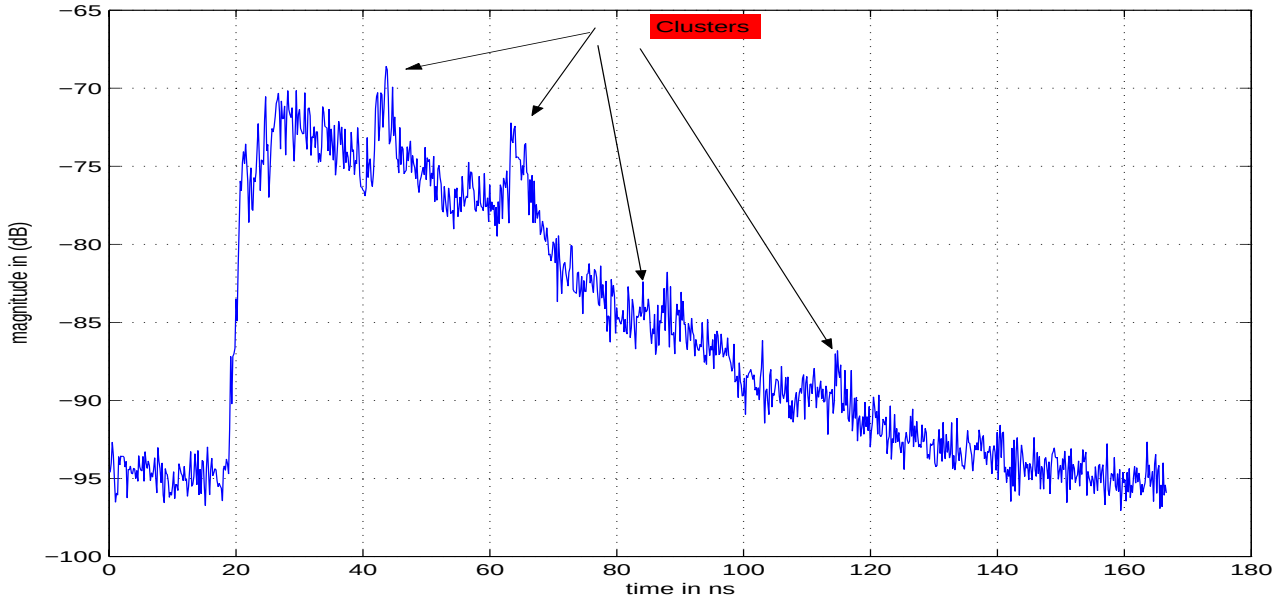

Figure 5.5: Power Intensity Profile in NLOS situation

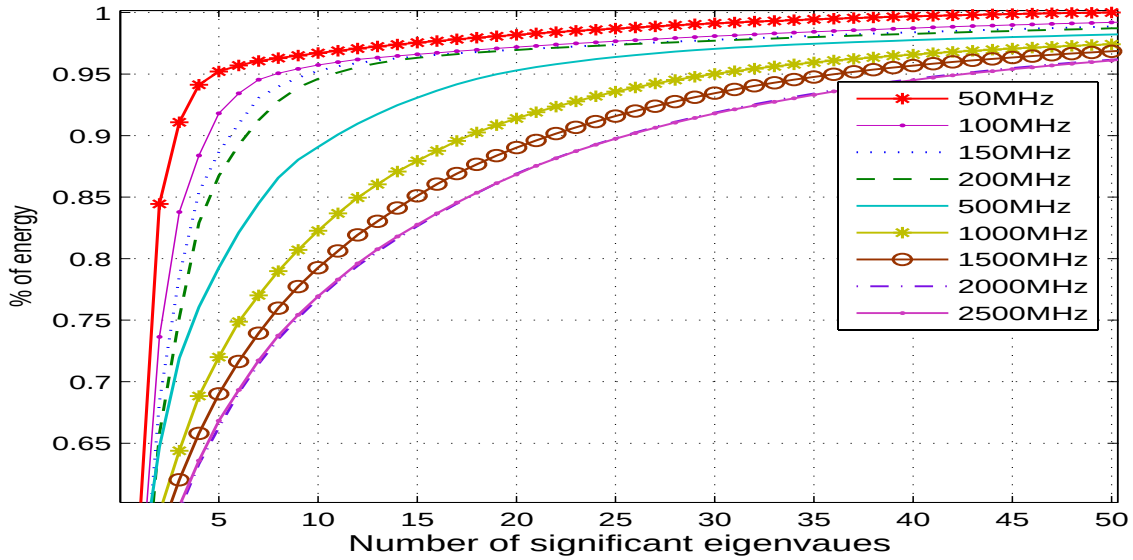

Figure 5.6: % of energy versus number of eigenvalues LOS, resolution 1 MHz low frequency range from 2 GHz to 5 GHz.

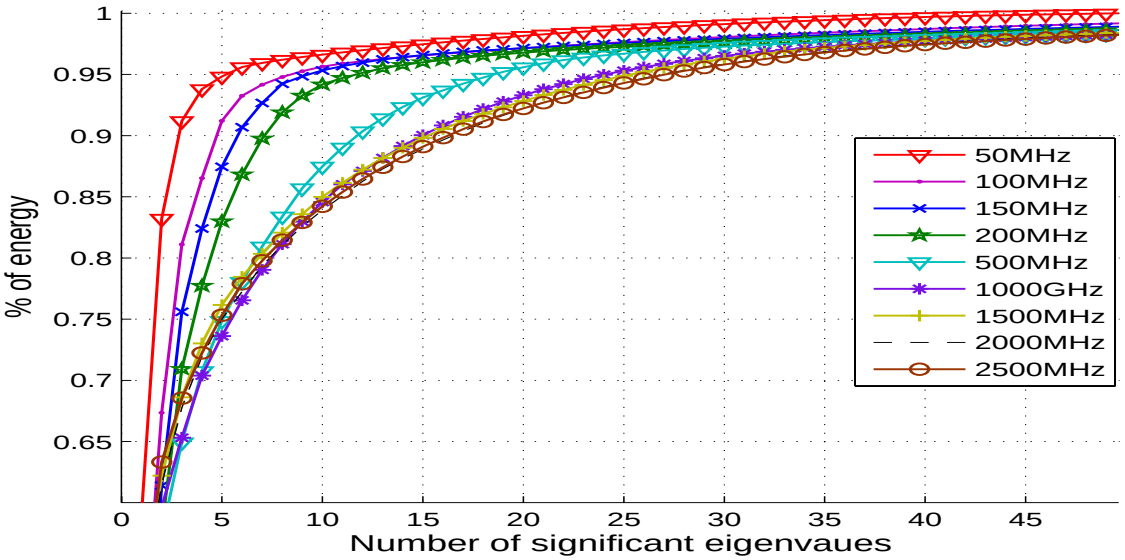

Figure 5.7: % of energy versus number of eigenvalues LOS, resolution 1 MHz high frequency range from 7 GHz to 9 GHz.

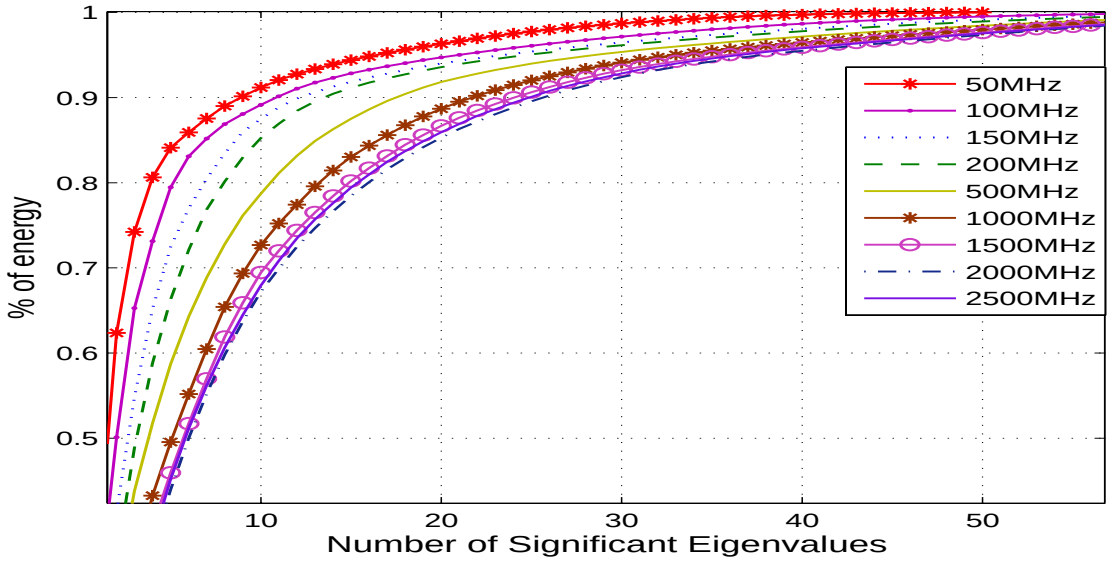

Figure 5.8: % of energy versus number of eigenvalues NLOS, resolution 1 MHz low frequency range from 2 GHz to 5 GHz.

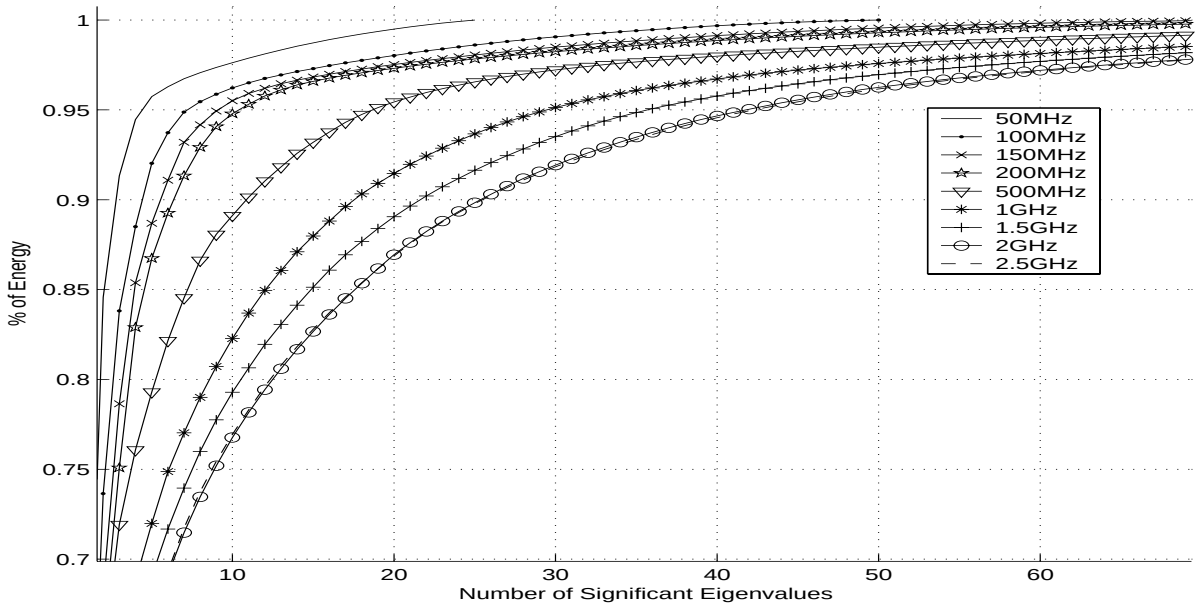

Figure 5.9: % of energy versus number of eigenvalues LOS, resolution 1 MHz low frequency range from 2 GHz to 5 GHz, sampling rate 2 MHz.

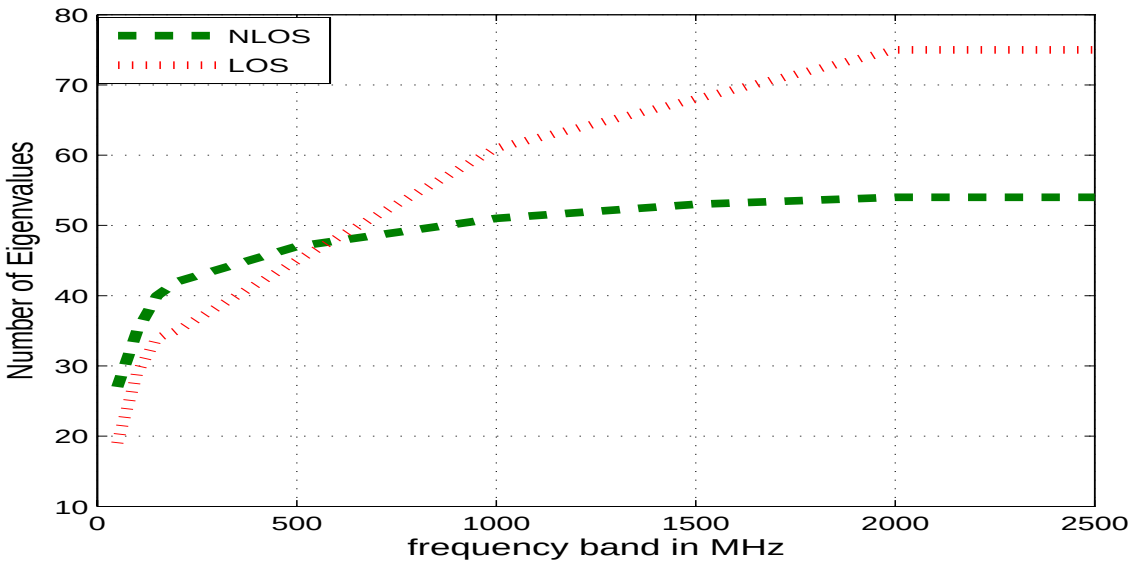

Figure 5.10: Evolution number of eigenvalue for LOS and NLOS.

Figure 5.10, plotted for 98% captured energy, shows that the number of significant eigenvalues increases with the channel bandwidth, although not linearly. We see that in both cases, the increase is linear until approximately 200 MHz, where a saturation effect begins to occur (we can approximate the number of significant eigenvalues evolution versus frequency bandwidth in NLOS case by $a \times \log(B)$, where a is a constant and B represents the frequency band) see Figure 5.2.3. This means that until this critical bandwidth the signal bandwidth does not provide sufficient resolution to resolve all eigenvalues, or equivalently the complete number of multipath components. Beyond this point, however, the channel is degenerate in the sense that all paths can be resolved. We note that the number of significant eigenvalues in the saturation region is markedly higher in the LOS case. This can be explained by the fact that the object placed between the transmitter and receiver also shadows a significant portion of NLOS components and the richness of the channel is therefore reduced.

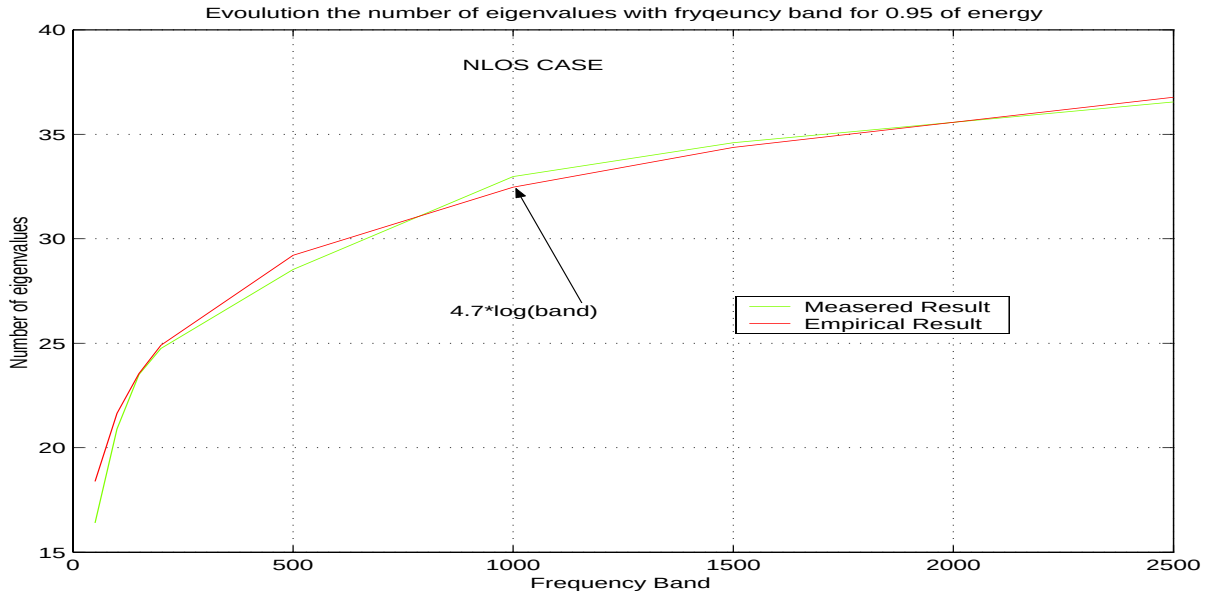

Figure 5.11: Empirical distribution of DoF versus bandwidth in NLOS

Eigenfunction Analysis in LOS and NLOS Situations

Figures 5.12, 5.13 and 5.14 show some sampled eigenfunctions in LOS settings corresponding to the most significant eigenvalues. These figures show that the channel exhibits a clustered behavior, as can be seen when we plot the CIR shown in figures 5.4 and 5.5. It is remarkable that from our analysis we see that paths from different clusters have comparable strengths in the same eigenfunction. As a result, these clusters are strongly statistically dependent as was described in the previous section.

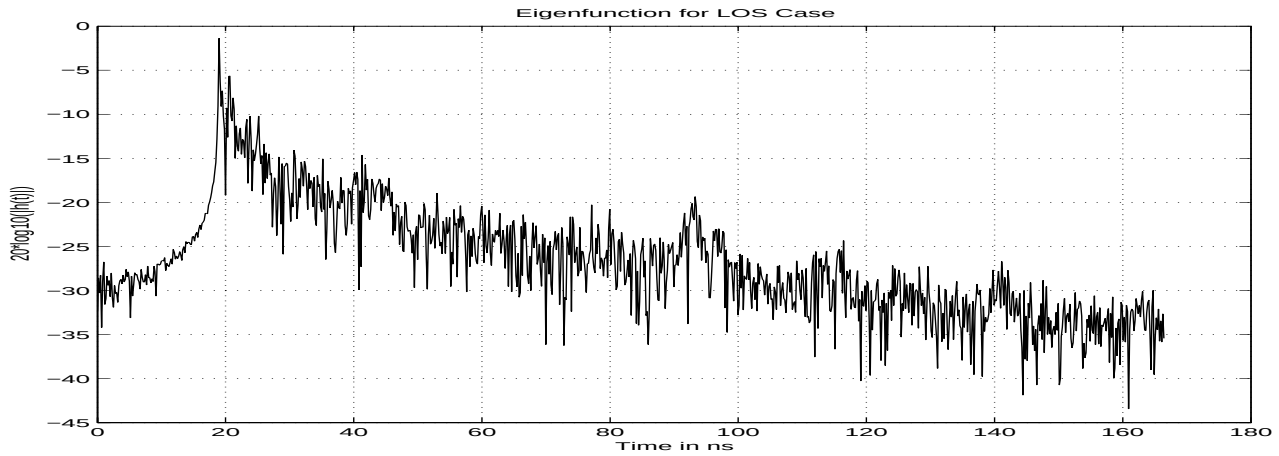

Figure 5.12: Eigenfunction corresponding to $\lambda_1 = 0.4445$ in LOS situation

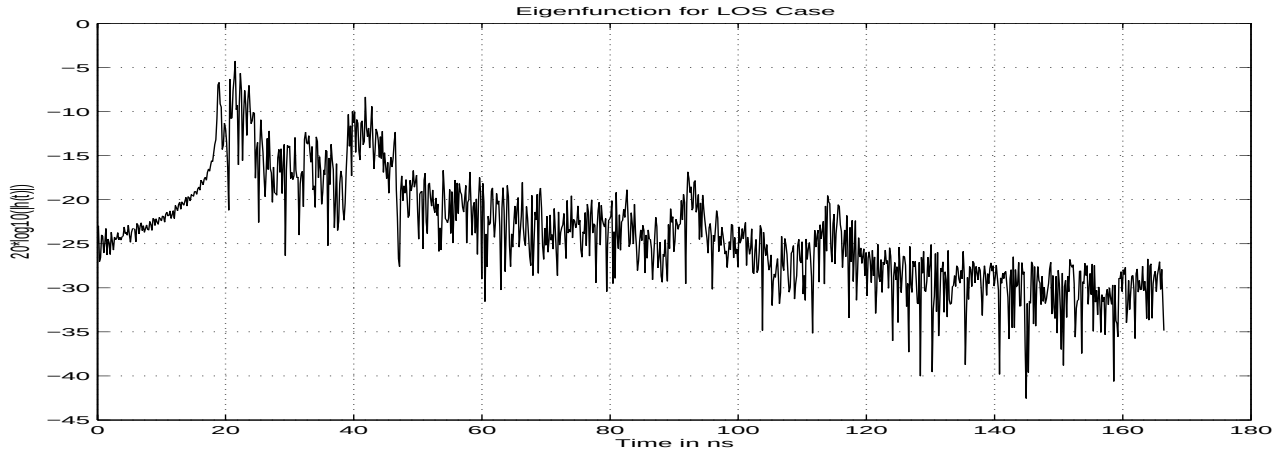

Figure 5.13: Eigenfunction corresponding to $\lambda_5 = 0.0314$ in the LOS situation

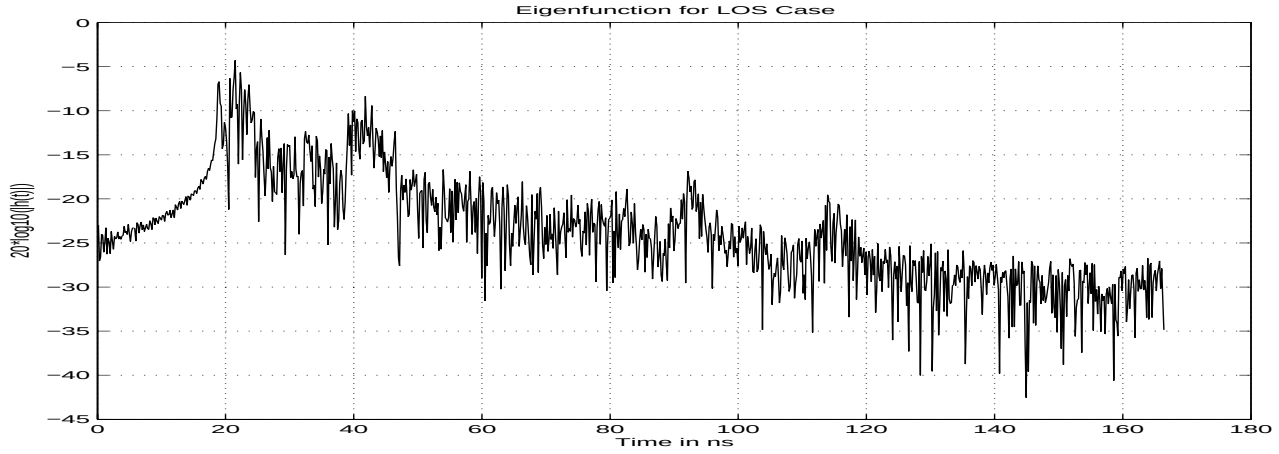

Figure 5.14: Eigenfunction corresponding to $\lambda_{10} = 0.0133$ in LOS situation

5.3 Information-Theoretic Criteria Based UWB Channel Modeling

In this section, we apply *Akaike information criterion* (AIC) and *Minimum Description Length* (MDL) to estimate the number of DoF (DoF) of an UWB channel (UWB) in an indoor environment. We evaluate our solution under both scenarios: LOS and NLOS.

In the Section 5.2, the growth of DoF of the channel is evaluated based on an empirical analysis. The goal of this Section is to analyze the impact of these extremely large systems bandwidth on the covariance matrix channel. We are primarily interested in assessing the growth in the number of DoF needed to characterize the channel as a function of the system bandwidth using the AIC and the MDL criterion. We are also interested in the root mean square (rms) delay spread behavior for a given threshold of received power (98% in the total received energy) as a function of the system bandwidth for both LOS and NLOS cases. Finally, an estimation of UWB channel entropy based on measurements is drawn. This confirms that the number of DoF increases sub-linearly with channel bandwidth.

5.3.1 Information Theoretic Criteria Based DoF Estimation

AIC and MDL are model-order determination algorithms that can also be used for determining how many signals are present in vector valued data. Suppose the $M \times 1$ complex vector $h(t)$ can be modeled as

$$h(t) = As(t) + n(t) \tag{5.14}$$

A is a rank(P) $M \times P$ complex matrix whose columns are determined by the unknown parameters associated with each signal. $s(t)$ is a $P \times 1$ complex vector whose p^{th} element is the waveform of the p^{th} signal, and $n(t)$ is a complex, stationary, and ergodic Gaussian process with zero mean and covariance matrix $E\{n(t)n'(t)\} = \sigma_n^2 I_n$. The problem is to determine P from N observations of $h(t)$; i.e., $h(t_1), ..., h(t_N)$. Furthermore, if P uncorrelated signals are present, the $M - P$ smallest eigenvalues of $\mathbf{R} = \mathbf{K}_{\mathbf{h}}^N$ (given in equation (5.6)) are all equal to the noise power σ_n^2, and the vector of parameters $\Theta^{(P)}$ specifying $\mathbf{R}$ can be described as:

$$\Theta^{(P)} = [\lambda_1, \lambda_2, ..., \lambda_{P-1}, \lambda_P, \sigma_n^2, \psi_1^T, \psi_2^T, ..., \psi_P^T] \tag{5.15}$$

The number of signals are determined from the estimated covariance matrix $\hat{\mathbf{R}}$. In the [MT85], the AIC criteria was adapted for detection of the number of signals. This procedure is recalled here in this simplified form.
If $\hat{\lambda_1}, \hat{\lambda_2}, ..., \hat{\lambda_M}$ are the eigenvalues of $\hat{\mathbf{R}}$ in the decreasing order then

$$AIC(k) = -2 \log \left(\frac{\prod_{i=k+1}^{p} \lambda_i(\mathbf{h})^{\frac{1}{(p-k)}}}{\frac{1}{p-k} \sum_{i=k+1}^{p} \lambda_i(\mathbf{h})} \right)^{N(p-k)} + 2k(2p-k) \tag{5.16}$$

and

$$MDL(k) = -\log \left(\frac{\prod_{i=k+1}^{p} \lambda_i(\mathbf{h})^{\frac{1}{(p-k)}}}{\frac{1}{p-k} \sum_{i=k+1}^{p} \lambda_i(\mathbf{h})} \right)^{N(p-k)} + \log(N) \frac{k(2p-k+1)}{4} \tag{5.17}$$

The number of DoF, possibly the number of significant eigenvalues, is determined as the value of $k \in \{0, 1, ..., p-1\}$ which minimizes the value of (5.16) or (5.17). In this work, the number of DoF represents the number of unitary dimension independent channels that constitute an UWB channel.

5.3.2 UWB Entropy Analysis

DoF Scaling versus the Bandwidth

Figures 5.15 (resp. figure 5.16) considers LOS (resp. NLOS) measurements settings, we plot the AIC and MDL functions for two different bandwidths typically 200 MHz and $6GHz$. The minimum of AIC or MDL curves give the number of significant eigenvalues. As a matter of fact, we see that the number of DoF increases with bandwidth but not linearly. TABLE 5.1 summarized some value of k that minimizes the AIC and MDL criterion. Thus, for 200 MHz bandwidth, we capture 98% of the energy with 29 significant eigenvalues whereas for 6 GHz channel bandwidths the number of eigenvalues is 50. To illustrate the relationship between number of (DoF) and system bandwidth, we

Table 5.1: The value of k minimizes AIC and MDL criterion

	Settings			
	LOS		NLOS	
ΔW	200 MHz	6 GHz	200 MHz	6 GHz
k_{AIC}	23	68	25	46
k_{MDL}	21	60	23	42

recall that for a signal with duration T and frequency band ΔW, the number of (DoF) of the signal space N_{dof} is given by [Gal68]

$$N_{dof} = T \cdot \Delta W + 1. \tag{5.18}$$

Generally [GS00], we find that if one transmits a band limited and time limited signal over a fading channel with rms delay spread T_d, the channel (DoF) N is approximately

$$N = T_d \cdot \Delta W. \tag{5.19}$$

The APDP is characterized by the first central moment (mean excess delay) τ_m and the square root of the second moment of the APDP root mean square τ_{rms} delay spread. Using the traditional definitions as found in [Rap89] (see Section 4.6 in Chapter 4). To investigate deeply the validity of this relationship for UWB channels, we measure the evolution of the τ_{rms} delay spread with the frequency bandwidth, for both LOS and NLOS cases, for one fixed threshold of received energy -20 dB attenuation regarding the first arriving path. Then we plot, on figure 5.17, the computed number of DoF following equation (5.19).

We then compare this result with the number of (DoF) obtained by AIC criterion from measurements. For 98% of the captured energy, we notice that the number of eigenvalues using the relationship in (5.19) increases linearly with the bandwidth for both LOS and NLOS case. In contrary, the number of eigenvalues calculated directly from measurements by AIC tends towards saturation beyond 2000 MHz frequency bandwidth for LOS case and beyond 1500 MHz frequency bandwidth for NLOS case. We remark also, that for lower frequencies (below 800 MHz for NLOS and 1500 MHz for LOS settings), the number of DoF by AIC is higher than that one obtained following equation (5.19).

In fact, the measured number of DoF based on AIC is computed from the total channel impulse response obtained by IFFT while in the other case we focus on the time limited channel impulse response truncated at T_d. Hence the difference between both computed DoF comes from energy outside the T_d interval.

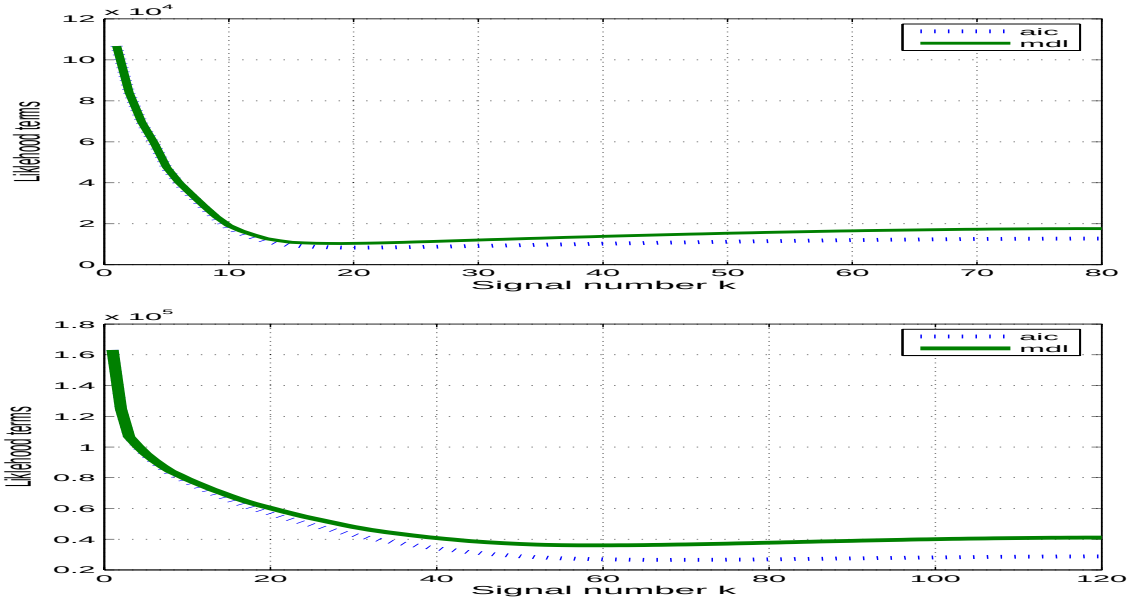

Figure 5.15: AIC and MDL for LOS 200 MHz (Top) and 6 GHz (bottom).

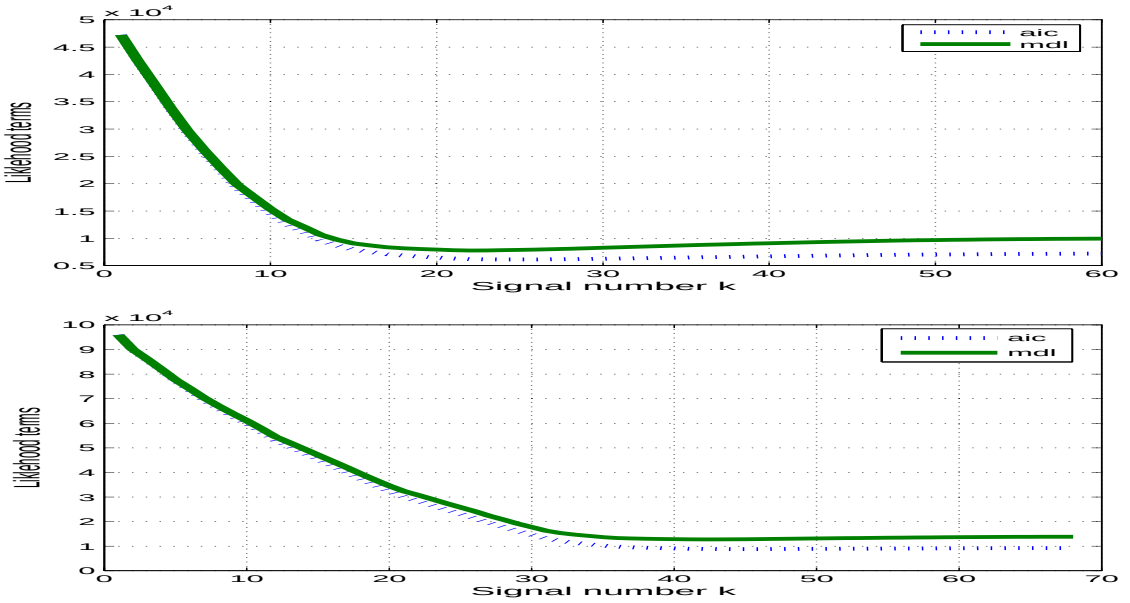

Figure 5.16: AIC and MDL for NLOS 200 MHz (Top) and 6 GHz (bottom).

Table 5.2: The delay Spread versus ΔW and power threshold

	Delay Spread (ns)			
	-10 dB threshold		-20 dB threshold	
ΔW	LOS	NLOS	LOS	NLOS
200 MHz	25	45	73	99
500 MHz	20	41	44	71
1000 MHz	15	40	41	70
1500 MHz	10	39	40	68
2000 MHz	9	39	37	68
2500 MHz	9	38	37	68
3000 MHz	9	38	37	68

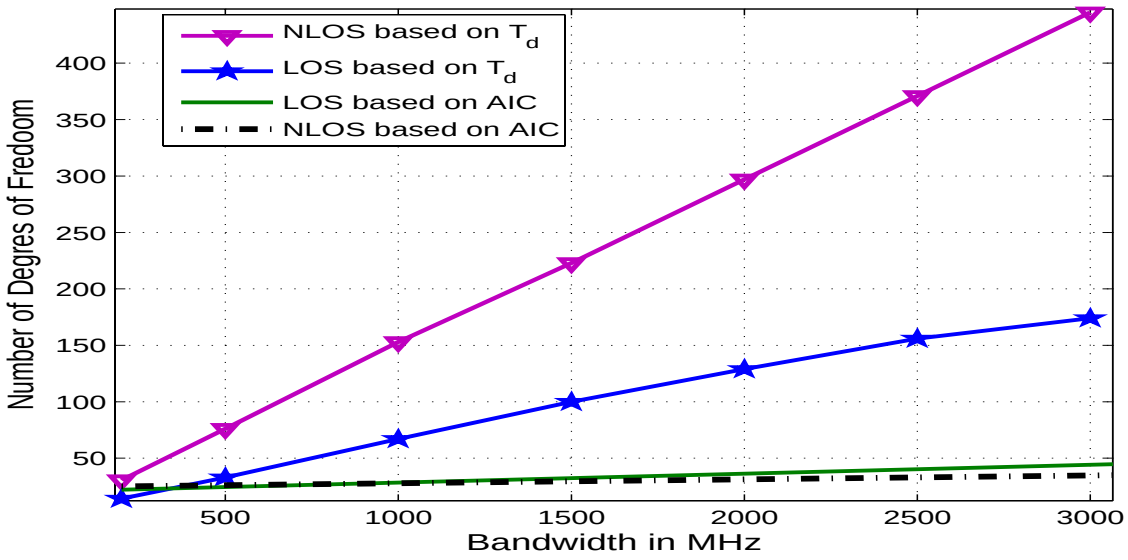

Figure 5.17: Evolution of the number of DoF for LOS and NLOS cases

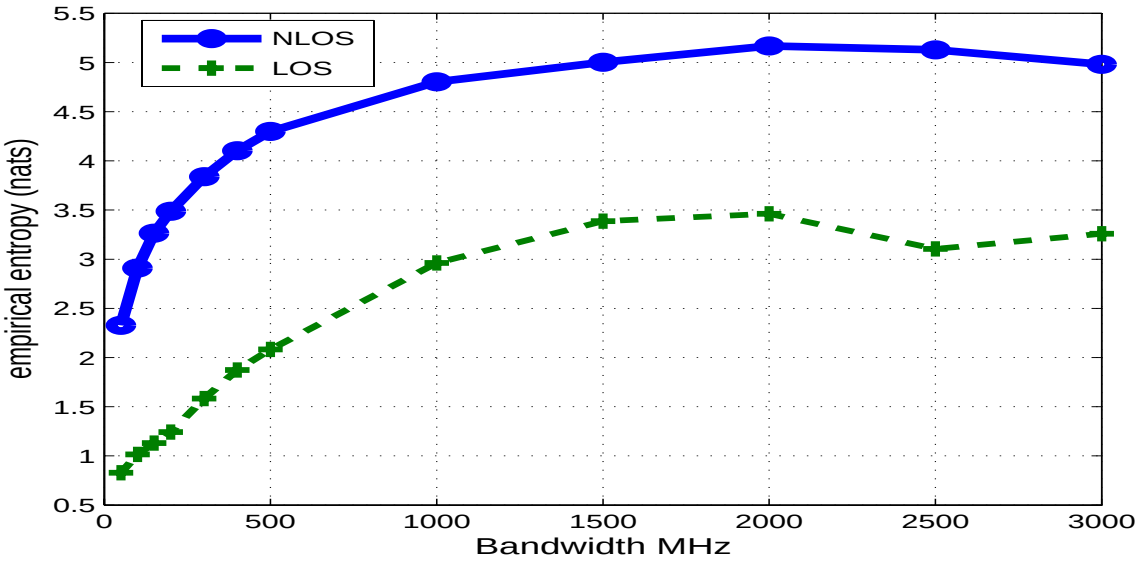

Figure 5.18: The entropy for UWB channel 6 GHz

UWB DoF and Entropy Analysis

The entropy is a measure of disorder of a system. Our system is the UWB channel and the disorder concerns the independent paths in this channel. As discuss above $\hat{R}$ is the estimated covariance matrix and the $\hat{\lambda}_k$ is the k^{th} eigenvalues of $\hat{R}$ and $\sum_k \hat{\lambda}_k = 1$. In [TS04] the Von Neumann entropy is given by

$$E(K) = -\text{tr}[\hat{R} \log \hat{R}]. \tag{5.20}$$

In this thesis the Von Neumann Entropy presents the Shannon entropy of eigenvalues.
Let $\hat{S}$ the empirical entropy

$$\hat{S} = -\text{tr}[\hat{R} \log \hat{R}] = -\sum_{k=1}^{L} \hat{\lambda}_k \log \hat{\lambda}_k \tag{5.21}$$

we call $\hat{S}$ empirical entropy because it is calculated based on estimated eigenvalues from a given set of channel measurements.

To confirm the results presented previously in the channel DoF saturation versus the channel bandwidth. We evaluate the channel entropy $\hat{S}$ for both LOS and NLOS settings. In Figure 5.18, we have plotted the measured $\hat{S}$ of the both LOS and NLOS scenarios with respect to the channel frequency band width. From this figure we constat that the $\hat{S}$ under NLOS case is more than $\hat{S}$ under LOS one. These show that the uncertainty increase with NLOS case. As explanation of these phenomenon is that the NLOS setting generates supplementary multipaths. Also, the figure shows the evolution of $\hat{S}$ versus channel bandwidth. As a matter of fact, we see that the entropy increases with bandwidth but not linearly. These confirms the saturation or the sub-linear behavior found on the DoF behavior.

5.4 Conclusion

In this Chapter, the second-order statistics of indoor UWB channels is characterized using channel sounding techniques. In the first Section, the energy of UWB channel impulse responses shows small variations, when compared to narrowband channels. The important results provided in this Section are twofold: Firstly, we have shown the evolution of the number of channel eigenvalues as a function of the system bandwidth for both LOS and NLOS scenarios where we see that the number of eigenvalues tends to saturate for the extreme bandwidth of UWB systems. This seems to suggest that all significant multipath components can be resolved. Secondly, we show that there is a strong statistical dependence between paths coming from different clusters, which is assumed not to be the case in most propagation models. In the second section we have used AIC and the MDL to estimate the number of (DoF) of an UWB channel in an in-door environment. We have also studied the evolution of the RMS delay spread behavior, T_d, as a function of frequency bandwidth based on a measurements campaign carried out at Eurecom Mobile Communication laboratory. We compared the results of AIC based technique with the number of (DoF) obtained using the product of T_d by the frequency bandwidth. This comparison pointed out that the number of DoF for a given UWB channel saturates beyond a certain frequency and does not increase linearly.

CHAPTER

6 NEW UWB CHANNEL MODELING BASED ON PHYSICAL APPROACH AND SAGE ALGORITHM

6.1 Introduction

To model the UWB propagation channel (i.e., path loss and multipath characteristics), field measurements must be performed and analyzed thoroughly. UWB channel models have been presented using the statistics channel parameters extracted based on time-domain and frequency-domain channel sounding techniques in different environments and under LOS and NLOS. However, these models did not include the effects of physical propagation phenomena on the channel, except the studies done in [CSW02] and [MBC+05].

The UWB radio channel is affected by various propagation mechanisms, namely reflection, transmission, scattering and diffraction. It can, therefore, be described by a set of multi path components (MPCs), each having a specific delay, angle of arrival, and angle of departure.

Several models are available that characterize the behavior of both, the indoor and the outdoor wireless multi-path channel. However, most of them focus on applications to narrowband and wideband wireless systems [Sch93, WS98]. With the emergence of UWB technology as a serious support for high data rate transmission for short–range indoor applications, new sets of indoor propagation measurements have been performed by many researchers e.g. [KP02, CWM02b, MFP05]. In this work, the data collected from channel measurements conducted at Eurecom [HKS05] are used. These measurements contain several LOS and NLOS environments. In [Mol05] an overview on UWB channel models found in literature is given. They all model the UWB channel as a sum of Dirac functions. The distortion of the Dirac pulses due to the interaction of the homogenous plane waves (HPW) at objects of finite size is not taken into account. In [Qiu04] this distortion of the MPCs at frequency bands relevant for UWB channels is studied. In this chapter, we propose a new UWB channel model which takes the distortion of the MPCs into account.

To investigate the proposed channel model and the efficiency algorithm used the estimate the parameters, we have in the first place evaluated the estimation process of a generated channel based on the diffraction and reflection mechanisms, and we have in the second place applied the same algorithm to our proposed channel model. The main objective of the parameters estimation process is to determine the laws distribution of the model parameters.

The reminder of the Chapter is organized as follows: Section 6.2 presents an UWB MPC response analysis based on measurement data. Section 6.3 describes the proposed channel model based on the physical analysis and the channel model parameter estimation. Lastly, in Section 6.4, we show and analyse new findings. At the end, we give a conclusion and an outlook on prospective work in Section 6.5.

6.2 Analysis of the UWB Impulse Response (Pulse Distortion)

The UWB impulse response is the result of the superposition of several MPCs. As a first step towards our new channel model we investigate the properties of a single MPC.
Qiu [Qiu04] presented the impact of large bandwidths on the impulse response due to diffraction. Based on a heuristic approach he proposes a model showing the relationship between delay spread and large bandwidths. In the sequel, we will analyze the reflection mechanisms for an UWB channel.

Using the expression of the reflection coefficient versus the frequency, Barnes [Bar91] derived the time domain channel impulse response (TD-CIR) expression.
The expression of the reflection coefficient versus the frequency and the incident angle, $R(\psi, s)$ expressed as:

$$R(\psi, s) = \pm \frac{\sqrt{s+2a} - \kappa\sqrt{s}}{\sqrt{s+2a} + \kappa\sqrt{s}} \tag{6.1}$$

with $\tau = \frac{\sigma}{\epsilon}$, $\beta = \frac{\sqrt{\epsilon_r - cos^2\psi}}{\epsilon_r sin\psi}$, $a = \tau/2$, $\kappa = \beta$ for vertical polarization and $a = \tau/2$, $\kappa = (\epsilon_r\beta)^{-1}$ for horizontal polarization.

Barnes [Bar91] derived the time domain expression of the reflected path $h_r(t)$ as:

$$h_r(t) = \left[K\delta(t) + \frac{4\kappa}{1-\kappa^2}\frac{\exp(-at)}{t}\sum(-1)^{n+1}nK^n I_n(at)\right] \tag{6.2}$$

Qiu in [Qiu04] derived the time domain impulse response due to diffraction for perfectly conducting half-plane as follow:

$$h_d(\tau) = \frac{\sqrt{2r/c}}{2\pi}\left[\frac{cos\frac{1}{2}(\varphi - \varphi_0)}{\tau + \frac{r}{c}cos(\varphi - \varphi_0)} - \frac{cos\frac{1}{2}(\varphi + \varphi_0)}{\tau + \frac{r}{c}cos(\varphi + \varphi_0)}\right]\frac{1}{\sqrt{\tau - r/c}}U(t - r/c) \tag{6.3}$$

c is the speed of light, τ is the path delay, φ and φ_0 are defined on figure 6.1. We plot on figure 6.2 the reference Dirac and the pulse used to examine the channel propagation phenomena analysis. Figures 6.3 and 6.4 show the response for reflection of Dirac and pulse signal respectively for different bandwidths. We plot on Figure 6.5 the response of diffracted pulse for different displacement types using the equation in (6.3).

Figure 6.6 shows the effect of the material constitutive parameters (ϵ: permittivity and σ: conductivity) on TD-CIR for a bandwidth equal to 1 GHz.

As we can see from this figure, the impulse response of a single MPC may show significant dispersion. These results clearly demonstrate that a single path of an UWB channel can experience a dramatical dispersion effect in time domain in the range of several nanoseconds. If we further recall that the RMS delay spread τ_{rms} for UWB channels ranges from 5 ns to 25 ns for indoor CM1-CM4 environments [MFP05], this dispersion should be taken into account to model UWB path response.

This implies that the UWB impulse response should not be represented by a set of Dirac functions. The large dispersion in time domain may also explain parts of the clustered behavior of the Power Delay Profile (PDP) observed in many UWB channel measurement campaigns [HKS05, MFP05]. This statement does not mean that we argue against clusters. It was shown several times

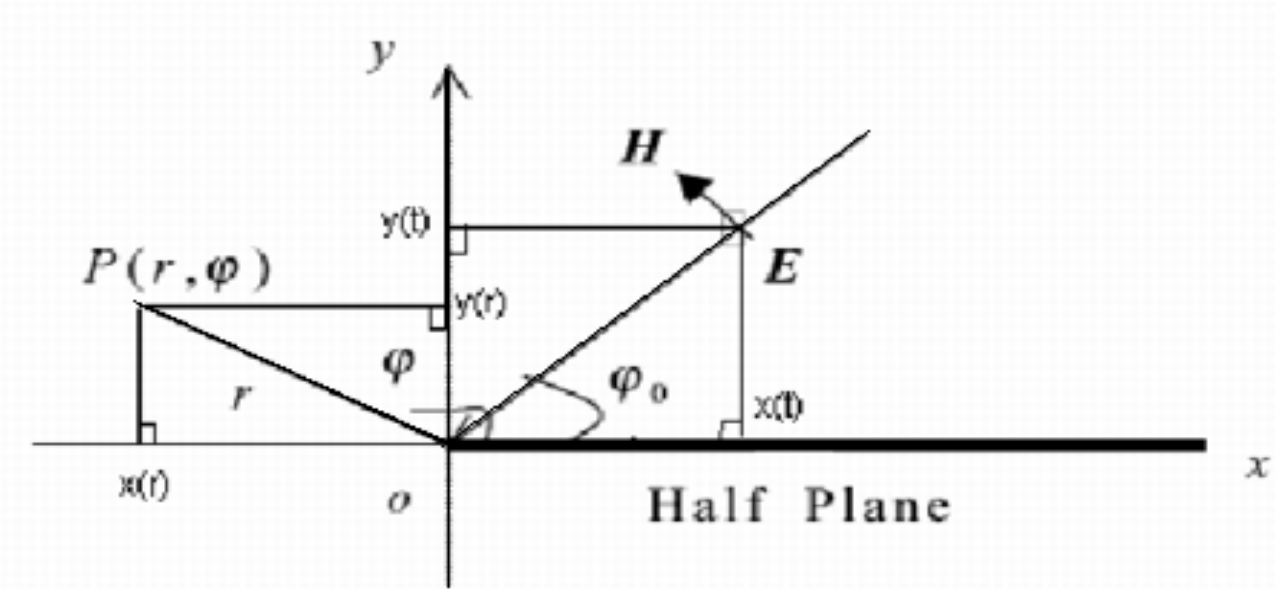

Figure 6.1: Diffraction at perfectly conducting half-plane.

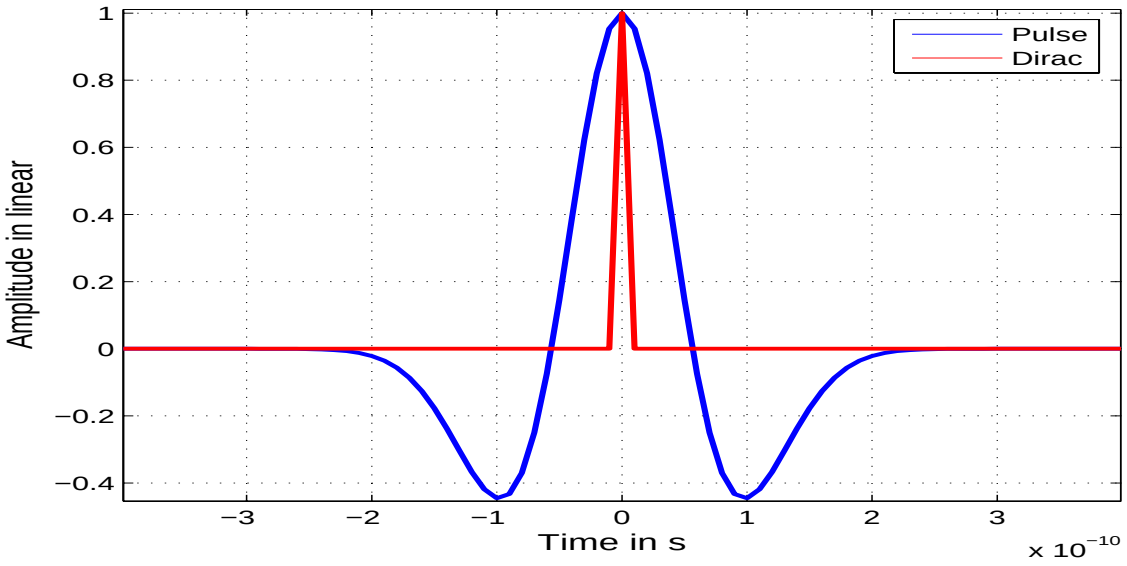

Figure 6.2: The pulse and dirac references

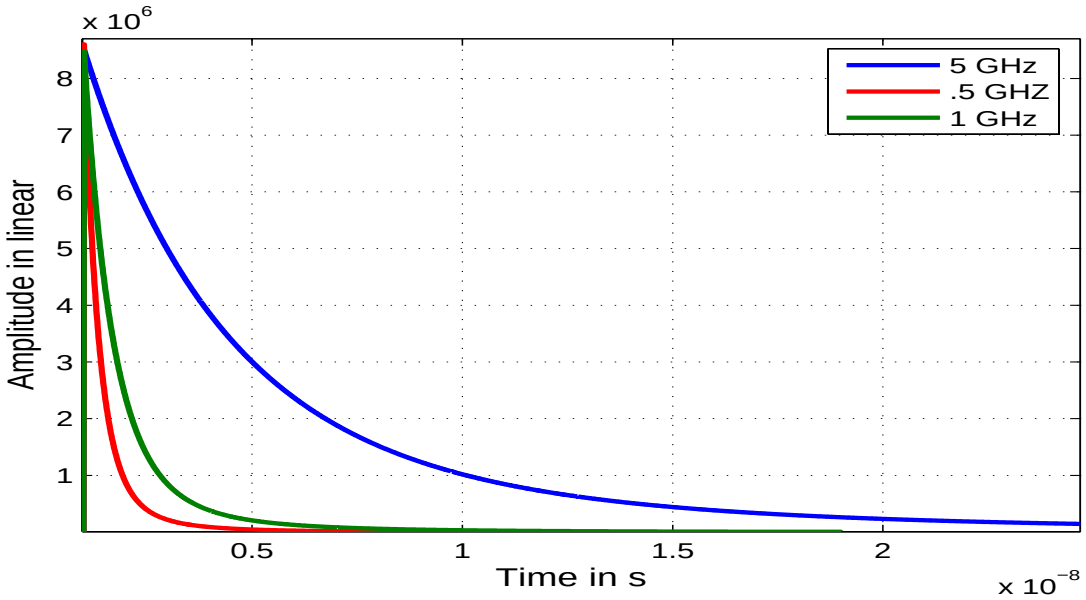

Figure 6.3: Reflection of Dirac versus channel bandwidth for a horizontal polarization with arc displacement, $\sigma_r = 0.001$ $\epsilon_r = 6$

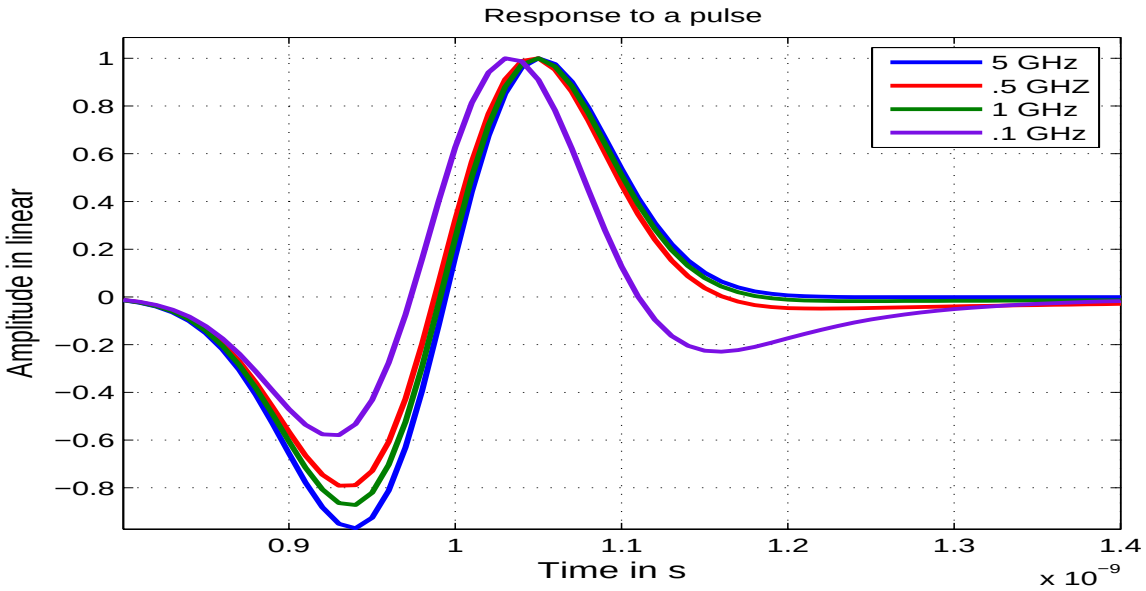

Figure 6.4: Reflection of pulse versus channel bandwidth for a horizontal polarization with arc displacement, $\sigma_r = 0.001$ $\epsilon_r = 6$

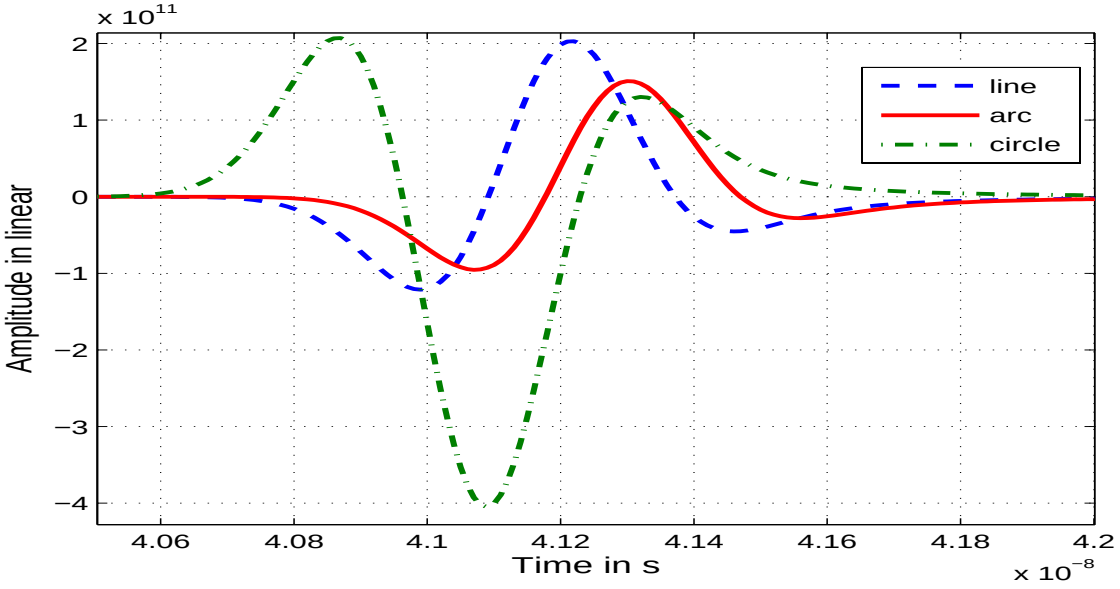

Figure 6.5: Diffracted pulse for the same frequency bandwidth and different displacement types.

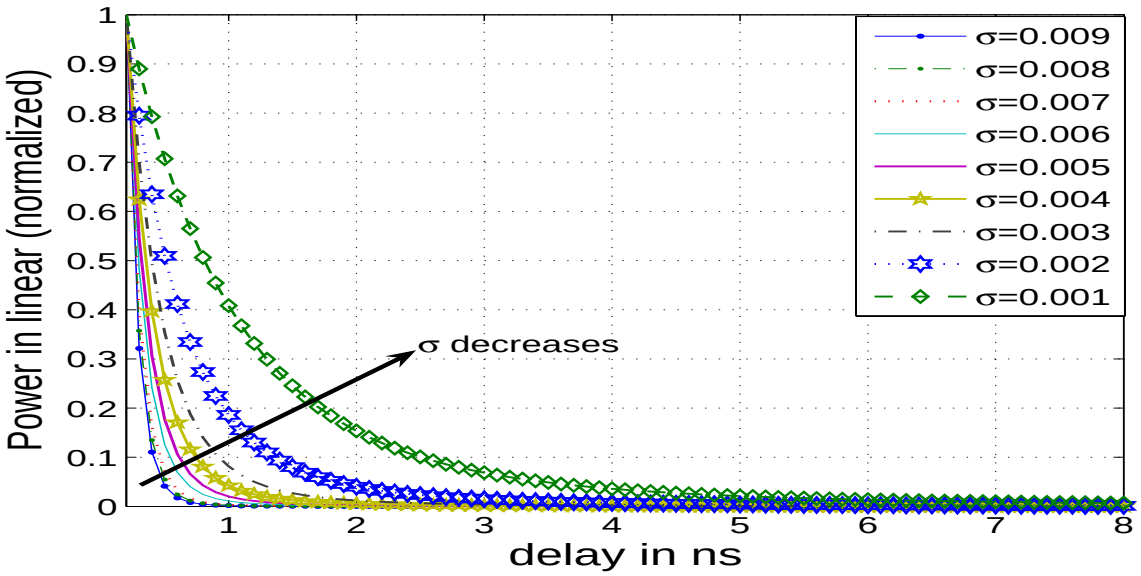

Figure 6.6: The path dispersion time versus σ with $W = 1GHz$, $\epsilon = 6$.

that cluster exist. But our idea influences the way clusters are built out of sets of MPCs. If each MPC has a certain time dispersion the PDP of a single reflection looks like the PDP of a cluster.

In the proposal IEEE 802.15.3a the channel impulse response is modeled using Saleh–Valenzuela approach, by a double sum as follows:

$$h(t) = \sum_{l=0}^{L-1} \sum_{k=0}^{K-1} \beta_{kl} exp(j\theta_{kl}) \delta(t - T_l - \tau_{kl}), \tag{6.4}$$

where L is the number of clusters and K is the number of echoes in each cluster and the APDP (Average Power Delay Profile) is expressed as:

$$E\beta_{kl}^2 = P(\tau_{kl}) = \Omega_0 exp\left(\frac{T_l}{\Gamma}\right) exp\left(\frac{\tau_{kl}}{\gamma}\right), \tag{6.5}$$

where Γ and γ are the decay constants of the clusters and of the echoes inside the clusters, respectively. This model states that all the paths are independent which is also different from what we can observe on Figure 6.6 which shows that some observed paths can be correlated due to time domain dispersion.

6.3 The Proposed UWB Channel Model

6.3.1 Channel Model Description

Based on the measurement and the physical analysis performed above, we propose a new simple channel model. The proposed model is given by:

$$h(\tau) = \sum_{l=1}^{L} g_l(\tau, \tau_l) u(\tau - \tau_l), \tag{6.6}$$

with $g_l(\tau, \tau_l)$ is the dispersed impulse response for the l^{th} path and L is the number of dominant paths. After analyzing UWB path impulse response for many scenario (different materials, incidence angles, distances,...), we propose as parameterizable path model next expression:

$$g_l(\tau, \tau_l) = g_l \exp\left(-(\tau - \tau_l)/\gamma_l\right), \tag{6.7}$$

The statistics of g_l, are considered to be Gaussian. Indeed, the considered environments are generally rich and contain different type of materials and different transmitter/receiver settings. This means that the parameters involved in the computation of diffracted or reflected paths (σ, ϵ_r, incidence angles, etc ...) can be seen as random an can be modeled using Gaussian distribution. For the statistics of τ_l, we chose to use a Poisson law which is generally used to model the delays Time of Arrival. The PDP of the modeled channel follows an exponential law as usually for wireless channels. γ_l is a parameter that can be chosen randomly from a specific set representing the observed dispersion due to reflection or diffraction mechanisms for a path l.

To simplify we make $\tau = t$ where t refers to times delay.

$$h(t) = \sum_{l=1}^{L} g_l(t, \tau_l) u(t - \tau_l). \tag{6.8}$$

The $u(t)$ is the Heaviside function and

$$g_l(t, \tau_l) = g_l e^{-(t-\tau_l)/\gamma_l} = \alpha_l e^{-t/\gamma_l}. \tag{6.9}$$

The signal parameters of the l^{th} path are τ_l arrival time or time delay, g_l is the complex amplitude and γ_l is the constant decay, the $g_l(t, \tau_l)$ is used to model the dispersed path over time. These parameters have intuitive meanings for an ideal surface reflector[1] in a homogeneous propagation path, with $\alpha_l = g_l e^{\tau_l/\gamma_l}$, the channel model becomes:

$$h(t) = \sum_{l=1}^{L} \alpha_l e^{-t/\gamma_l} u(t - \tau_l). \tag{6.10}$$

6.3.2 Channel Model Parameters Estimation

Let the observation Y have the probability distribution $f(y, \theta_{true})$ where θ_{true} is a parameter vector residing in a subset Θ of p-dimensional space C^p. Given a measurement realization $Y = y$, our goal is to compute the penalized maximum-likelihood estimate $\hat{\theta}$ of θ_{true} defined by:

$$\hat{\theta} = \arg\max_{\theta} \phi(\theta) \tag{6.11}$$

where

$$\phi(\theta) = \log f(y, \theta) - P(\theta) \tag{6.12}$$

and P is an optional penalty function. Analytical solution for $\hat{\theta}$ are often unavailable due to the complexity of f, the coupling in P, or both. Thus one must resort to iterative methods. One of the most widely used procedures is the Expectation Maximization (EM) algorithm [Moo97]. In this work we have used a SAGE algorithm. This later is derived from EM algorithm.

The parameters to estimate are L, α_l, γ_l and τ_l. The number of MPCs L in the observed UWB signal $Y(t)$ is derived by using the Maximum Description Length (MDL) algorithm and the Akaike Information Criterion (AIC) [SHKA05b]. Before estimating α_l, γ_l and τ_l We start by estimating γ_l. To do so, we use a method based on an approximation by regression (we can see the γ_l as a slope in each path). To estimate the parameters $\theta_l = [\alpha_l, \tau_l]$, we use SAGE algorithm. Our global estimation scheme is depicted on Figure 6.7.

Let $Y(t)$ our observation of incomplete data (observable data) and t denote the discreet time.

$$Y(t) = \sum_{l=1}^{L} \alpha_l e^{-\beta_l t} u(t - \tau_l) + \nu(t), \quad \beta_l = \frac{1}{\gamma_l}, \tag{6.13}$$

where $\nu(t)$ is an Additive White Gaussian Noise (AWGN) mean null with variance σ_n^2.

In the problem of estimating superimposed signal (6.13), the individual signals is given by

$$X_k(t; \theta_k) = \alpha_k e^{-\beta_k t} u(t - \tau_k) + \nu(t). \tag{6.14}$$

The relationship between the admissible data $X_k(t; \theta_k)$ (the noise $\nu(t)$ is included in the complete data.) for θ_k and the incomplete data $Y(t)$ is expressed as

$$Y(t) = X_k(t; \theta_k) + \sum_{l \neq k}^{L} \alpha_l e^{-\beta_l t} u(t - \tau_l), \tag{6.15}$$

[1] the reflector it is the object which causes the reflection of the path.

$$X_k(t;\theta_k) = Y(t) - \sum_{l\neq k}^{L} \alpha_l e^{-\beta_l t} u(t-\tau_l). \tag{6.16}$$

The $X_k \sim \mathcal{N}(\mu_x, \sigma_n^2)$ and the $Y \sim \mathcal{N}(\mu_y, \sigma_n^2)$. We assume that no overlap in clusters, the SAGE algorithm is based on the calculation of conditional expectation of the log-likelihood $Q(\theta_k, ; \theta^i)$ of X_k [FHay], the θ_k and θ^i refer to the parameter to be estimate and the estimated parameters at iteration i. Since $X_k(t)$ is not observable one can try to estimate it based on the observation $Y(t) = y(t)$ of the incomplete data and a previous estimate $\hat{\theta}^i$ of θ. A natural estimate of $X_k(t)$ is its conditional expectation given $Y(t) = y(t)$ and assuming $\theta = \hat{\theta}^i$ [FTH+17]. The probability density function of θ_k for the observation $X_k(t;\theta_k) = x_k(t;\theta_k)$ based on the $\hat{\theta}^i$ and $Y(t) = y(t)$ is defined as follows:

$$\begin{aligned}
f(X;\theta_k,\theta^i|Y=y) &\cong K e^{-\frac{1}{2\sigma_n^2}\sum_{t=1}^{N}(X_k(t)-\mu_x)(X_k(t)-\mu_x)}, && (6.17)\\
&\cong K e^{-\frac{1}{2\sigma_n^2}\sum_{t=1}^{N}(X_k(t)X_k(t)-X_k(t)\mu_x-\mu_x X_k(t)+\mu_x^2)}, && (6.18)\\
&\cong K e^{-\frac{1}{2\sigma_n^2}\sum_{t=1}^{N}(X_k(t)^2-2X_k(t)\mu_x+\mu_x^2)}, && (6.19)\\
&\cong K' e^{-\frac{1}{2\sigma_n^2}\sum_{t=1}^{N}(-2X_k(t)\mu_x+\mu_x^2)}, && (6.20)
\end{aligned}$$

where $K' = K e^{-\frac{1}{2\sigma_n^2}\sum_{t=1}^{N} X_k(t)^2}$.

The log-Likelihood function is given by:

$$\Lambda(X;\theta_k,\theta^i|Y=y) = \log f(X;\theta_k,\theta^i|Y=y). \tag{6.21}$$

$$\Lambda(X;\theta_k,\theta^i|Y=y) \cong c' - \frac{1}{2\sigma_n^2}\sum_{t=1}^{N}(-2X_k(t)\mu_x + \mu_x^2), \tag{6.22}$$

where N is the length of interval D.

$$\Lambda(X;\theta_k,\theta^i|Y=y) \cong c' + \frac{1}{\sigma_n^2}\sum_{t=1}^{N}\mu_x(X_k(t) - \frac{1}{2}\mu_x). \tag{6.23}$$

A maximum-Likelihood estimate (MLE) of θ_k based on the observation $y(t)$ is the value[2] of this vector which maximizes $\Lambda(X;\theta_k,\theta^i|Y=y)$, where $y(t)$ is defined. Finally, we can calculate the $Q(\theta_k;\theta^i)$:

$$\begin{aligned}
Q(\theta_k;\theta^i) &= E\{\Lambda(X;\theta_k,\theta^i|Y=y)|Y=y\}\\
&\cong E\{c' + \frac{1}{\sigma_n^2}\sum_{t=1}^{N}\mu_x(X_k(t) - \frac{1}{2}\mu_x)\}\\
&\cong c' + \frac{1}{\sigma_n^2}\sum_{t=1}^{N}\mu_x(E\{X_k(t)|Y=y\} - \frac{1}{2}\mu_x) && (6.24)
\end{aligned}$$

[2]For the sake of simplicity we assume that this value is unique.

where $E\{X_k(t)|Y=y\} = E\{X_k(t)\} - R_{xy}R_{yy}^{-1}\{y - Ey\}$ and $E\{X_k(t)|Y=y\} = \mu_x - \sigma_n^2\sigma_n^{-2}\{y - \mu_y\}$

$$\begin{aligned} Q(\theta_k;\theta^i) &\cong c + \frac{1}{\sigma_n^2}\sum_{t=1}^{N}\mu_x(\mu_x - \{y-\mu_y\} - \frac{1}{2}\mu_x) \\ &\cong c + \frac{1}{\sigma_n^2}\sum_{t=1}^{N}\mu_x(\frac{1}{2}\mu_x - (y-\mu_y)) \end{aligned} \tag{6.25}$$

We substitute the μ_x and μ_y by their expansions, $\mu_x = \alpha_k e^{-\beta_k(t-\tau_k)}u(t-\tau_k)$ and $\mu_y = \sum_{l\neq k}^{L}\alpha_l e^{-\beta_l t}u(t-\tau_l)$ respectively.

$$Q(\theta_k;\theta^i) \cong c + \frac{1}{\sigma_n^2}\sum_{t=1}^{N}\alpha_k e^{-\beta_k t}u(t-\tau_k)(\frac{1}{2}\alpha_k e^{-\beta_k t}u(t-\tau_k) - (y - \sum_{l\neq k}^{L}\alpha_l e^{-\beta_l t}u(t-\tau_l))) \tag{6.26}$$

The MLE's of the parameters $\hat{g}_k$, $\hat{\tau}_k$ of a single impinging wave: $\{\hat{\tau}_k, \hat{g}_k\} = \arg_{\tau,g}\max\{Q(\theta_k;\theta^i)\}$.

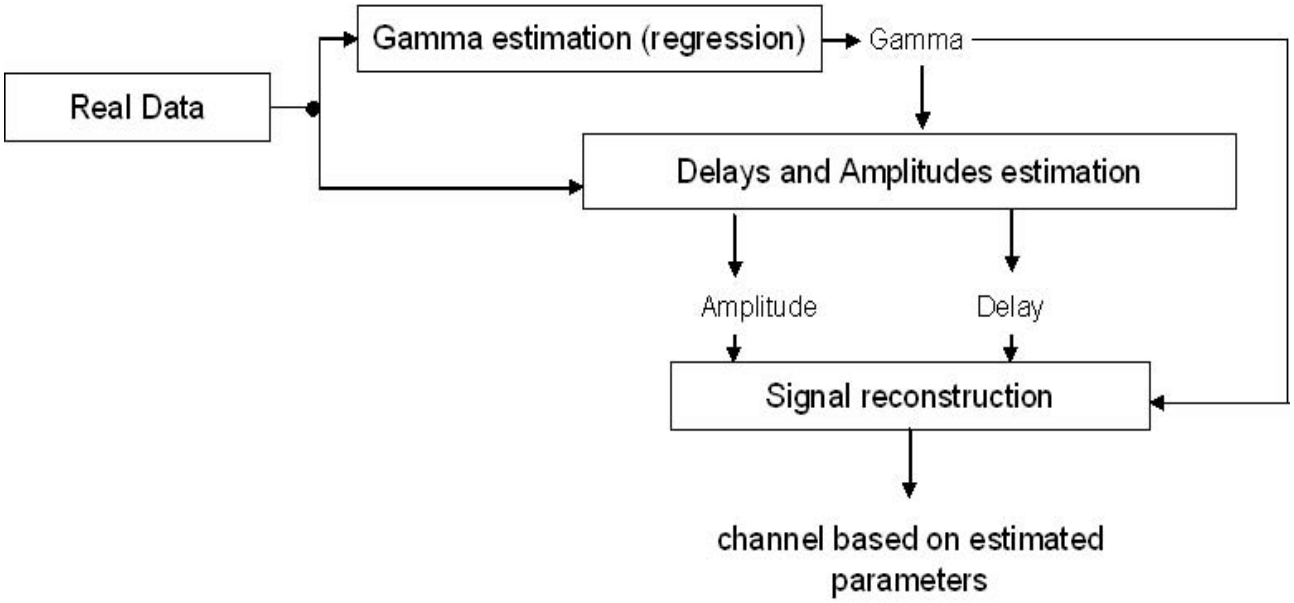

Figure 6.7: Bloc diagram for channel model parameters estimation.

6.4 Results

6.4.1 UWB Channel Model Implementation

The analytical channel is implemented, using Matlab Tools, based on equations derived in [Qiu04] and [Bar91]. The nature of the environment (dense, number of reflecting/diffracting scatterers, geometry, etc...) is fully parameterizable. For the statistical model, we propose as a first approach to model γ_l,

Table 6.1: Small scale statistics

	$\tau_{rms,L=50}$ ns	$\tau_{m,L=50}$ ns	$\tau_{rms,L=100}$ ns	$\tau_{m,L=100}$ ns
mean	11.7953	9.6071	11.3588	8.3215
min	6.0284	2.3504	7.1747	3.6765
max	15.3522	18.4709	14.6920	16.5753

α_l and τ_l using lognormal distribution and exponential distribution respectively.
Figure (6.10) shows the power delay profile for simulated analytical channel with $L = 100$, $\bar{\gamma} = 1.5$ and time resolution $0.1667ns$ corresponding $W = 6\ GHz$. We can see from this figure that the simulated channel exhibits the same clustered behavior as what was observed from UWB channel measurements [HKS05].

The PDP is generally characterized by the first central moment (mean excess delay) τ_m and the square root of the second moment (root mean square delay spread), τ_{rms}.

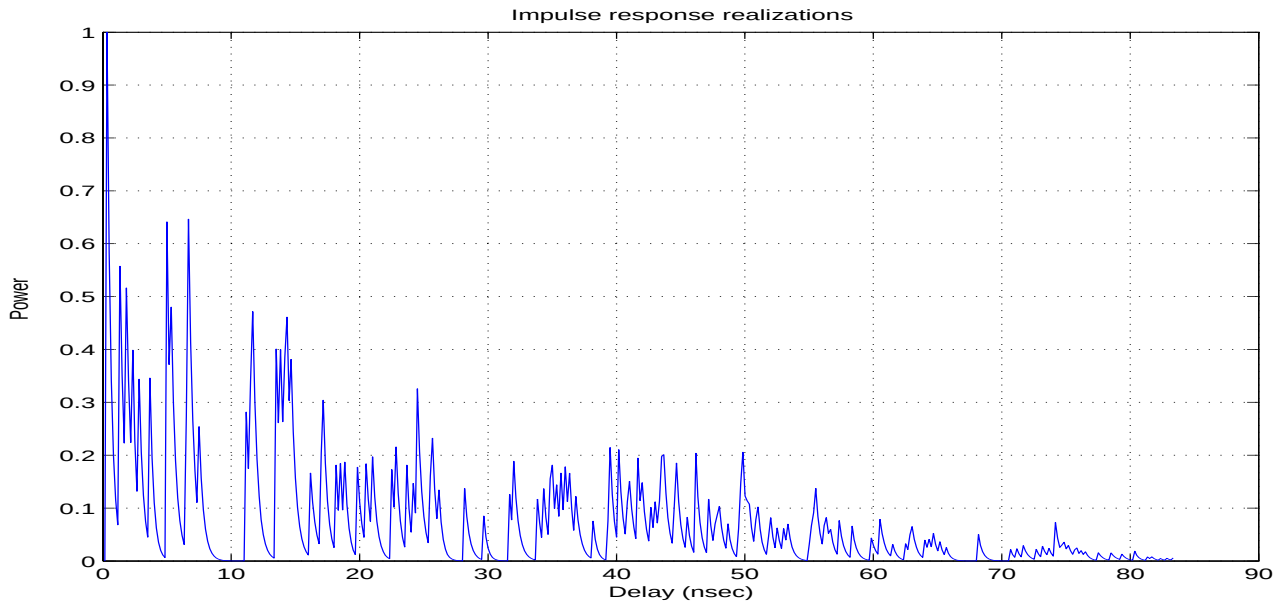

Figure 6.8: Simulated UWB Channel Impulse Response realization (1) $L = 100$.

The resulting small scale statistics are given in Table 6.4.1. These results represent all 500 realizations (Note in computing these results the power delay profiles (PDPs) were normalized). Comparing the results for the different environments (commanded by L number of multi path and γ material considerations) reveals some relative trends for the mean excess delay, max excess delay, RMS delay spread, and the number of paths.

Figure 6.11 presents comparison between the real and simulated channel function transfer in frequency domain. This shows that the simulated channel is close to real one.

Figures 6.12 and 6.13 shows the cumulative distribution function of τ_m and τ_{rms} for the analytical channel, respectively. These results show that the statistics of the simulated model are in agreement with the hose published in the literature and the real channel.

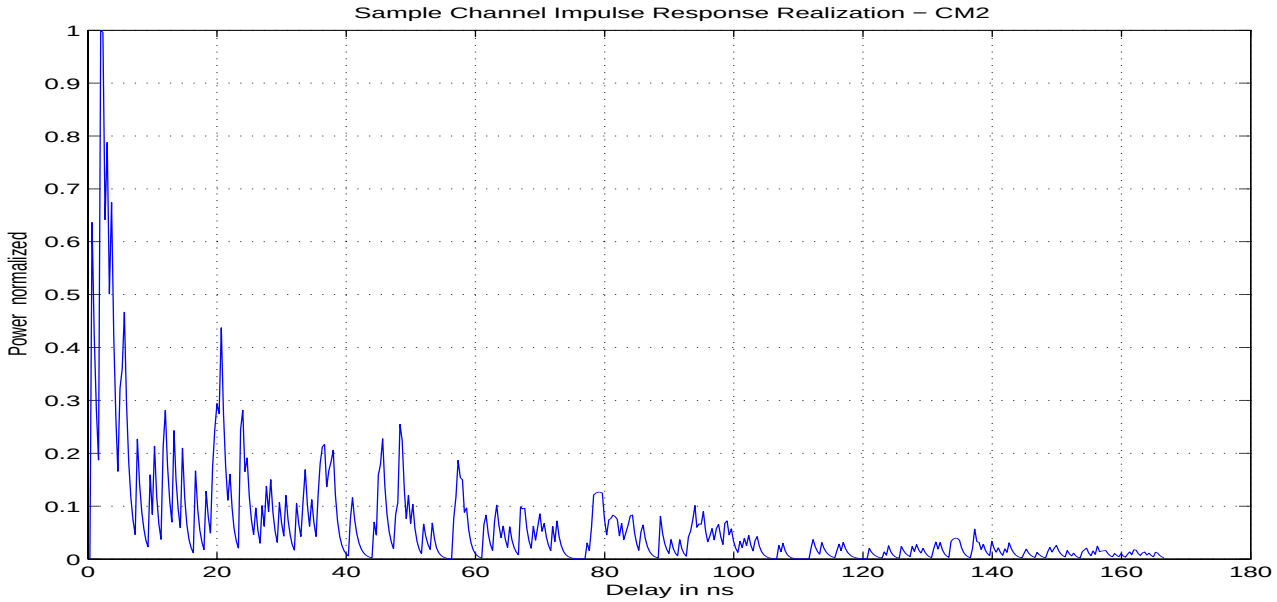

Figure 6.9: Simulated UWB Channel Impulse Response realization (2) $L = 70$.

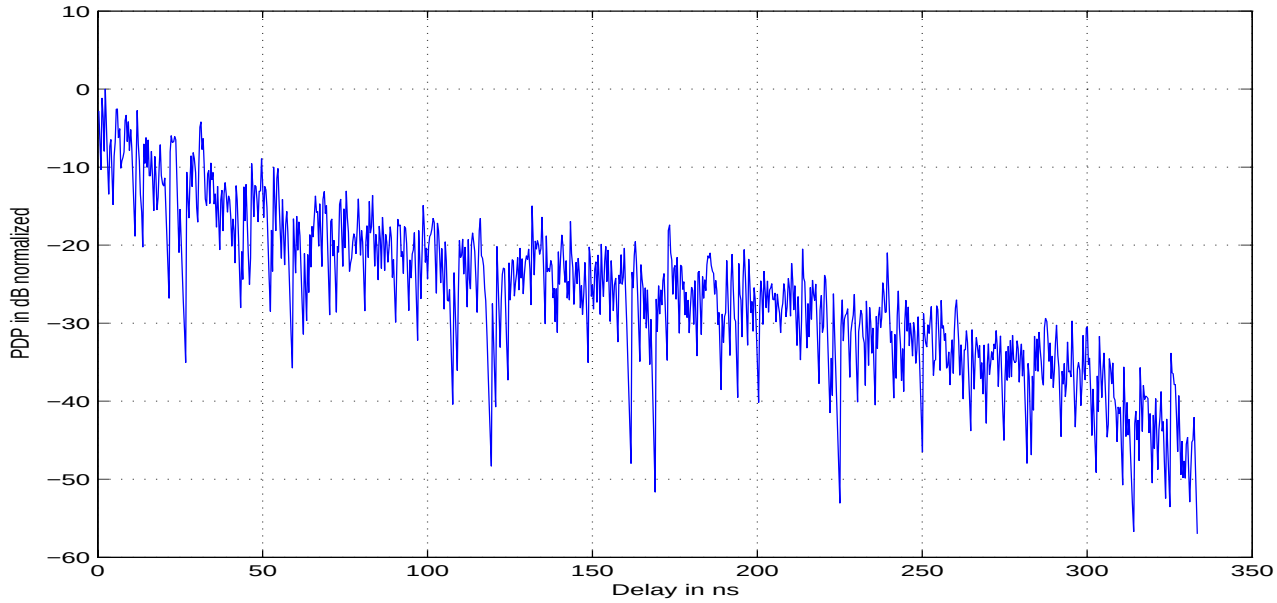

Figure 6.10: The power delay profile estimated from simulated channel $L = 100$.

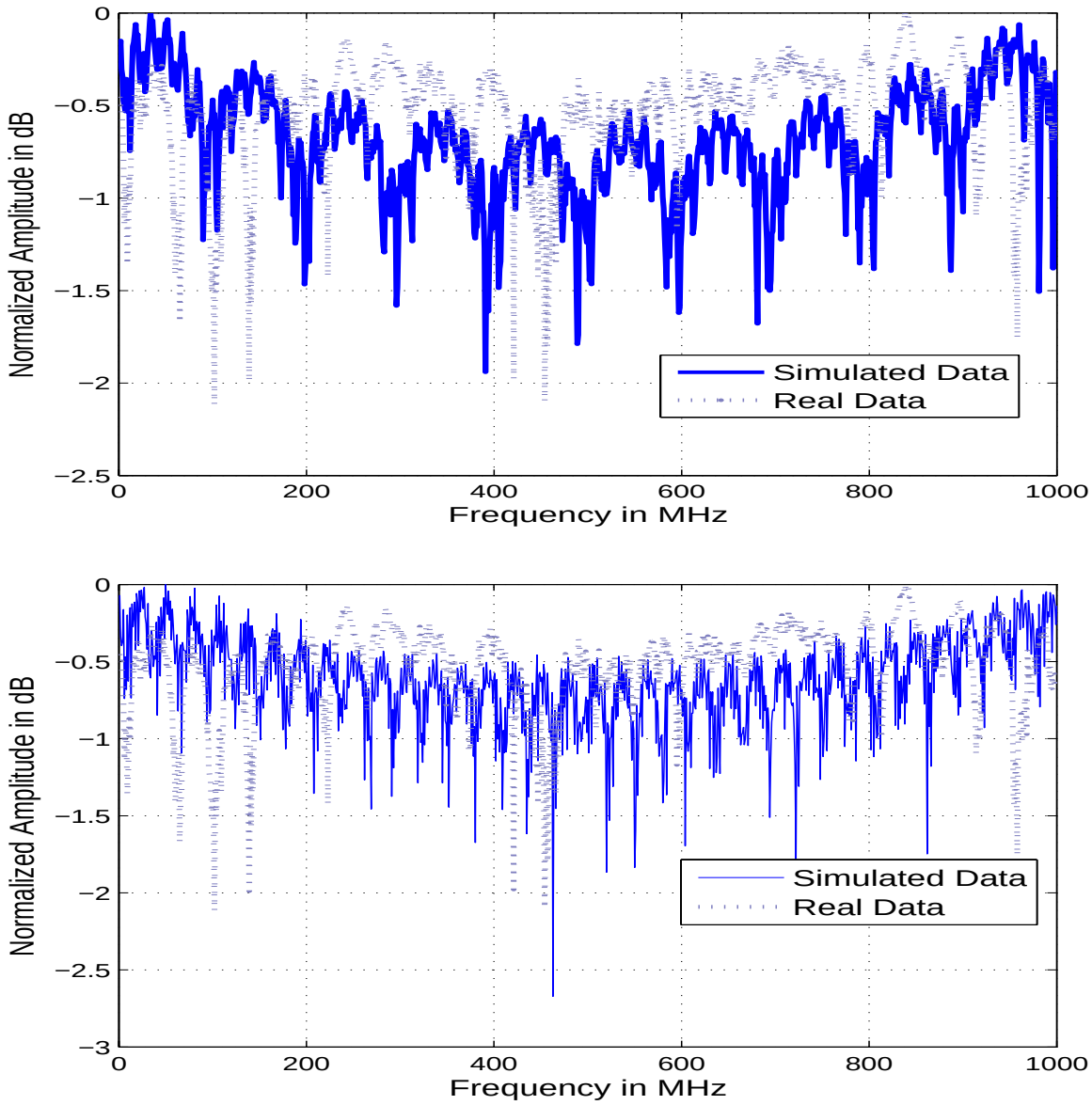

Figure 6.11: Comparison between the frequency response for real and simulated channel 1 GHz. Two different realizations.

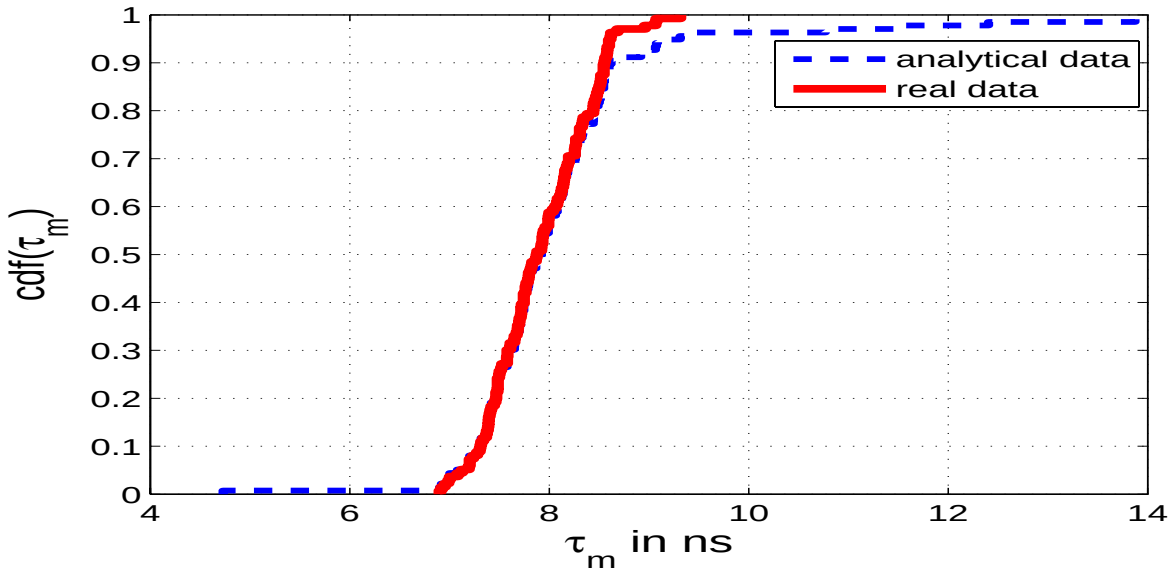

Figure 6.12: τ_m from simulated analytical channel

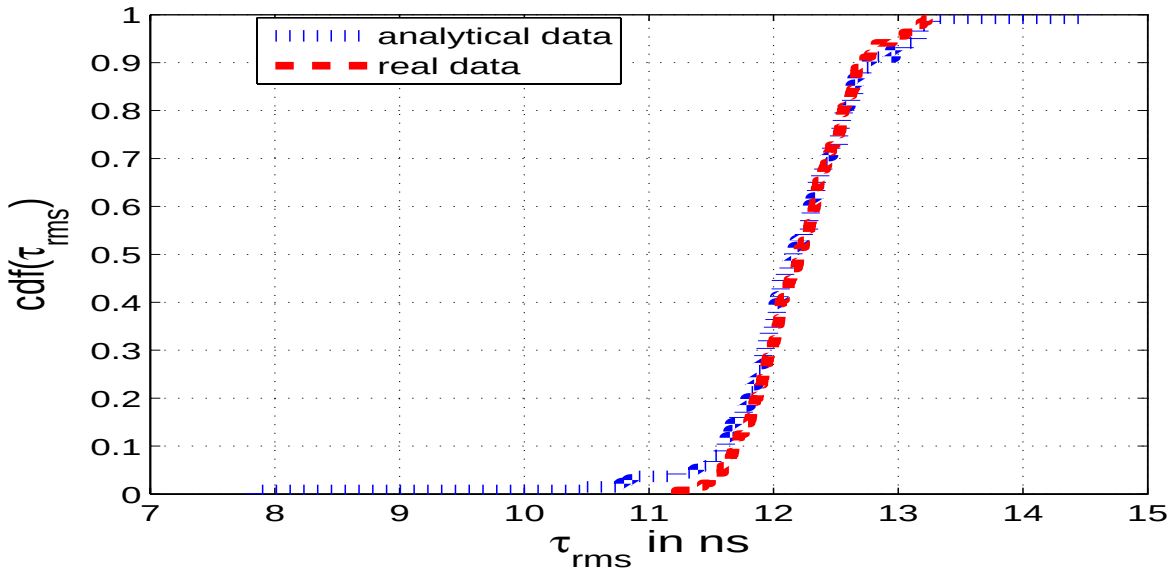

Figure 6.13: τ_{rms} both from simulated analytical channel

6.4.2 Channel Parameters Estimation

In this part, we focus on the estimation of the channel parameters using the model presented in equation (6.6). In Figures 6.14 and 6.15, we show the impulse responses of the analytical[3] channel and the measured channel [HKS05] and compare them to channel built based on our parameter estimates.

In Figure 6.16, we show single realizations of the impulse responses of the simulated based on the model in equation (6.8) and compare them with one based on our parameters estimates. The Figure shows the good agreement with original and estimated channels.

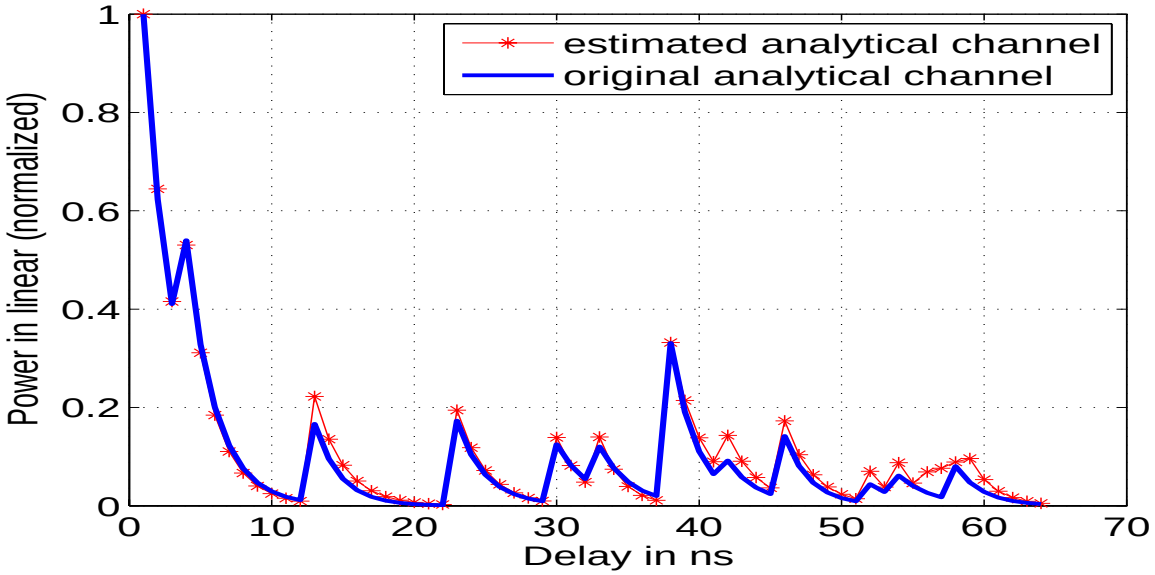

Figure 6.14: Estimated impulse response of the analytical channel 1 GHz.

6.5 Conclusion

In this chapter, we have combined results from channel measurement data and the physical channel propagation phenomena to derive a new statistical UWB channel model. We started by analyzing, based on simulations, the effects of different physical propagation phenomena using analytical time domain expressions of reflected and diffracted paths. These simulations have demonstrated that on the contrary of the narrow and wide bandwidth, the channel behavior in UWB context is completely different. After that, we have presented the new UWB channel model, a mathematical description of the model is discussed and the corresponding parameters extraction derivations, based on SAGE algoritm, are presented. According to the obtained results, we can conclude that the proposed model presents a good fit to measurement data and is easy to implement.

[3]The analytical channel is constructed using a set of responses of paths generated by diffraction or reflection mechanisms.

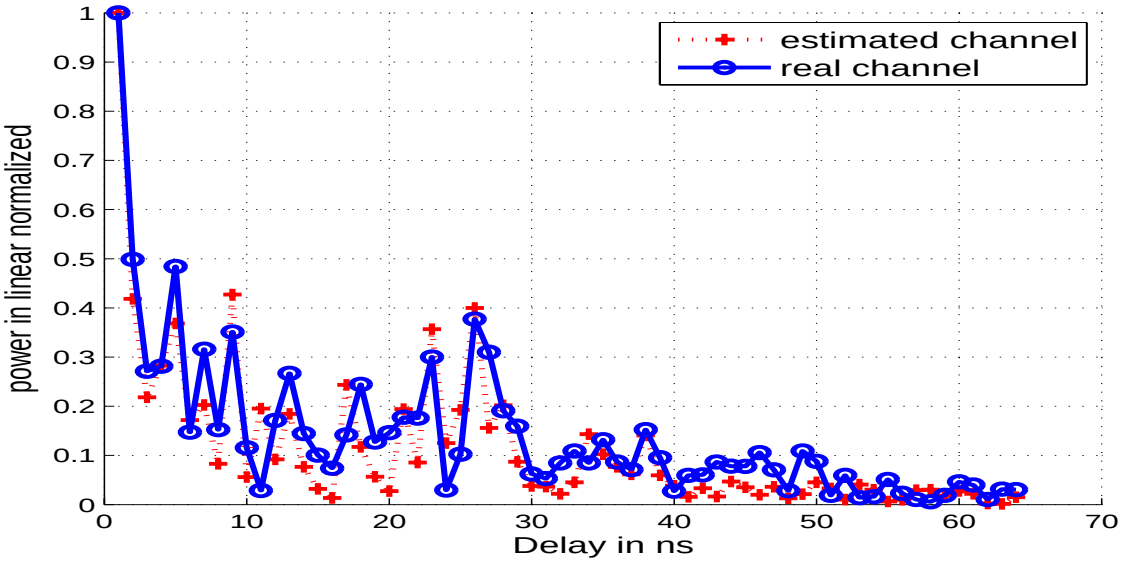

Figure 6.15: Estimated impulse response of the measured channel 1 GHz.

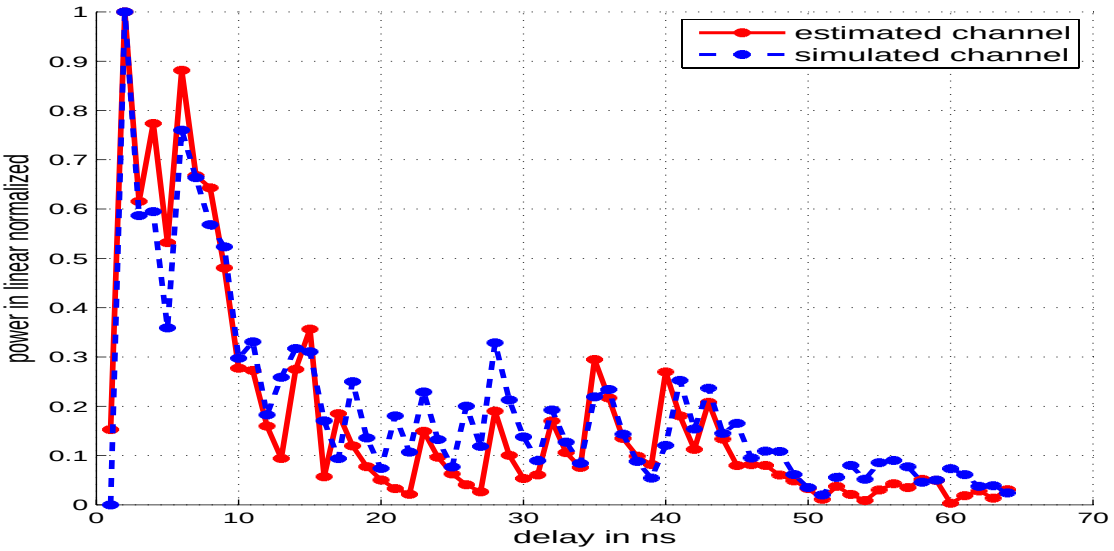

Figure 6.16: Estimated impulse response of the simulated channel $\bar{\gamma} = 1.5$, $L = 40$.

CHAPTER

7

CONCLUSIONS AND FUTURE WORKS

7.1 Conclusion

This thesis has discussed a variety of topics related to ultra-wideband characterization and modeling. Strong work characterizing the indoor UWB channel was presented. Based on those findings issues on UWB channel behavior and properties, a novel UWB channel model is presented. Numerous statistical characterizations of the indoor UWB channel, based on measurement data, were presented in Chapter 4. In this Chapter we have investigated ultra wideband propagation channels in different environments, and established a statistical model that captures the main behavior of the channel. We found that the power variation can be described by a Weibull distribution model. We have also observed that no correlation between the path loss and the frequency bandwidth of interest. On the other hand, a correlation between path loss and central frequency is detected. The small-scale fading for all environments is described by a Rayleigh distribution, except for the first components in channel impulse response. Finally, the RMS delay spread was found to be about between 3.6 ns and 15.2 ns for LOS and about between 9.6 ns and 15.6 ns and . This value is much smaller than that of conventional narrowband systems. In Chapter 5, based on the measurement, the UWB channel total received energy and the number of eigen-values of channel are evaluated empirically. The evaluation of total received energy shows that the energy of UWB channel impulse responses suffer small variations, when compared to narrowband channels. We have also presented two different techniques based on information theory arguments, namely the AIC and the MDL, to estimate the number of DoF of an UWB channel in an in-door environment. The evolution of the scaling of DoF, extracted using AIC and MDL, versus the bandwidth was also analyzed and compared to the product of the rms delay spread with the bandwidth. This comparison, highlights the fact that the number of DoF for a given UWB channel saturates beyond a certain frequency bandwidth and does not increase linearly. Also an estimation of UWB channel entropy is provided to justify the DoF scaling behavior with the channel bandwidth. Motivated by these strong results found in chapters 4 and 5, we decided to investigate the underlying physical phenomena that govern the channel behavior and to propose a more realistic UWB channel model. In chapter 6, section 6.2, the frequency dependent distortion of UWB pulse is tested, when passing through various materials for different channel bandwidths. It was shown thus that for many common materials, the time dispersion per path is different over the same UWB channel bandwidth. Based on these results, we have proposed a new statistical UWB channel model taking into account the effect of physical phenomena, like the reflection and the diffraction, at large bandwidths. Finally, the extraction of the parameters of the model is performed using the well known SAGE algorithm and first results are given. The proposed model presents a good fit to measurements data and is easy to implement. Indeed, a set of four parameters, namely the number of MPCs, the MPC amplitude, the MPC delay and the MPC decay constant, describes the whole model.

7.2 Contributions

The present thesis has provided numerous original contributions to UWB channel characterization and modeling research areas like:

- Complete state of the art on the published UWB channel models within last five years.
- Providing a large UWB channel measurement data base carried out at Eurecom Institute. This database was used within the FP6 European project NEWCOM/Project B [saa05] to validate many UWB channel models and to address UWB channel performance.
- Results on the effect of the antennas response on UWB channel behavior (using Intel measurements).
- Statistical characterization of indoor (some results are also available for outdoor environment) small scale and large scale effects using Eurecom UWB measurement database.
- Empirical and theoretical characterization of UWB DoF using information theory arguments. These findings were completely new in the literature and this work was pionner to highlight the non linear scaling of UWB DoF versus the bandwidth. Many recent works published in the literature refer to our results [PM07, PM06b, PM06a, HRS07, RHS07, HS07, UH06, KCG+05, CFT07, CFAT06b, SK04] and [Sou05, Ano06, dLNMDF06, dLNMD06, dLNDH06, HV05].
- New statistical LOS model for indoor UWB channels.
- Estimation of channel parameters of the proposed model using SAGE algorithm

7.3 Future Works

The future works will focus on the improvement of the proposed UWB channel model to take into account the variability of the parameters of the model with respect to the bandwidth and the central frequency of interest.
Another focus will concern the investigation of localization issues taking advantage from UWB high temporal resolution.

APPENDIX

A

APPENDIX

A.1 UWB Channel Model Parameters Estimation Using Sage Algorithm

In the 6.3.1, we found that the MLE's of the parameters $\hat{\alpha}_k, \hat{\beta}_k, \hat{\tau}_k$ of a single impinging wave:

$$\{\hat{\alpha}_k, \hat{\beta}_k, \hat{\tau}_k\} = \arg\max_{\alpha,\beta,\tau} Q(\theta_k; \theta^i)\}$$

here we present the estimators for different parameters $\{\hat{\alpha}_k$, $\hat{\beta}_k$ and $\hat{\tau}_k\}$ we have

$$Q(\theta_k;\theta^i) \cong c + \frac{1}{\sigma_n^2}\sum_{t=1}^{N} \alpha_k e^{-\beta_k t}u(t-\tau_k)(\frac{1}{2}\alpha_k e^{-\beta_k t}u(t-\tau_k) - (y - \sum_{l\neq k}^{L} \alpha_l e^{-\beta_l t}u(t-\tau_l)) \quad \text{(A.1)}$$

$$\cong c + \frac{1}{\sigma_n^2}\sum_{t=1}^{N} \alpha_k e^{-\beta_k t}u(t-\tau_k)(\frac{1}{2}\alpha_k e^{-\beta_k t}u(t-\tau_k) - (y - GA)) \quad \text{(A.2)}$$

$$\cong c + \frac{1}{\sigma_n^2}\sum_{t=1}^{N} \alpha_k e^{-\beta_k t}u(t-\tau_k)(\frac{1}{2}\alpha_k e^{-\beta_k t}u(t-\tau_k) - (y - GA)) \quad \text{(A.3)}$$

where $GA = \sum_{l\neq k}^{L} \alpha_l e^{-\beta_l t}u(t-\tau_l))$.

The estimator of α_k:

$$\frac{\partial Q(\theta_k;\theta^i)}{\partial \alpha_k} = 0$$

let $A_k = e^{-\beta_k t}u(t-\tau_k)$,

$$\frac{\partial Q(\theta_k;\theta^i)}{\partial \alpha_k} = \frac{\partial}{\partial \alpha_k}\left[c + \frac{1}{\sigma_n^2}\sum_{t=1}^{N}\alpha_k A_k(\frac{1}{2}\alpha_k A_k - (y - GA))\right] \tag{A.4}$$

$$= \frac{1}{\sigma_n^2}\sum_{t=1}^{N}A_k(\frac{1}{2}\alpha_k A_k - (y - GA)) + \sum_{t=1}^{N}\alpha_k A_k(\frac{1}{2}A_k)) \tag{A.5}$$

$$= \frac{1}{\sigma_n^2}\sum_{t=1}^{N}(\frac{1}{2}\alpha_k A_k^2 - A_k(y - GA)) + \sum_{t=1}^{N}\alpha_k(\frac{1}{2}A_k^2)) \tag{A.6}$$

$$= \sum_{t=1}^{N}\alpha_k A_k^2 - A_k(y - GA) \tag{A.7}$$

$$= 0 \tag{A.8}$$

Then

$$\sum_{t=1}^{N}\alpha_k A_k^2 = \sum_{t=1}^{N}A_k(y - GA)$$

the A_k is depends on the time t then

$$\hat{\alpha}_k^{i+1} = \frac{\sum_{t=1}^{N}e^{-\hat{\beta}_k^i t}u(t-\hat{\tau}_k^i)(y(t) - \sum_{l=k}^{L}\hat{\alpha}_l^i e^{-\hat{\beta}_l i t}u(t-\hat{\tau}_l^i))}{\sum_{t=1}^{N}e^{-2\hat{\beta}_k^i t}u^2(t-\hat{\tau}_k^i)}.$$

The estimator of β_k:

$$\frac{\partial Q(\theta_k;\theta^i)}{\partial \beta_k} = 0$$

we have $\frac{\partial}{\partial \beta_k}A_k = -tA_k$.

$$\frac{\partial}{\partial \beta_k}\left[c + \frac{1}{\sigma_n^2}\sum_{t=1}^{N}\alpha_k A_k(\frac{1}{2}\alpha_k A_k - (y - GA))\right] = 0$$

$$\frac{1}{\sigma_n^2}\left[c\sum_{t=1}^{N}(-t)A_k(\frac{1}{2}\alpha_k A_k - (y - GA)) + \sum_{t=1}^{N}\frac{1}{2}\alpha_k(-t)A_k^2\right] = 0$$

$$\sum_{t=1}^{N}t\alpha_k A_k^2 = \sum_{t=1}^{N}tA_k(y - GA)$$

$$\sum_{t=1}^{N}t\alpha_k e^{-2\beta_k t}u^2(t-\tau_k) = \sum_{t=1}^{N}te^{-\beta_k t}u(t-\tau_k)(y - GA)$$

$$\sum_{t=1}^{N} te^{-2\beta_k t}u^2(t-\tau_k) = \frac{1}{\alpha_k}\sum_{t=1}^{N} te^{-\beta_k t}u(t-\tau_k)(y-GA). \tag{A.9}$$

Equation (A.9) can be rewritten using matrix formula as follows:

$$\underline{B}^T\ \underline{U}\ \underline{1} = \underline{B}'^T\ \underline{U}'\ \underline{1} \tag{A.10}$$

where

$$\underline{B} = \begin{bmatrix} e^{-2\beta_k} \\ e^{-4\beta_k} \\ . \\ . \\ . \\ e^{-2N\beta_k} \end{bmatrix}, \underline{U} = \begin{bmatrix} 1u^2(1-\tau_k) \\ 2u^2(2-\tau_k) \\ . \\ . \\ . \\ Nu^2(N-\tau_k) \end{bmatrix}, \underline{B}' = \frac{1}{\alpha_k}\begin{bmatrix} e^{-\beta_k} \\ e^{-\beta_k} \\ . \\ . \\ . \\ e^{-N\beta_k} \end{bmatrix},$$

$$\underline{U}' = \begin{bmatrix} 1u(1-\tau_k)(y(1)-GA) \\ 2u(2-\tau_k)(y(2)-GA) \\ . \\ . \\ . \\ Nu(N-\tau_k)(y(N)-GA) \end{bmatrix},$$

and $\underline{1} = \underbrace{[1,...,1]}_{1\times N}$ the (A.9) become:

$$\underline{B}^T\ R = \underline{B}'^T\ R' \tag{A.11}$$

where $R = \underline{U}\ \underline{1}$ a full rank matrix then $det(R) \neq 0$ and $R' = \underline{U}'\ \underline{1}$

$$\underline{1}'\underline{B}^T\ RR^{-1} = \underline{1}'\underline{B}'^T\ R'R^{-1} \tag{A.12}$$

$$\log(\underline{1}'\underline{B}^T) = \log(\underline{1}'\underline{B}'^T\ R'R^{-1}) \tag{A.13}$$

$$\log(\underline{1}'\underline{B}^T) = \log(\underline{1}'\underline{B}'^T) + \log(R'R^{-1}) \tag{A.14}$$

Let

$$\underline{1}'\underline{B}^T = \begin{pmatrix} e^{-2\beta_k} & e^{-2\beta_k} & . & . & . & e^{-2\beta_k} \\ e^{-4\beta_k} & e^{-4\beta_k} & . & . & . & e^{-4\beta_k} \\ . & . & . & . & . & . \\ . & . & . & & & \\ . & . & . & . & . & . \\ e^{-2N\beta_k} & e^{-2N\beta_k} & . & . & . & e^{-2N\beta_k} \end{pmatrix}$$

$$\underline{1}'\underline{B}'^T = \begin{pmatrix} e^{-1\beta_k} & e^{-1\beta_k} & . & . & . & e^{-1\beta_k} \\ e^{-2\beta_k} & e^{-2\beta_k} & . & . & . & e^{-2\beta_k} \\ . & . & . & . & . & . \\ . & . & . & & & \\ . & . & . & . & . & . \\ e^{-N\beta_k} & e^{-N\beta_k} & . & . & . & e^{-N\beta_k} \end{pmatrix}$$

$$V = \begin{pmatrix} 1 & 1 & . & . & . & 1 \\ 2 & . & . & . & . & 2 \\ . & . & . & . & . & . \\ . & . & . & . & . & . \\ . & . & . & . & . & . \\ N & N & . & . & . & N \end{pmatrix}$$

$$-2\beta_k V + \beta_k V = \log(R'R^{-1}) \tag{A.15}$$

$$\hat{\beta_k}^{i+1} = -V^{-1}\log(R'R^{-1}) = \frac{1}{\hat{\gamma_k}^{i+1}}$$

The estimator of τ_k: we have $< u >' = \delta$ in distribution sense.

$$\frac{\partial Q(\theta_k;\theta^i)}{\partial \tau_k} = 0$$

we have $\frac{\partial}{\partial \tau_k} A_k = e^{-\beta_k}\frac{1}{\tau_k}\delta(t-\tau_k)$.

$$\frac{\partial}{\partial \tau_k}\left[c + \frac{1}{\sigma_n^2}\sum_{t=1}^{N}\alpha_k A_k(\frac{1}{2}\alpha_k A_k - (y - GA))\right] = 0$$

$$\sum_{t=1}^{N}\alpha_k e^{-\beta_k t}\frac{1}{\tau_k}\delta(t-\tau_k t)(\frac{1}{2}\alpha_k A_k - (y-GA))$$
$$+\alpha_k e^{-\beta_k t}u(t-\tau_k)(\frac{1}{2}\sum_{t=1}^{N}\alpha_k e^{-\beta_k}\frac{1}{\tau_k}\delta(t-\tau_k)) = 0$$

$$\sum_{t=1}^{N}\alpha_k e^{-\beta_k t}\frac{1}{\tau_k t}\delta(t-\tau_k)(\frac{1}{2}\alpha_k e^{-\beta_k t} - (y-GA))$$
$$+\alpha_k e^{-\beta_k t}u(t-\tau_k)(\frac{1}{2}\sum_{t=1}^{N}\alpha_k e^{-\beta_k t}\frac{1}{\tau_k}\delta(t-\tau_k)) = 0$$

then

$$\hat{\tau}_k^{i+1} = -\frac{1}{\hat{\beta}_k^i}\log\left(\frac{y(t) - \sum_{l=k}^{L}\hat{\alpha}_l^i e^{-\hat{\beta}_l^i t}u(t-\hat{\tau}_l^i)}{\hat{\alpha}_k^i}\right)$$

BIBLIOGRAPHY

[A.99] Balanis C. A. *Antenna theory: analysis and design*. 2nd edition, John Wiley and Sons, Inc, 3rd edition, 1999.

[AA03] M. Lobeira et al. A. Alvarez, G. Valera. New channel impulse response model for uwb indoor system simulations. In *IEEE Vehicular Technology Conference, VTC Spring, Seoul, Korea*, pages 1–5, April 2003.

[AMR02] B. Woerner A. Muqaibel, A. Safaai-Jazi and S. Riad. Uwb channel impulse response characterization using deconvolution techniques. In *IEEE International Midwest Symposium on Circuits Systems, Tulsa Oklahoma*, pages 605–608, 4-7 August 2002.

[And84] T.W. Anderson. *An Introduction to Multivariate Statistical Analysis*. 2nd Ed., Wiley New York, 1984.

[Ano06] Hicham Anouar. *Design and Optimization of Multiple Access Protocols for Ad Hoc Wireless Networks*. PhD thesis, l' Ecole Nationale Supérieure, des Télécommunications (ENST), Jun 2006.

[App] Application requirement analysis. ieee p802.15-03/0489r4.

[AVL+03] A. Alvarez, G. Valera, M. Lobeira, R. Torres, and J. L. Garcia. New channel impulse response model for uwb indoor system simulations. In *IEEE VTC-Fall*, pages 1–5, Sep 2003.

[Bar91] P. R. Barnes. On the direct calculation of a transient plane wave reflected from a finitely conducting half plane. *IEEE Trans. on Electromagnetic Compatibility*, 33(2), May 1991.

[BD91] W.R. Braun and U. Dersch. A physical mobile radio channel. *IEEE Transactions on Vehicular Technology*, 40(2):472–482, May 1991.

[BDSJea03] R. M. Buehrer, W. A. Davis, A. Safaai-Jazi, and et al. Characterization of the ultra-wideband channel. In *IEEE Conference on Ultra Wide Band Systems and Technologies, Reston, VA, USA*, pages 26–31, Novomber 2003.

[Bel63] A. P. Bello. Characterization of randomly time-variant linear channels. *IEEE Transactions on Communications Systems*, 11(4):360–393, 1963.

[Bel64] A. P. Bello. Time-frequency duality. *IEEE Transactions on Information Theory*, 10(1):18–33, 1964.

[BWXea04] K. Balakrishnan, K. C. Wee, S. Xu, and et al. Characterization of ultra-wideband channels : Small-scale parameters for indoor & outdoor office environments. *Document technique IEEE 802.15- 04/385*, Jully 2004.

[CDC05] W. Ciccognani, A. Durantini, and D. Cassioli. Time domain propagation measurements of the uwb indoor channel using pn-sequence in the fcc compliant band 3.66 ghz. *IEEE Transactions On Antennas And Propagation*, 53(4):1542–1549, April 2005.

[CFAT06a] A. Chehri, P. Fortier, H. Aniss, and P. M Tardif. Uwb spatial fading and small scale characterization in underground mines. *Communications, 2006 23rd Biennial Symposium on*, pages 213 – 218, May 29 - June 1 2006.

[CFAT06b] A. CHEHRI, P. FORTIER, H. ANISS, and P.-M. TARDIF. Uwb spatial fading and small scale characterization in underground mines. In *23rd IEEE Biennial Symposium on Communications, Kingston, Ontario,*, pages 213–218., 29 mai - 1er juin 2006.

[CFT07] A. CHEHRI, P. FORTIER, and P.M. TARDIF. Eigen-analysis of uwb channel in underground mines based on information theoretic criteria. In *IEEE International Conference Communication, Glasgow, Écosse*, 24-28 juin 2007.

[CKL04] C. C. Chong, Y. Kim, and S. S. Lee. Uwb indoor propagation channel measurements and data analysis in various types of high-rise apartments. In *IEEE Vehicular Technology Conference, VTC Fall, Los Angeles, CA, USA,*, pages 150–154, September 2004.

[CKL05] C.-C. Chong, Y. Kim, and S.-S. Lee. Statistical characterization of the uwb propagation channel in various types of high-rise apartments. In *Wireless Communications and Networking Conference*, pages 944 – 949, March 2005.

[CKYL05] Chia-Chin Chong, Young-Eil Kim, Su Khiong Yong, and Seong-Soo Lee. *Statistical characterization of the UWB propagation channel in indoor residential environment*, volume 5, chapter WIRELESS COMMUNICATIONS AND MOBILE COMPUTING, pages 503–512. Wiley InterScience (www.interscience.wiley.com). DOI: 10.1002/wcm.310, 2005.

[Com] Ultra Lab (Ulra-Wideband Radio Communication). *U.S.S Curtis Propagation Measurements*. http:ultra.use.eduulabUSScurtis.html.

[Com02] Federal Communications Commission. First report and order in the matter of revision of part 15 of the commission's rules regarding ultrawideband transmission systems. Technical report, ET-Docket 98153, FCC 02-48 released, 22 April 2002.

[Cor07] Intel Corporate. Ultra-wideband (uwb) technology. Technical report, http://www.intel.com/technology/comms/uwb/, 13, Februry 2007.

[CP02] D. Cheung and C. Prettie. A path loss comparison between the 5 ghz unii band (802.11a) and the 2.4 ghz ism band (802.11b). *Document technique, Intel Corporation*, Janaury 2002.

[CSMZ99] J. M. Cramer, R. A. Scholtz, and Win M. Z. Spatio-temporal diversity in ultra wideband radio. In *IEEE Wireless Communications and Networking Conference*, pages 888–892, 1999.

[CSW02] R. J. M. Cramer, R. A. Scholtz, and M. Z. Win. Evaluation of an ultrawide band propagation channel 50, pp. , may 2002. *IEEE Trans. Antennas Propagat*, 50(2):561570, May 2002.

[CTS04] W. J. Chang, J. H. Tarng, and M. J. Shen. Radio bandwidth on the averaged power-delay profiles of uwb indoor channels. In *COST 273 Workshop, Gothenburg, Sweden*, January 2004.

[CWM01] D. Cassioli, M. Z. Win, , and A. R. Molisch. A statistical model for the uwb indoor channel. In *IEEE IEEE VTC01 Spring Conference (VTC)*, page 11591163, October 2001.

[CWM02a] D. Cassioli, M. Z. Win, and A. F. Molisch. The ultra-wide bandwidth indoor channel: From statistical models to simulations. *IEEE Journal on Selected Areas in Communications*, 20(6):1247–1257, Aug 2002.

[CWM02b] D. Cassioli, M. Z. Win, and A. F. Molish. The ultra-wide bandwidth indoor channel-from statistical model to simulation. *IEEE Journal on Selected Areas Communications*, 20(6):1247–1257, Aug 2002.

[DHG] Jason A. Dabin, Alexander M. Haimovich, and Haim Grebel. A statistical ultra-wideband indoor channel model and the effects of antenna directivity on path loss and multipath propagation. *IEEE JOURNAL ON SELECTED AREAS IN COMMUNICATIONS*, 24(4):2006, April.

[DJ99] D. Dickson and P. Jett. Application specific integrated circuit implementation of a multiple correlator for uwb radio applications. In *IEEE Conference*, pages 1207–1210, October 1999.

[dLNDH06] Raul Liberato de Lacerda Neto, M. Debbah, and A. Menouni Hayar. Channel division multiple access. In *1st IEEE International Conference on Wireless Broadband and Ultra-Wideband Communications (AusWireless'06), New South Wales, Australia*, March 13-16 2006.

[dLNMD06] R.L. de Lacerda Neto, A. Menouni, and M. Debbah. Channel division multiple access based on high uwb channel temporal resolution. In *Vehicular Technology Conference, 2006. VTC-2006 Fall. 2006 IEEE 64th*, Spet 19-23 2006.

[dLNMDF06] R.L. de Lacerda Neto, A. Menouni, M. Debbah, and B.H. Fleury. A maximum entropy approach to ultra-wideband channel modeling. In *Speech and Signal Processing, ICASSP 2006 Proceedings. 2006 IEEE International Conference on*, June 19-23 2006.

[DMAS86] R. B. DAgostino and Eds. M. A. Stephens. *Goodness-of-Fit Techniques*. New York, NY, USA: Marcel Dekker, 1986.

[DMB06] B. M. Donlan, D. R. McKinstry, , and R. M. Buehrer. The uwb indoor channel: Large and small scale modeling. *IEEE TRANSACTIONS ON WIRELESS COMMUNICATIONS*, 5(10):2863–2873, October 2006.

[DNHea03] J. A. Dabin, N. Nan, A. M. Haimovich, and et al. The effect of antenna directivity on pathloss and multipath propagation in uwb indoor wireless channels,. In *IEEE Conference on Ultra Wideband Systems and Technologies, Reston, VA, USA*, pages 305–309, Novomber 2003.

[DSY00] Wayne E. Stark Do-Sik Yoo, VictorW.-K. Cheng. An index of frequency selectivity frequency mean square correlation. In *Vehicular Technology Conference Proceedings, 2000. VTC 2000-Spring Tokyo. 2000 IEEE 51st*, pages 15–18, May 2000.

[Dur04] D. Cassioli Et A. Durantini. Statistical characterization of uwb indoor propagation channels based on extensive measurement campaigns. In *International Symposium on Wireless Personal Multimedia Communications, Abano Terme, Italy,*, pages 236–240, September 2004.

[DVB+04] BM. Donlan, S. Venkatesh, V. Bharadwaj, RM Buehrer, and AJ. Tsai. The ultra-wideband indoor channel. In *IEEE Vehicular Technology Conference (VTC 2004-Spring)*, pages 208–212, 2004.

[ea04] B. Kannan et al. Uwb channel characterization in office. Technical report, Tech. Rep. Document IEEE, 802.15-04-0439-00-004a,, 2004.

[ea05] S. Emami et al. Uwb, tech. rep. document. *Report*, 2005.

[FCC02] Federal communications commission: Fcc press release, feb 2002. Technical report, http://www.fcc.gov/Bureaus/Engineering/Technology/News/Releases/2002/, February 2002.

[FHay] J. A. Fessler and A. O. Hero. Complete-data spaces and generalized em algorithms. In *IEEE Conf. Acoustic and Speech and Signal Processing*, chapter 1-4. 1993, May.

[Foe02] J. Foerste. Channel modeling sub-committee report final (doc.: Ieee 802-15-02/490r1-sg3a). In *IEEE P802.15 Working Group for Wireless Personal Area Networks (WPANs), Feb. 2002. [Online] Available: http://grouper.ieee.org/groups/802/15/pub/2002/Nov02/*, November 2002.

[FPM03] J.R. Foerster, M. Pendergrass, and A.F. Molisch. A channel model for ultra wideband indoor communication. In *International Symposium on Wireless Personal Multimedia Communication*, October 2003.

[FSJL95] E. Funk, S. Saddow, L. Jasper, and A. Lee. ultra-wideband pulse generation using photoconductive switching. In *Digest of the LEOS Summer Topical Meetings*, pages 55–56, 1995.

[FTH+17] B.H. Fleury, M. Tschudin, R. Heddergott, D. Dahlhaus, and K.L. Pedersen. Channel parameter estimation in mobile radio environments using the sage algorithm. In 3, editor, *IEEE Journal in Selected Aerea Communication*, Octobet, 1999 17. 434-450.

[Gal68] R. G. Gallager. *Information Theory and Reliable Communication*. John Wiley and Sons, Inc. New York, NY, USA, 1968.

[GGAK03] S. S. Ghassemzadeh, L. J. Greenstein, and et al. A. Kavcic. Uwb indoor path loss model for residential and commercial buildings. In *IEEE Vehicular Technology Conference,VTC Fall, Orlando, FL,*, pages 629–633, September 2003.

[GGS+05] S. S. Ghassemzadeh, L. J. Greenstein, T. Sveinsson, A. Kavcic, and V. Tarokh. Uwb delay profile models for residential and commercial indoor environments. *IEEE Transactions On Vehicular Technology*, 54(4), July 2005.

[GJR+04] SS Ghassemzadeh, R. Jana, C. Rice, Turin W, and V. Tarokh. Measurement and modeling of an ultra-wide bandwidth indoor channel. *IEEE Transactions on Communications 2004; 52(10):*, 52(10):1786–1796, 2004.

[GJRT02] S. S. Ghassemzadeh, R. Jana, C. W. Rice, and W. Turin. A statistical path loss model for in-home uwb channels,. In *IEEE Conference on Ultra Wideband Systems and Technologies, Baltimore, MD, USA*, pages 59–64, May 2002.

[Gol49] M. J. E. Golay. *Notes on digital coding*. 1949.

[Gre83] Y. Grenier. Time-dependent arma modelling of non stationary signals. *IEEE Transaction On ASSP*, 4(31):899–911, 1983.

[GS00] A. Ganesan and A. M Sayeed. Bandwidth-efficient exploitation of the degrees of freedom in a multipath fading channel. In *Information Theory, 2000. Proceedings. IEEE International Symposium on, Italy*, page 161, 25-30 June 2000.

[GSCea00] S. J. Gunderson, R. Scholtz, K. Chugg, and et al. Shipboard environment characterization, appendix a : Naval total asset visibility tests on the uss curtiss. In *Document technique, UltRaLab*, page http://ultra.usc.edu/New_Site/papers/NTAV_Appendix_A_USC.pdf, 2000.

[Ha02] Hovinen and al. A proposal for a selection of indoor uwb path loss model. Technical report, [Online] Available: http://grouper.ieee.org/groups/802/15/pub/2002/Jul02, 02280r1P802.15, July 2002.

[HD94] H.Hashemi and D.Tholl. Statistical modeling and simulation of the rms delay spread of indoor radio propagation channels. *IEEE Transactions on Vehicular Technology*, February 1994.

[H.H93a] H.Hashemi. Impulse response modeling of indoor radio propagation channels. *IEEE Journal on Selected Areas in Communications*, September 1993.

[H.H93b] H.Hashemi. The indoor radio propagation channel. In *proceedings of the IEEE*, July 1993.

[HHP02a] V. Hovinen, M. Hamäläinen, and T. Pätsi. Ultra-wideband indoor radio channel models: preliminary results. In *IEEE Conference on Ultra-wideband Systems and Technologies (UWBST '02), Baltimore, MD USA,2002*, pages 75–79, May 2002.

[HHP02b] V. Hovinen, M. Hämäläinen, and T. Pätsi. Ultra wideband indoor radio channel models: Preliminary results. In *IEEE Conference on Ultra Wide Band Systems and Technologies (UWBST '02), Baltimore, MD, USA*, pages 75–79, May 2002.

[HKS05] A. Menouni Hayar, R. Knopp, and R. Saadane. Subspace analysis of indoor uwb channels. *EURASIP Journal on applied signal processing, special issue on UWB - State of the art*, 1(3):287–295, 2005.

[HRS07] Gautham Hariharan, Vasanthan Raghavan, and Akbar M. Sayeed. Capacity of sparse wideband channels with partial channel feedback. *Submitted to European Transactions on Telecommunications, New Directions in Information Theory*, June 2007.

[HS07] Gautham Hariharan and Akbar M. Sayeed. Non-coherent capacity and reliability of sparse multipath channels in the wideband regime. In *2nd Information Theory and Applications Workshop, San Diego*, Jan 2007.

[HT94] H. Hashemi and D. Tholl. Statistical modeling and simulation of the rms delay spread of indoor radio propagation channels. *IEEE Transactions on Vehicular Technology*, 43(1):110–119, February 1994.

[HTK05] K. Haneda, J. Takada, and T. Kobayashi. On the cluster properties in uwb spatio-temporal residential measurement. In *COST 273 Workshop, Bologna, Italy,*, Jan 2005.

[HV05] A. Menouni Hayar and G. M. Vitetta. Channel models for ultra-wideband communica-tions: an overview. In *Proc. of the 14th IST Mobile Wireless Summit 2005, Dresden, Germany*, June 19-23 2005.

[Jay03] E. T. Jaynes. *Probability Theory: The Logic of Science*. Cambridge, 2003.

[J.F01] Srinivasa Somayazulu David Leeper J.Foerster, Evan Green. Ultra wideband techonology for short or medium range wireless communications. *Intel Technology Journal, 2th Quarter*, 2001.

[JHH04] T. Jämsä, V. Hovinen, and L. Hentilä. Comparison of wideband and ultra-wideband channel measurements. In *COST 273 Workshop, Gothenburg, Sweden*, Jan 2004.

[JK03] N. Danièle Á. Álvarez M. Lobeira J. L. García G. Valera R. P. Torres (CAN) J. Keignart, J. B. Pierrot. Radio channel sounding results and model. Deliverable number: D31, ist-2001-32710, U.C.A.N., 2003.

[KCG+05] M. Kamoun, S. Chaillou, J. Gosteau, L. e Mazet, M. Courville, and P Duhamel. Data rate upper bounds for uwb link with ieee 802.15.3a channel model. In *Ultra-Wideband, 2005. ICU 2005. 2005 IEEE International Conference on*, pages 764 – 768, 5-8 Sept 2005.

[KD02] J. Keignart and N. Daniele. Subnanosecond uwb channel sounding in frequency and temporal domain. In *IEEE Conference on Ultra Wide Band Systems and Technologies, Baltimore, MD, USA*, pages 25–30, may 2002.

[KD03] J. Keignart and N. Daniele. Channel sounding and modelling for indoor uwb communications. In *Workshop on Ultra Wideband Systems, Oulu, Finland*, Juan 2003.

[KL95] G. Kadel and R. Lorenz. Impact of the radio channel on the performance of digital mobile communication systems. In *IEEE Int. Symp. on Personal, Indoor and Mobile Radio Communications (PIMRC)'95,*, pages 419–423, 1995.

[KP02] J. Kunisch and J. Pamp. Measurement results and modeling aspects for uwb radio channel. In *IEEE Conference Ultra Wideband Systems and Technologies*, pages 19–23, 21-23 May 2002.

[KPDR] J. Keignart, J. B. Pierrot, N. Daniele, and P. Rouzet. Uwb channel modeling contribution from cea-leti and stmicroelectronics (doc: Ieee p802.15-02/444-sg3a). Technical report, submitted to IEEE P802.15 Working Group for Wireless Personal Area Networks (WPANs), Oct. 2002. [Online] Available: http://grouper.ieee.org/groups/802/15/pub/2002/Nov02/.

[KWAea04a] J. Karedal, S. Wyne, P. Almers, and et al. Statistical analysis of the uwb channel in an industrial environment. In *IEEE Vehicular Technology Conference, VTC Fall, Los Angeles, CA, USA*, pages 81–85, September 2004.

[KWAea04b] J. Karedal, S. Wyne, P. Almers, and et al. Uwb channel measurements in an industrial environment. In *IEEE Global Telecommunications Conference, Dallas, TX, USA*, pages 3511–3516, Novomber 2004.

[MA00] M.Kaveh and A. Abdi. newblock performance comparison of three different estimators for nakagami m-parameter using monte carlo simulation. *IEEE Communication Letters*, 4(1):119–121, 2000.

[MASJWR06] A. Muqaibel, A. Attiya A. Safaai-Jazi, B. Woerner, and S. Riad. Path-loss and time dispersion parameters for indoor uwb propagation. *IEEE Transactions on Wireless Communications*, 5(3):550– 559, March 2006.

[MBC+05] A.F. Molisch, K. Balakrishnan, D. Cassioli, C.-C Chong, and J. Karedal J. Kunisch H. Schantz K. Siwiak S. Emami, A. Fort. A comprehensive model for ultrawideband propagation channels. In *IEEE Global Telecommunications Conference (GLOBECOM)*, pages 3648–3653, November 2005.

[MFP05] A. F. Molisch, J. R. Foerster, and M. Pendergrass. Channel models for ultrawideband personal area networks. *IEEE Wireless Communications*, 10(6):14–21, December 2005.

[MMH+02] G. Matz, A.F. Molisch, F. Hlawatsch, M. Steinbauer, and I. Gaspard. On the systematic measurement errors of correlative mobile radio channel sounders. *IEEE Transaction on Communications*, 50(5):808–821, May 2002.

[Mol] A. F. Molisch. Uwb propagation channels,.

[Mol05] A. F. Molisch. Ultrawideband propagation channels–theory, measurement,and models. *(invited paper) IEEE Transaction Vehicular Technology*, 2005.

[Moo97] T. Moon. The expectation–maximization algorithm. *IEEE Signal Processing Magazine*, pages 47–60, 1997.

[MT85] M.Wax and T.Kailath. Detection of signals by information theoretic criteria. *IEEE Trans. on Acoustics n Acoustics,Speech, and Signal Processing*, 33(2):387–392, April 1985.

[MZW98] R. A. Scholtz M. Z. Win. On the robustness of ultra-wide bandwidth signals in dense multipath environments. *IEEE Communications Letters*, 2(2):51–53, February 1998.

[OE01] G. R. Opshaug and P. Enge. Gps and uwb for indoor navigation. In *Institute of Navigations GPS Conference Salt Lake City, UT, USA*, September 2001.

[OI04] M. Hamalainen Oppermann and J. Iinatti. *UWB Theory and Applications*. John Wiley Sons Inc., 2004.

[OWY83] A.V. Oppenheim, A.S. Willsky, and I.T. Young. *Signals and Systems*. Prentice-Hall, London, 1983.

[Pam02] J. Kunisch Et J. Pamp. Measurement results and modelling aspects for the uwb radio channel. In *IEEE Conference on Ultra Wideband Systems and Technologies, Baltimore, MD, USA*, pages 19–23, May 2002.

[PB02] M. Pendergrass and W. Beeler. Empirically based statistical ultra wideband (uwb) channel model (doc: Ieee 802-15-02/240sg3a). Technical report, IEEE P802.15 Working Group for Wireless Personal Area Networks (WPANs), June 2002. [Online] Available: http://grouper.ieee.org/groups/802/15/pub/2002/Jul02/, July 2002.

[PCR+02] C. Prettie, D. Cheung, L. Rusch, , and M. Ho. Spatial correlation ofuwb signals in a home environment. In *IEEE Conf. Ultra Wideband Systems and Technologies*, page 6569, May 2002.

[PCRH02] C. Prettie, D. Cheung, L. Rusch, and M. Ho. Spatial correlation of uwb signals in a home environment. In *IEEE UWBST*, pages 65–69, May 2002.

[PM96] John G. Proakis and Dimitris G. Manolakis. *Digital Signal Processing: Principles, Algorithms and Applications*. 3rd Edition, New Jersey, 1996.

[PM06a] D. Porrat and U. Mitra. Synchronization of ppm over wideband multipath channels. In *IEEE 2006 International Zurich Seminar on Communications*, February 2006.

[PM06b] D. Porrat and U. Mitra. Timing acquisition of wideband ppm systems over multipath. In *2006 IEEE International Symposium on Information Theory Seattle, Washington, USA*, July 2006.

[PM07] D. Porrat and U. Mitra. Multipath delay profile acquisition for ultrawideband ppm systems. *to appear in the IEEE Journal on Selected Areas in Communicaitons, special issue on performance limits of ultra-wideband systems*, 2007.

[PPV03] P. Pagani, P. Paunch, and S. Vinton. A study of the ultra-wideband indoor channel: Propagation experiment and measurement results. In *COST273 TD(030)060*. Jan 2003.

[Qiu04] R. C. Qiu. A generalized time domain multipath channel and its application in ultra-wideband (uwb) wireless optimal receiver design part ii: Physics-based system analysis. *IEEE Transaction on Wireless Communication*, 3(6), November 2004.

[Rap89] T. S. Rappaport. Characterization of uhf multipath radio channels in factory buildings. *IEEE Transaction Antennas Propagation*, 37(8):1058–1069, August 1989.

[Rap02] TS Rappaport. .*Wireless Communications: Principles and Practice*. Prentice Hall PTR: Upper Saddle River, NJ, USA, (2nd edn) edition, 2002.

[RHS07] Vasanthan Raghavan, Gautham Hariharan, and Akbar M. Sayeed. Capacity of sparse multipath channels in the ultra-wideband regime. In *to appear in IEEE Journal on Selected Topics in Signal Processing, Performance Limits of Ultra-Wideband Systems*, 2007.

[Ria86] S. Riad. The deconvolution problem: An overview. *Proceedings of the IEEE Publication*, 74:82–85, Jan 1986.

[RK03] J. Romme and B. Kull. On the relation between bandwidth and robustness of indoor uwb communication. In *IEEE Ultra Wide Bandewidtth System Technology Conference (UWBS03)*, November 2003.

[Ros99] J. P. Rossi. Influence of measurement conditions on the evaluation of some radio channel parameters. *IEEE Transaction on Vehicular Technology*, 48:1304–1316, 1999.

[RPCQL03] L. Rusch, C. Prettie, D. Cheung, and M. Ho Q. Li. Characterization of uwb propagation from 2 to 8 ghz in a residential environment. Technical report, Intel, 2003.

[SA99] A. M. Sayeed and B. Aazhang. Joint multipath-doppler diversity in mobile wireless communications. *IEEE Transaction communication on*, pages 123–132, Jan 1999.

[Saa03] R. Saadane. Empirical eigenanalysis of indoor uwb propagation channel. Master's thesis, Faculty of Sciences, Mohammed V University, Rabat, November 2003.

[saa05] Eurecom database and fp6 european project newcom/project. Technical report, http://newcom.ismb.it/public/index.jsp, December 2005.

[SAH06] R. Saadane, D. Aboutajdine, and A. Menouni Hayar. A statistical uwb channel model based on physical analysis. In *IEEE Advanced International Conference on Telecommunications and International Conference on Internet and Web Applications and Services (AICT-ICIW'06)*, page 80, 2006.

[SAH07] R. Saadane, D. Aboutajdine, and A. Menouni Hayar, editors. *Ultra Widebandwidth Large and Small scale Characterization With Different Environments*. IEEE ICTIS'07 conference Fez, Morocco, 3-5 April 2007.

[SAHK07] R. Saadane, D. Aboutajdine, A. Menouni Hayar, and R. Knopp. Uwb channel and degrees of freedom evaluations. *International Journal on Wireless and Optical Communications Special Issus in Ultra Wide*, 4(2):1–13, April 2007.

[SBS66] M. Schwart, W. R. Bennet, and S. Stein. *Communication Systems and Techniques*. New York: McGraw-Hill, 1966.

[Sch93] R. A. Scholtz. Multiple access with time-hopping impulse modulation. In *IEEE Military Communications Conference*, pages 447–450, October 1993.

[Sch04] U. Schuster. Indoor uwb channel measurements from 2 ghz to 8 ghz. In *Document technique IEEE 802.15-04/447, IEEE 802.15Working Group forWireless Personal Area Networks (WPANs),*, October 2004.

[SH06] R. Saadane and A. Menouni Hayar. Ultra wide bandwidth channel models. In *Newcom report ProjectB/WPRB1/DRB1.3*. October 2006.

[SHA07] R. Saadane, A. Menouni Hayar, and D. Aboutajdine. Ultra-wideband channel statistical characterization in different laboratories. Technical report, Faculty of sciences Rabat, Eurecom Institue, France, 2007.

[SHAH07a] R. Saadane, A. Menouni Hayar, D. Aboutajdine, and Helmut Hofstetter. New statistical uwb channel model based on physical approach: Validation using sage algorithm. *To be submitted to IEEE Jornal in Selected Topics in Signal Processing*, 2007.

[SHAH07b] R. Saadane, A. Menouni Hayar, D. Aboutajdine, and Helmut Hofstetter, editors. *Propagation phenomenon Analysis for Statistical UWB channel model*. Accepted to International Conference in Communications and Networking in China, IEEE WCN Chinacom, 2007.

[SHKA05a] R. Saadane, A. Menouni Hayar, R. Knopp, and D. Aboutajdine. On the estimation. In *ICMS'2005, International Conference on Modeling and Simulation Marrakech, Morocco,*, 22-25 November 2005.

[SHKA05b] R. Saadane, A. Menouni Hayar, R. Knopp, and D. Aboutajdine. On the estimation of the degrees of freedom of in-door uwb channel. In *IEEE Vehicular Technology Conference VTC Spring'05*, 29th May - 1st June 2005.

[SHKD04] R. Saadane, A. Menouni Hayar, R. Knopp, and D.Aboutajdine. Empirical eigenanalysis of indoor uwb propagation channels. In *IEEE Global Telecommunications Conference*, November 29-December 3 2004.

[Shn89] D.A. Shnidman. The calculation of the probability of detection and the generalized marcum q–function. *IEEE Transaction on Informtion Theory*, 35(2):389–400, March 1989.

[SK04] Y. Souilmi and R. Knopp. On the achievable rates of multiband ultra-wideband systems. *International Journal of Wireless Information Networks*, 10(4), October 2003, 2004. 2004.

[Sou05] Youness Souilmi. *Analysis of Signalling and Coding Schemes for Non-Coherent Ultra-Wide bandwidth Systems*. PhD thesis, l' Ecole Nationale Supérieure, des Télécommunications (ENST), Juin 2005.

[SP78] D. Slepian and H.O. Pollak. Prolate spheroidal wave functions, fourier analysis, and uncertainty- i. *Bell System Technical Journal*, 40:43–64, May-June 1978.

[SSGT02] L. J. Greenstein S. S. Ghassemzadeh and V. Tarokh. The ultra wideband indoor multipath loss model (doc: Ieee p802.15-02/282-sg3a and ieee p802.15-02/283-sg3a),. Technical report, submitted to IEEE P802.15 Working Group for Wireless Personal Area Networks (WPANs), June 2002. [Online] Available:http://grouper.ieee.org/groups/802/15/pub/2002/Jul02/, July 2002.

[Stu96] G. L. Stueber. *Principles of Mobile Communication*. Kluwer, 1996.

[SV87] A. Saleh and R. A Valenzuela. A statistical model for indoor multipath propagation. *IEEE Journal Selected Areas Communication*, 5(2):128–137, February 1987.

[SV02] A. M. Sayeed and V. V. Veeravalli. Essential degrees of freedom in space-time fading channels. In *13th IEEE Intern. Symp. Pers. Indoor, Mobile Radio Commun.*, pages 1512–151, Sept 6, Sept. 2002.

[SW02] T. Svantesson and J. Wallace. Statistical characterization of the indoor mimo channel based on los/nlos measurements. In *Conference Record of the Thirty-Sixth Asilomar Conference on Signals, Systems and Computers*, pages 1354 –1358, Novomber 2002.

[Tay95] J. D. Taylor. *Introduction to ultra wideband radar systems*. CRC Press, Inc., Boca Raton, FLUSA, 1995.

[THK05] A. Taparugssanagorn, L. Hentilä, and S. Karhu. Time-varying autoregressive process for ultra-wideband indoor channel model. In *IST Mobile Wireless Communications Summit*, 19-22 June 2005.

[TJT02] W. Turin, R. Jana, and V. Tarokh. Autoregressive modeling of an indoor uwb channel. In *EEE Conference on Ultra Wideband Systems and Technologies*, 2002.

[TS04] K. Tsuda and W. S.Noble. Learning kernels from biological networks by maximizing entropy. *Bioinformatics DOI: 10.1093/bioinformatics/bth906*, 1(20):326–333, 2004.

[TT00] I. E. Telatar and D. N. C. Tse. Capacity and mutual information of wideband multipath fading channels. *IEEE Trans. on Information Theory*, 2(2):1384–1400, July 2000.

[UH06] U.G.Schuster and H.Boumlcskei. Ultra wideband channel modeling on the basis of information-theoretic criteria. *IEEE Transactions on Wireless Communications*, to appear:to appear, 2006.

[VS99] R.G. Vaughan and N. Scott. Super-resolution of pulsed multipath channels for delay spread characterization. *IEEE Transaction on Communication*, 47(3):343–347, March 1999.

[W.C74] W.C.Jakes. *Microwave Mobile Communications*. John Wiley and Sons, New York, 1974.

[Wil94] D.B. Williams. Counting the degrees of freedom when using aic and mdl to detect signals. *IEEE Transactions on Signal Processing.*, 42(11):3282–3284, November 1994.

[WS98] M. Z. Win and R. A. Scholtz. Impulse radio: how it works. *IEEE Communications Letters*, 2(2):36–38, February 1998.

[www] www.skycross.com. Skycross, http://www.skycross.com/Products/uwb.asp.

[Yan02] S. M. Yano. Investigating the ultra-wideband wireless channel. In *IEEE VTC-Spring*, pages 1200–1204, May 2002.

[ZAS+03] T. Zasowski, F. Althaus, M. Stager, A.Wittneben, and G. Troster. Uwb for noninvasive wireless body area networks: Channel measurements and results. In *IEEE UWBST*, pages 285–289, November 2003.

[ZAZ06] W. Zhang, T.D. Abhayapala, and J. Zhang. Uwb spatia - frequency channel characterization. In *Vehicular Technology Conference, 2006. VTC 2006-Spring. IEEE 63rd*, pages 2732– 2736, Juan 2006.